TWDB Contract No. 2100012507
Final Report
Received: September 14, 2021

Numeric Well Log Simulations and Core Testing for the Edwards-Trinity (Plateau) Aquifer

Texas Water Development Board Contract #2100012507

Prepared for:
Texas Water Development Board

Prepared by:
Carlos Torres-Verdín
Zoya Heidari
Reynaldo Casanova
Almostafa Alhadi
Camilo Gelvez

August 2021

This page is intentionally blank.

Numeric Well Log Simulations and Core Testing for the Edwards-Trinity (Plateau) Aquifer

Texas Water Development Board Contract #2100012507

By
Carlos Torres-Verdín
Zoya Heidari
Reynaldo Casanova
Almostafa Alhadi
Camilo Gelvez
The University of Texas at Austin

August 2021

Executive Summary

The Texas Water Development Board (TWDB) Brackish Resources Aquifer Characterization System (BRACS) department contracted this work as part of their data collection efforts for their study on the brackish groundwater resources of the Edwards-Trinity (Plateau) Aquifer. For this project, we located, described, photographed and measured petrophysical properties for the Edwards-Trinity Plateau aquifers from six cores managed by the Bureau of Economic Geology. The core descriptions include lithology, mineralogy, hydrogeologic units, bedding thickness, color, sedimentary structures, and other significant features. We conducted laboratory measurements on 24 core samples which were obtained from 4 rock classes of the Trinity hydrogeologic unit and one representative rock class of the Edwards hydrogeologic unit. The core descriptions and photographs are available by request from the TWDB BRACS department. We performed nuclear magnetic resonance (NMR), total porosity, permeability, and electrical measurements on the core samples to quantify basic rock properties.

In addition, we assessed formation water salinity by numerical simulations of well logs of five wells located in the Edwards-Trinity (Plateau) Aquifer to accurately estimate rock and fluid properties of the different formations of both hydrogeologic units. We digitized all available logs image files into LAS files. In order to understand the numerical simulations results, we generated several synthetic models with a base-case simulation of sandstone, limestone, and dolomite with water of varying salinity to determine the sensitivity of factors influencing the calculations of water salinity from resistivity and spontaneous potential logs. We encountered that the main factors to consider are mud-filtrate invasion radius and formation factor variability, such as changes in total porosity and cementation exponent (m). Deeply invaded formations might impact the electrical resistivity logs response, which could escalate into high errors in the formation water salinity estimations. Percent error in water quality calculations was quantified for several sources including calculation method and well log type. Additionally, we investigated the impact of acquiring the electrical resistivity logs using induction and laterolog tools. We observed that induction tools are more reliable tools for the types of lithology and in-situ water of the Edwards-Trinity (Plateau) Aquifer. Ultimately, we found our numerical simulations of well logs to provide an alternative and reliable solution for estimating formation water salinity in geohydrology under the presence of mud-filtrate invasion. The well log LAS files and the simulation model files are available by request from the TWDB BRACS department.

Table of Content

List of Figures

List of Tables

1 Provided core list

Table 1-1 and Table 1-2 contain a summary of the information provided by the TWDB. Tables include general information for cores location and estimated depths and tops for possible formation and hydrogeological units available. In addition, nearby well logs were provided for the majority of wells with available cores along with well logs for simulations and other well log datasets including porosity logs. All well log sets were digitized in LAS format.

Five wells were selected as primary wells for core description and sampling. The cores from three of these wells are located at the Austin Core Research Center (CRC) available at the Bureau of Economic Geology (BEG), and other two are located at the CRC Midland facilities.

Table 1-1. Original list of wells with available cores in Edwards and Trinity hydrogeologic units. General information.

Accession number	Location	County	Field name	Well number	Formation	Hydrostratigraphic unit	Type
S08027	Midland CRC[a]	Crocket	Isabel Vaughan	15	-	Edwards, Trinity	Whole Core
S05823	Midland CRC[a]	Edwards	Higgins	1	-	Edwards, Trinity	Whole Core
C02692	Austin CRC[a]	Val Verde	Massie West	CT-3	Paluxy	Trinity	Whole Core
C06078	Austin CRC[a]	Val Verde	Hinds	1	Glen Rose	Edwards, Trinity	Slabbed Core
C02508	Austin CRC[a]	Val Verde	Murray	8	Cretaceous	Trinity	Whole Core

[a] CRC = core research center.

Table 1-2. Original list of wells with available cores in Edwards and Trinity hydrogeologic units. Depths of interest and nearby well logs.

Accession number	Core top (ft)	Core bottom (ft)	Edwards bottom (ft)	Trinity bottom (ft)	Nearby well log	Edwards logged bottom (ft)	Trinity logged bottom(ft)
S08027	453	1,452	510	620	Shannon # 1	440	520
S05823	594	922	609	1,184	A.P. Shankllin # 1	130	1,100
C02692	363	389	349	849	CT-22	330	600
C06078	0	392	270	1,112	N/A	-	-
C02508	709	712	679	1,786	Harding	463	1,730

2 Cores location, lithology and hydrogeologic intervals

BEG representatives assisted in locating the cores for two core viewings, description and sampling. The first session, March 15th to March 18th was at the Austin CRC. During this session, only wells Massie West CT-3 and Murray-8 were available for sampling. These wells only have 26 ft and 3 ft of core available, respectively. We included secondary cores from Massie West fields to increase the length of available cores for sampling purposes and were included in the core-viewing task. Though well Hinds-1 could not be sampled (it is a slabbed core), we took photographs and describe the full length of this core.

For the second core viewing session on April 26th and 27th, the cores located at the Midland CRC facilities were to be transferred to BEG at Austin. However, we identified that core for well Isabel_Vaughan-15 only had 10 ft available in Edwards hydrogeological unit and no cores available in Trinity unit. In addition, well Higgins-1 only had available cores for the depth intervals of 594-600 ft (6 ft) in Edwards unit, and 856-861.2 ft, 872-883 ft, 906-911 ft, and 917-922 ft (26.2 ft) in Trinity unit. After consulting with TWDB, the Well Yates-100-D was located and included into the study.

Figure 2-1 shows the geographic location of wells with available cores and nearby well logs, and Figure 2-2 illustrates the location of these wells in the map of the Edwards-Trinity Plateau area in West Texas (Kuniansky and Ardis, 2004). We reviewed published literature about the Edwards-Trinity Plateau aquifers; Kuniansky and Ardis (2004) and Anaya and Jones (2009) present the main characteristics of these hydrogeologic units, including a detailed explanation of the main formations, geologic transition, and facies description. Figure 2-3 and Figure 2-4 display the correlation chart for the Edwards-Trinity Plateau aquifers system divided in four main regions from northwest to southeast: 1) Trans-Pecos, 2) Edwards Plateau, 3) Hill Country, and 4) Balcones Fault Zone. Based on the stratigraphic units' correlations and the geologic formation information by Kuniansky and Ardis (2004) and Anaya and Jones (2009), we redefined Edwards and Trinity tops along with their main formations, presented in Table 1-1 and Table 1-2, in order to comprise consistent data and an adequate description of the cores. The reinterpreted and modified information is available in Table 2-1 and Table 2-2, and it is highlighted in light yellow for comparison with the provided original information.

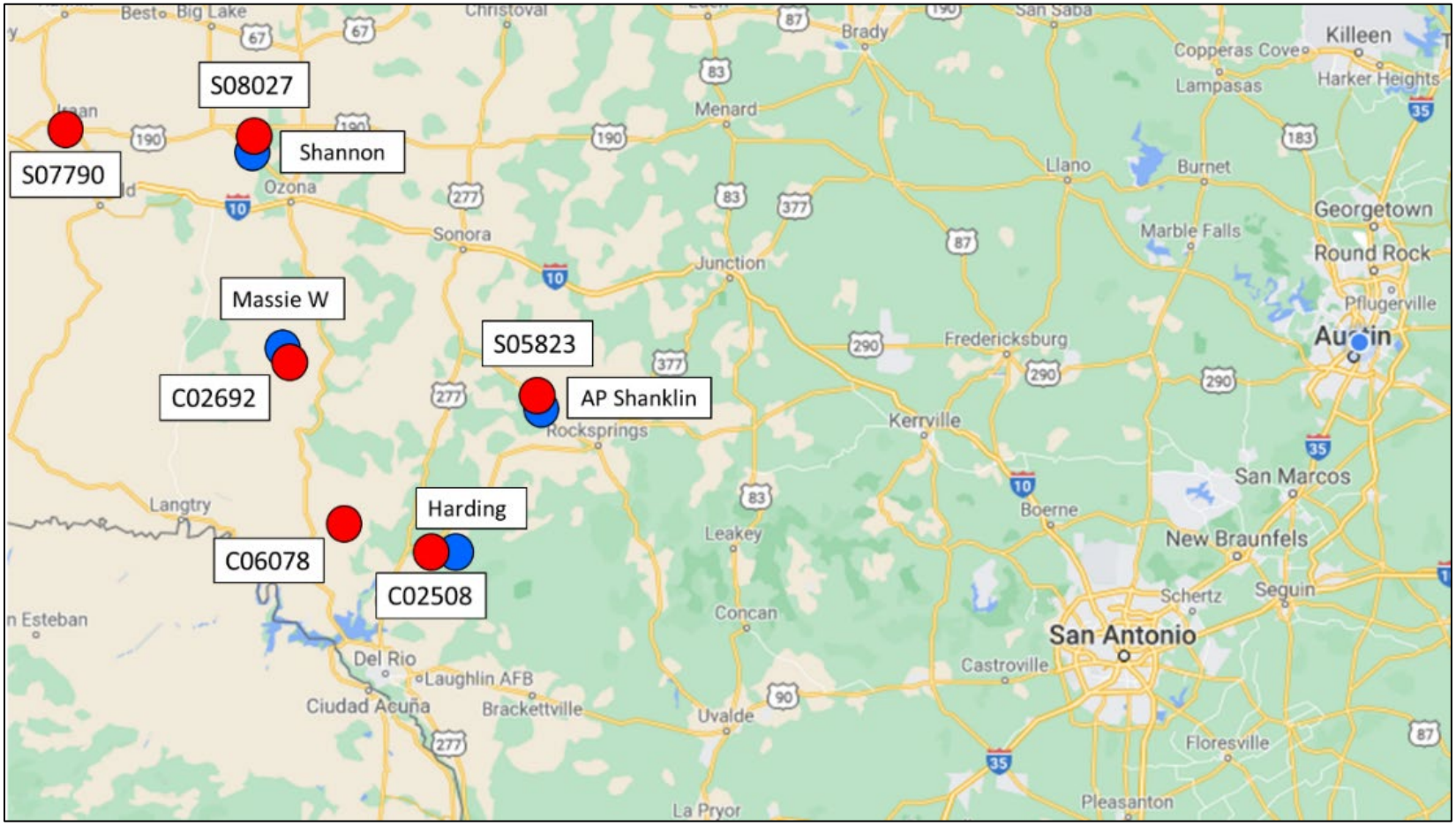

Figure 2-1. Geographic location of wells with available cores shown with red dots and nearby well logs shown with blue dots.

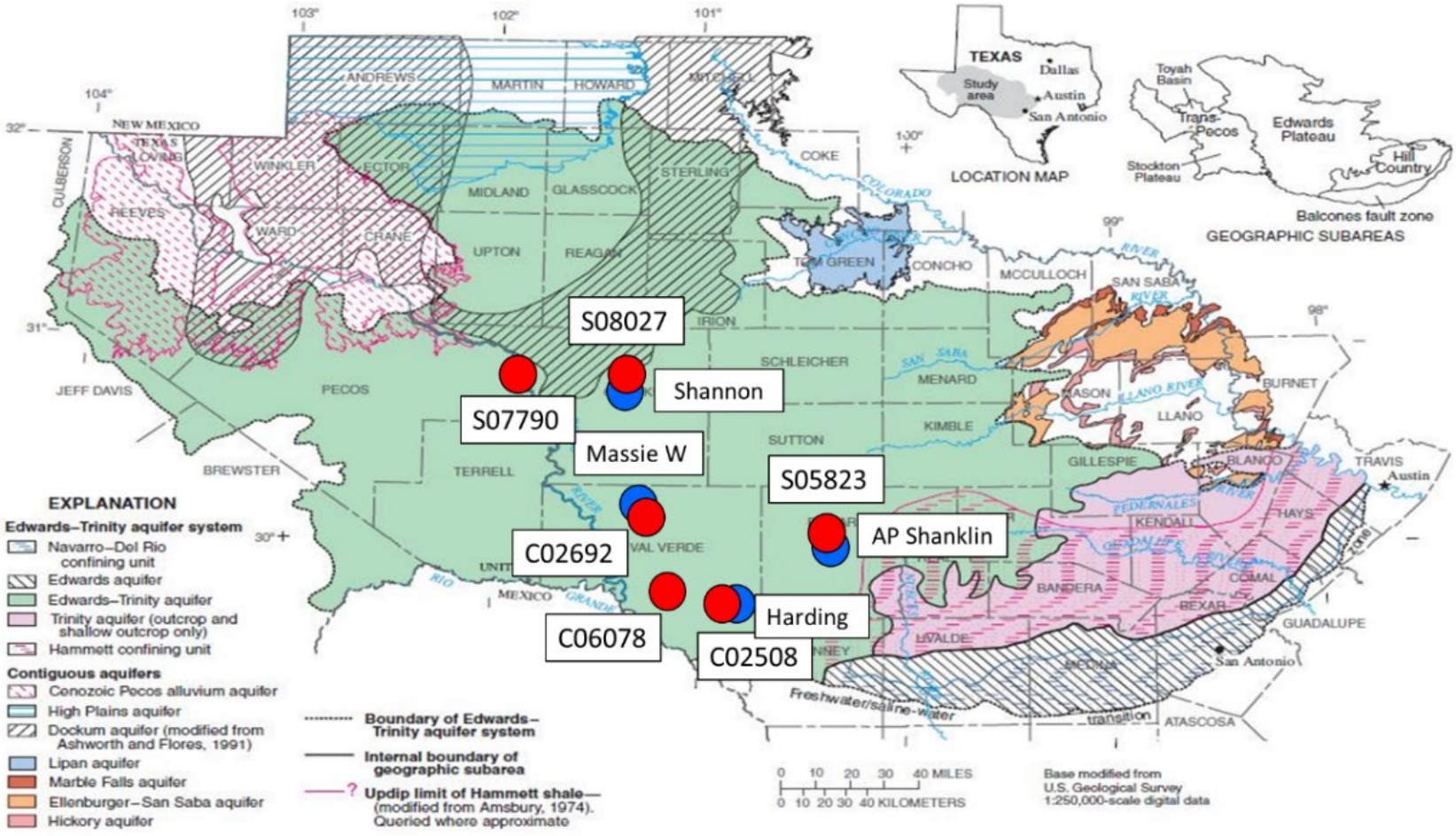

Figure 2-2. Edwards-Trinity Plateau map including wells with available cores shown with red dots and nearby well logs shown with blue dots. Modified from Kuniansky and Ardis (2004).

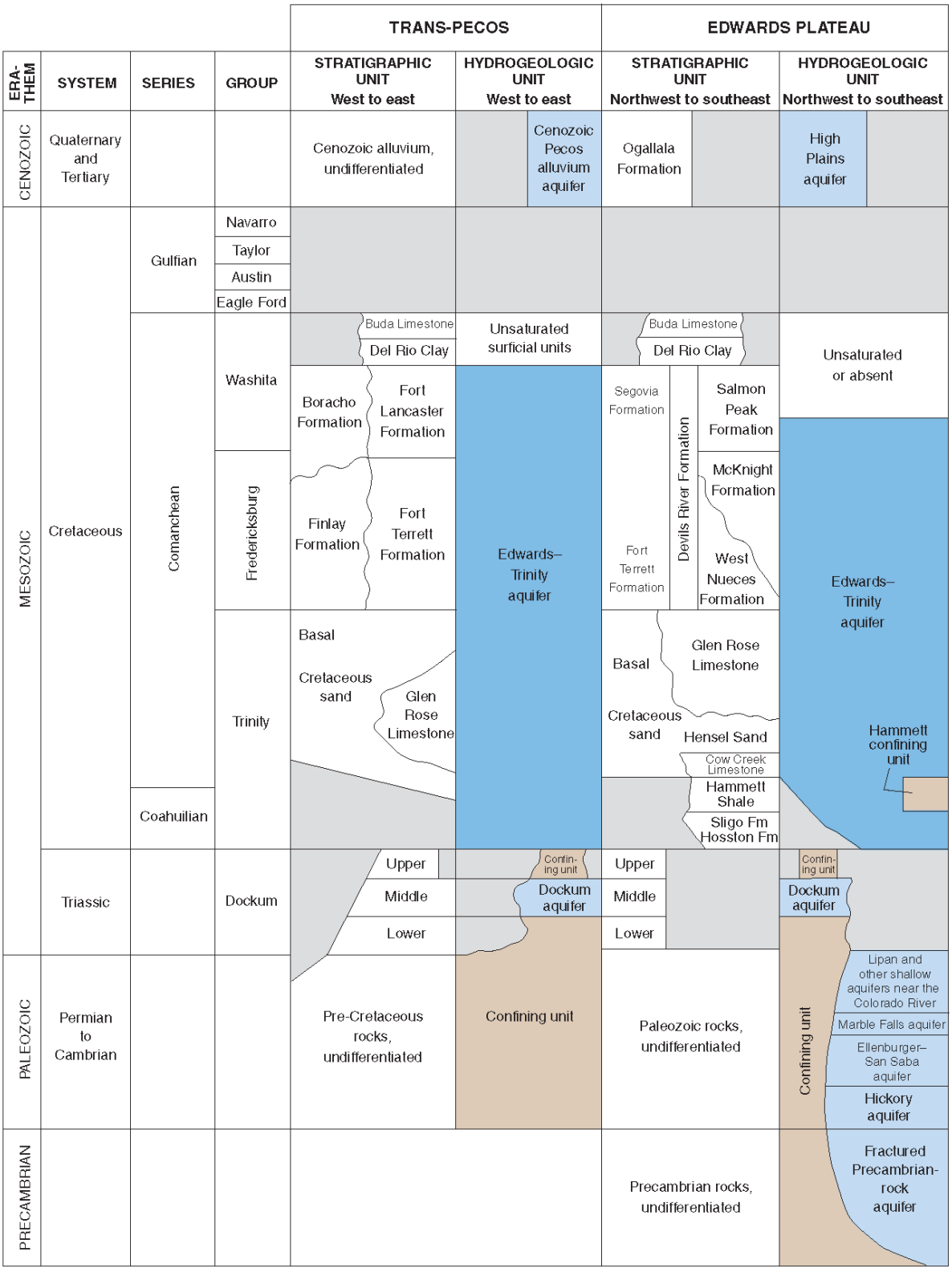

Figure 2-3. Geology correlation chart for Trans-Pecos and Edwards Plateau (Kuniansky and Ardis, 2004).

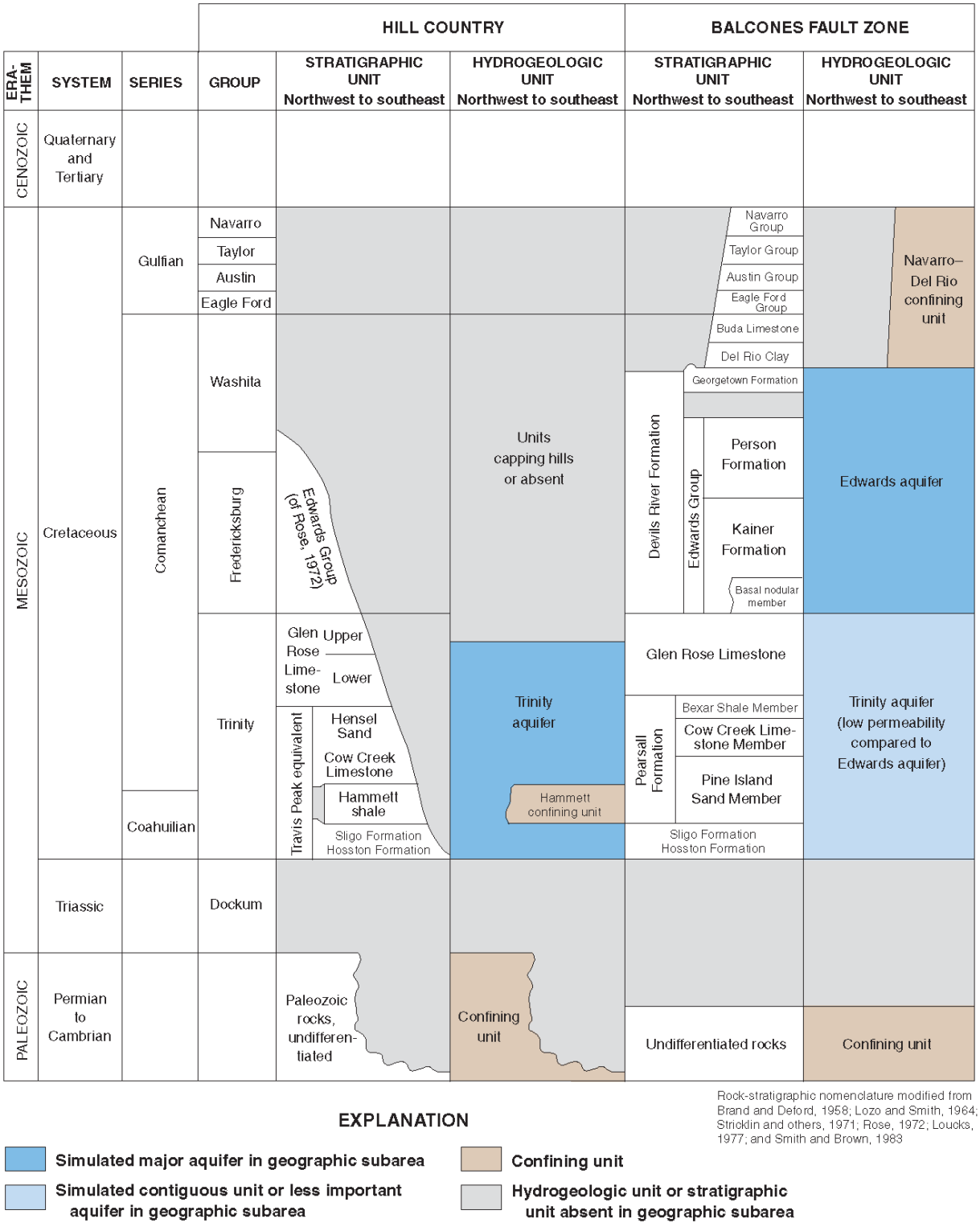

Figure 2-4. Geology correlation chart for Hill Country and Balcones Fault Zone (Kuniansky and Ardis, 2004).

Table 2-1. Final list of wells selected for the project with updated formation names.

Accession number	Location	County	Field name	Well number	Formation	Hydrostratigraphic unit	Type
S08027	Midland CRC [a]	Crocket	Isabel Vaughan	15	Fort Terrett,	Edwards	Whole Core
S05823	Midland CRC [a]	Edwards	Higgins	1	Fort Terrett, Glen Rose	Edwards, Trinity	Whole Core
S07790	Midland CRC [a]	Pecos	Yates	100-D	Hosston	Trinity	Slabbed Core
C02692	Austin CRC [a]	Val Verde	Massie West	CT-3	Fort Terrett, Cretaceous, Glen Rose	Edwards, Trinity	Whole Core
C02693	Austin CRC [a]	Val Verde	Massie West	CT-4	Glen Rose	Trinity	Whole Core
C02699	Austin CRC [a]	Val Verde	Massie West	CT-10	Glen Rose	Trinity	Whole Core
C02698	Austin CRC [a]	Val Verde	Massie West	CT-9	Glen Rose	Trinity	Whole Core
C06078	Austin CRC [a]	Val Verde	Hinds	1	Fort Terrett, Glen Rose	Edwards, Trinity	Slabbed Core
C02508	Austin CRC [a]	Val Verde	Murray	8	Glen Rose	Trinity	Whole Core

[a] CRC = core research center.

Table 2-2. Final list of wells selected for the project with updated core depths and units tops.

Accession number	Core top (ft)	Core bottom (ft)	Edwards bottom (ft)	Trinity bottom (ft)	Nearby well log	Edwards logged bottom (ft)	Trinity logged bottom(ft)
S08027	453	463	510	620	Shannon # 1	440	520
S05823	594	922	609	1,184	AP Shankllin # 1	130	1,100
S07790	414	464	153	496	N/A	-	-
C02692	363	389	349	849	CT-22	330	600
C02693	343	365	304	834	CT-22	330	600
C02699	397	421	344	874	CT-22	330	600
C02698	442	463	414	944	CT-22	330	600
C06078	0	392	270	1,112	N/A	-	-
C02508	709	712	679	1,786	Harding	463	1,730

3 Photographs and basic core descriptions

This section includes core photographs of nine total cores available at the Austin and Midland Core Research Centers. Table 2-1 and Table 2-2 present a list and information for the primary and secondary cores. Photographs including scale and depth reference are available for all nine cores and are divided in folders according to their original location.

In addition, we include independent basic core descriptions for all six primary cores. Each report indicates various facies lithology, depth of intervals, geological formation, hydrogeologic unit, sedimentary structures, color, and a brief description of grain size, distribution, texture, mineralogy and geological features.

Listing of the Edwards-Trinity Plateau core descriptions are available in an Excel file; for download purposes, the following is the link to the Excel file of the Edwards-Trinity Plateau core descriptions: https://utexas.box.com/s/w8khydri8hkk0iuyd1fd2qupxdcuklaa

For download purposes the core photographs are located via the following downloadable link: https://utexas.box.com/s/w8khydri8hkk0iuyd1fd2qupxdcuklaa

4 Sample analyses

The main objective of this task is to analyze 15 to 25 representative core samples of various Edwards/Trinity rock classes. The petrophysical properties should include at least porosity, permeability, porosity factor (m), and nuclear magnetic resonance (NMR).

4.1 Methods and equipment

This section of the report presents the methodology and equipment used to obtain porosity, permeability, and electrical measurements in the core samples acquired in wells located in the Edwards-Trinity Plateau.

4.1.1 Sample preparation

We cut 38 core samples that represent the main rock classes of Edwards/Trinity formations and analyzed 24 samples through laboratory measurements. Table 4-1 describes the main geological features of each rock class and

Table 4-2 shows the core samples IDs, the location of each core sample, and the name of the wells from which cores ate taken. We classified the core samples based on the rock features and main diagenesis as discussed in task 1. We analyzed four rock classes of Trinity formation and one rock class of Edwards formation based on the rock availability and selection of the more representative core samples for each formation. Figure 4-1 to 4-5 show pictures of the analyzed core samples.

We saturated the core samples with 3 wt. % potassium chloride brine (KCl), which has a resistivity of 0.22 ohm-m to inhibit the clay and prevent core samples from swelling. In the

saturation process, we initially dried the samples at low temperatures (approximately 65 F) to eliminate the sample damage. Then, we situated the core samples in vacuum equipment for 12 to 24 hours depending on the sample porosity. Finally, we introduced the brine to the sample in the vacuum and left them for 4 to 12 hours to be saturated. We faced some challenges in the cutting and preparation process for the first rock class in the Trinity formation. Most rock samples in this rock class absorb water, swell, and break (Figure 4-6). Furthermore, some core samples get damaged during the measurements processes, when the samples get exposed to water.

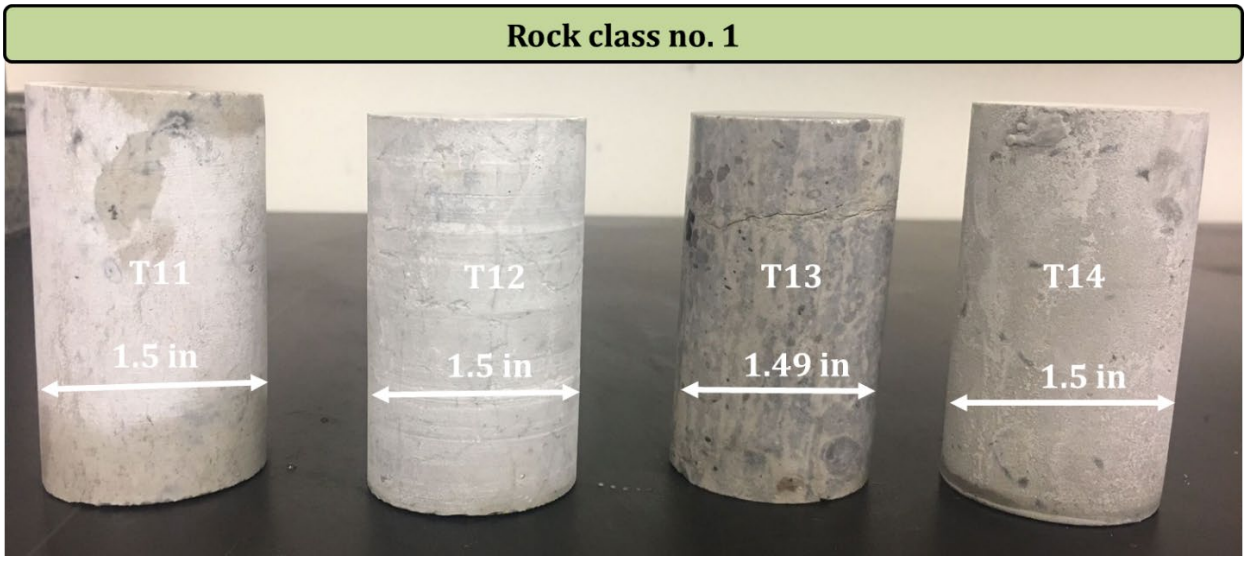

Figure 4-1. Rock class 1: pictures of analyzed core samples.

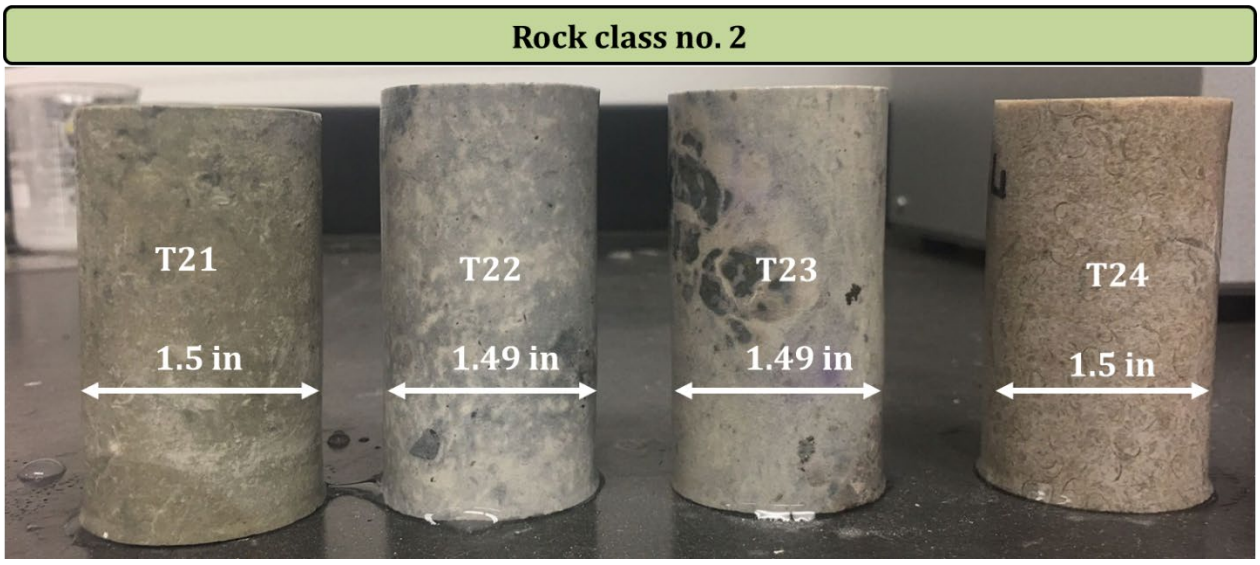

Figure 4-2. Rock class 2: pictures of analyzed core samples.

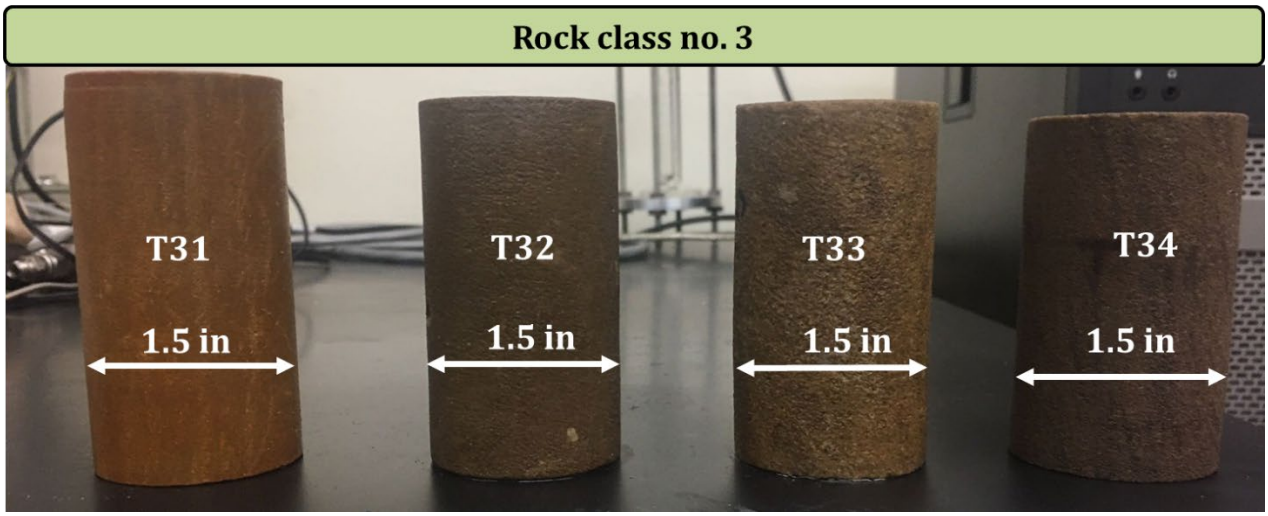

Figure 4-3. Rock class 3: pictures of analyzed core samples.

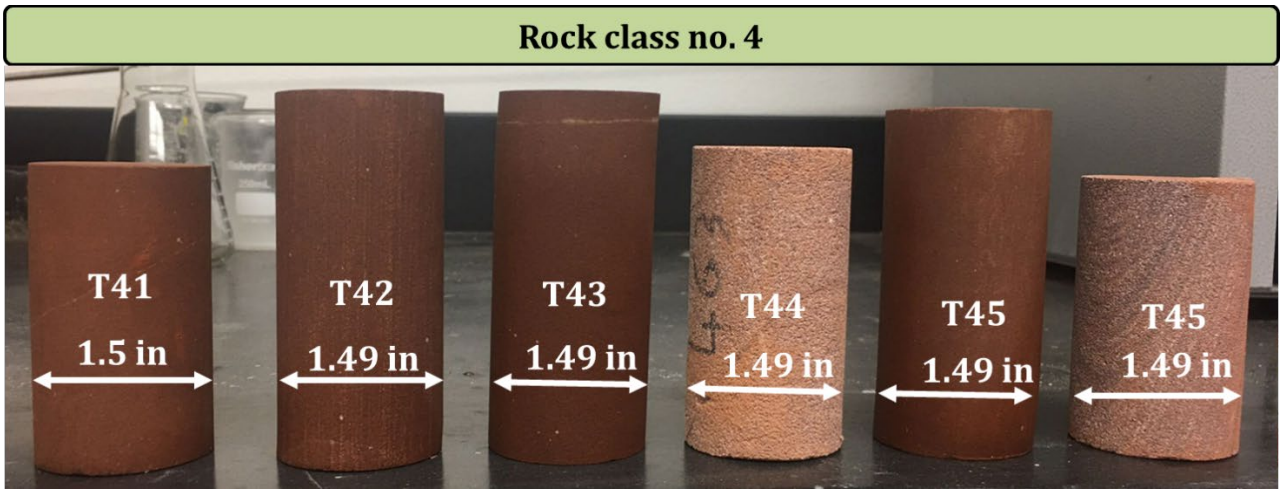

Figure 4-4. Rock class 4: pictures of analyzed core samples.

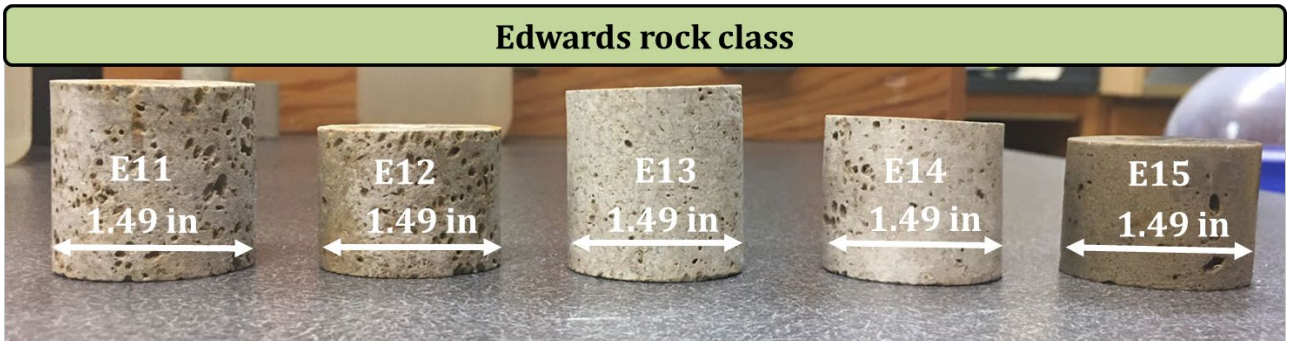

Figure 4-5. Edwards rock class: pictures of analyzed core samples.

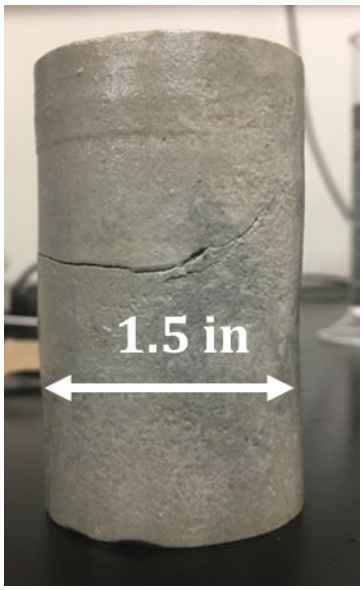

Figure 4-6. Rock class 1: an example of a damaged core sample.

Table 4-1. Geological description for each rock class.

Rock Class	Description	Formation	Samples analyzed
1	White to light gray, brittle limestone, embedded trace clay and gypsum, presence of bioturbation, and micro vugs.	Trinity	T11, T12, T13, T14
2	White to light grey, brittle to soft limestone, embedded evaporates.	Trinity	T21, T22, T23, T24, T25
3	Brownish to tan mudstone with crossbedding and embedded dolomite. Poorly consolidated, friable and presence of small fracs	Trinity	T31, T32, T33, T34
4	Red Massive well-sorted sandstone with a wide range of grain sizes, embedded calcite clasts and dark clays. Cross-bedded white calcarous thin layers	Trinity	T41, T42, T43, T44, T45
Edwards	White to brownish, limestone with Calcareous mudstone with embedded dolomite crystals, traces of evaporites, and large-size vugs	Edwards	E11, E12, E13, E14, E15

Table 4-2. Location of the core samples.

Core ID	Class	Formation	Well #	Core depth (ft)
T11	Class 1	Trinity	C02699	410
T12		Trinity	C02699	420
T13		Trinity	C02699	407.5
T14		Trinity	C02698	442
T15		Trinity	C02693	343
T21	Class 2	Trinity	C02698	445
T22		Trinity	C02698	444.5
T23		Trinity	C02698	446
T24		Trinity	C02698	444
T25		Trinity	C02698	447
T31	Class 3	Trinity	C02698	454
T32		Trinity	C02698	456
T33		Trinity	C02698	455
T34		Trinity	C02692	380
T41	Class 4	Trinity	S07790	451
T42		Trinity	S07790	447
T43		Trinity	S07790	446
T44		Trinity	S07790	463
T45		Trinity	S07790	455
E11	Edwards	Edwards	S08027	460
E12		Edwards	S08027	460.2
E13		Edwards	S08027	462
E14		Edwards	S08027	462.2
E15		Edwards	S08027	457

4.1.2 Permeability measurements

The selected rock classes cover a wide range of permeability values, which requires different measurement techniques for permeability assessments, such as using gas permeameter, core-flood, and pulse-decay permeameter.

Brine permeability measurements

We initially used gas permeameter and brine core flood method to estimate the permeability of the detected rock classes. We were able to measure the permeability of class 3 core samples and one core sample of Edwards class using brine core-flood method. When we applied the aforementioned methods to the rest of the core samples, both systems reached their maximum pressure, and the fluids did not penetrate the core samples.

Gas permeability measurements (pulse-decay method)

To measure the permeability of tight core samples, we used pressure-decay measurements which were acquired for all the dried core samples. In this technique, the core sample is placed in a core holder connected to an upstream tank filled with nitrogen. Then, an upstream valve is opened, and the gas expands across the sample either to the atmosphere or vacuum. The differential pressure versus time is recorded and the permeability values are obtained through the data analysis procedure. We dried the samples at 65°C for at least 48 hours to remove any moisture in them. Then, we used a GCTS pulse-decay permeameter (PDP) to obtain the permeability values for all core samples at room temperature (25°C). After we placed the dried core sample in a Hassle-type core holder, we applied a confining pressure of 1,400 psi around the core sleeve using a hydraulic oil pump. Next, we established a pore pressure of 800 psi using nitrogen (N_2) as the pore fluid. We allowed N_2 pressure to equilibrate before conducting any measurements on the core samples. After the pore pressure was equilibrated, we applied a small pressure pulse by decreasing the downstream pressure to 10 psi. Finally, we recorded the decline in the differential pressure and the increase in downstream pressure as the pressure pulse traveled through the core sample. The recorded data was processed to obtain the gas permeability using an in-house data processing algorithm based on the formulation introduced by Jones (1999).

4.1.3 Electrical measurements

We used multifrequency impedance analyzer equipment to measure the electrical resistivity of core samples which are saturated with 3 wt.% KCl brine. The measured electrical resistivity and the estimated porosity are then used through the application of Archie's model to estimate the porosity exponent (m). The Winsauer coefficient (a) was assumed to be equal to 1.

4.1.4 NMR and porosity measurements

We measured the relaxation time of the transverse magnetization decay (T_2) using a 2-MHz Magritek NMR Rock Core Analyzer with a CPMG pulse sequence. We set the interexperiment delay to be 5s, the minimum signal-to-noise ratio (SNR) to 200, and the echo spacing to 100 μs. We measured the T_2 distribution of each fully brine-saturated core sample. 23 core samples were analyzed, and results are shown in the results section.

4.1.5 Porosity measurements

Porosity can be estimated using weight measurements and NMR measurements. We avoid using the weight method to estimate porosity of the core samples because it requires drying the rock samples either at high temperature or at low temperature for a long time (more than 30 hours). From our initial tests, such processes resulted in damaging the core samples. Therefore, we used NMR measurements to reliably estimate the porosity of the core samples.

4.2 Results

This section contains the results and observations for the permeability measurements, NMR measurements, porosity measurements and electrical measurements performed on all core samples.

4.2.1 Permeability measurements

Figure 4-7 to Figure 4-10 show the detected flow rate at different levels of pressure difference applied to the core samples T32, T33, T34, and E14. We used brine core-flood method for assessment of permeability in these core samples. Figure 4-11 to Figure 4-22 show the pressure decay as a function of time for the rest of the core samples. We used pluse-decay technique for assessment of permeability in these core samples.

The selected core samples cover a wide range of permeability even within the same rock class. We were unable to estimate the permeability of rock class 1 because the core samples were damaged either by the heating process or saturation process. Rock class 2 has very low permeability ranging from 0.0005 to 0.08 mD. Rock class 3 has a wide range of permeability from 7 mD to 1,378 mD which can indicate the presence of microfractures in some core samples. Rock class 4 has permeability values ranging from 0.0028 mD to 0.096 mD. It should be noted that from inspection of the pulse-decay data, it seems that the low permeability of some of the samples makes them fall in the margin of reliability of the PDP equipment for assessment of permeability. Therefore, those permeability estimates could be biased.

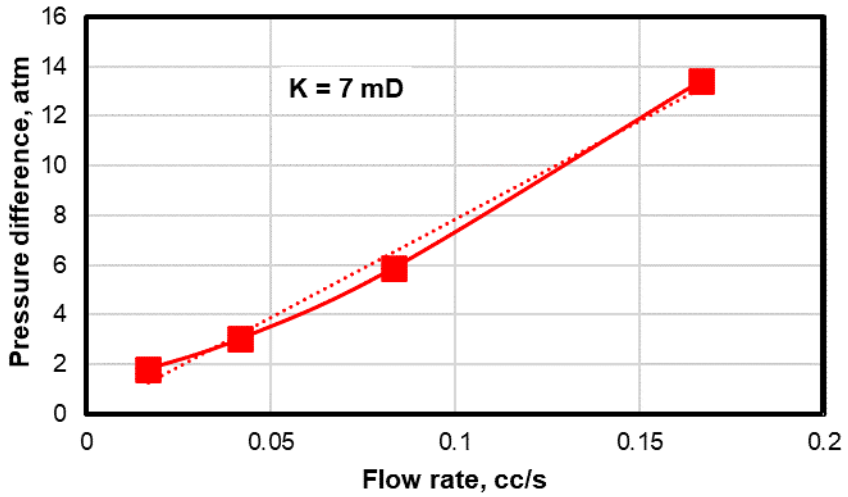

Figure 4-7. **Rock class 3: permeability assessment for sample T32. This plot shows the detected flow rate at different levels of pressure difference applied to the core sample. 3 wt.% KCl brine is used to perform the flow experiments. Dot line is the slope which used to estimate permeability value**

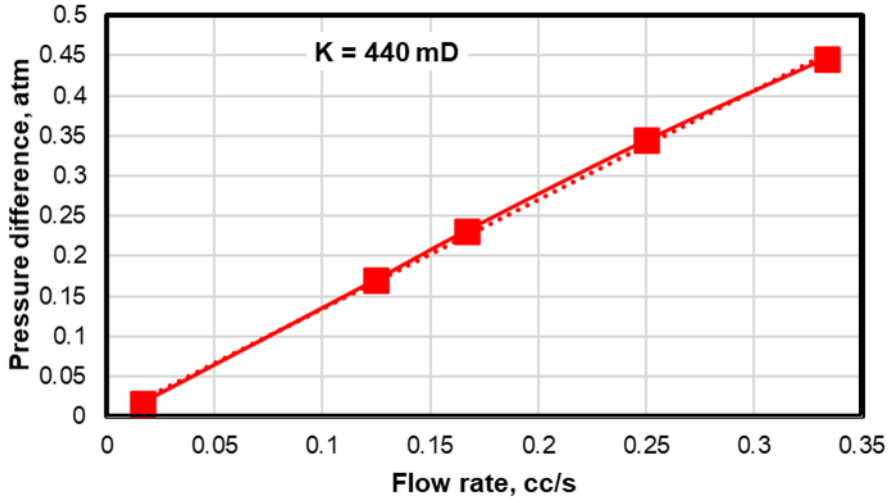

Figure 4-8. **Rock class 3: permeability assessment for sample T33. This plot shows the detected flow rate at different levels of pressure difference applied to the core sample. 3 wt.% KCl brine is used to perform the flow experiments. Dot line is the slope which used to estimate permeability value**

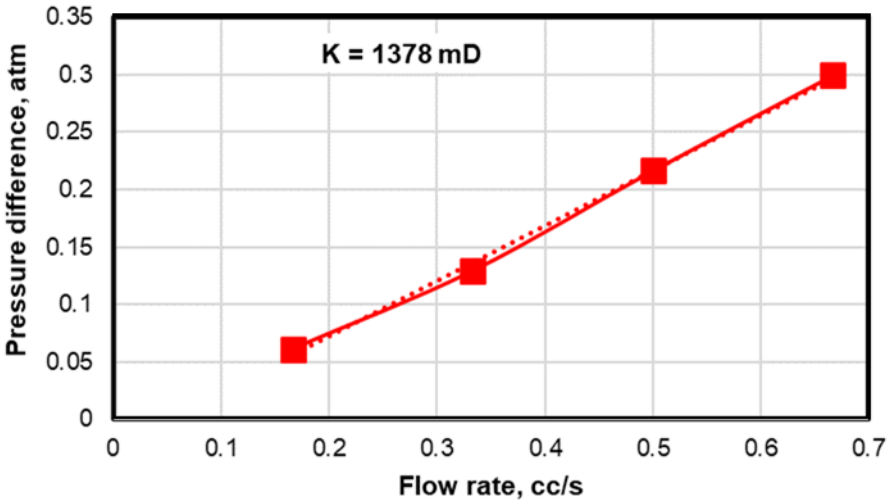

Figure 4-9. **Rock class 3: permeability assessment for sample T34. This plot shows the detected flow rate at different levels of pressure difference applied to the core sample. 3 wt.% KCl brine is used to perform the flow experiments. Dot line is the slope which used to estimate permeability value**

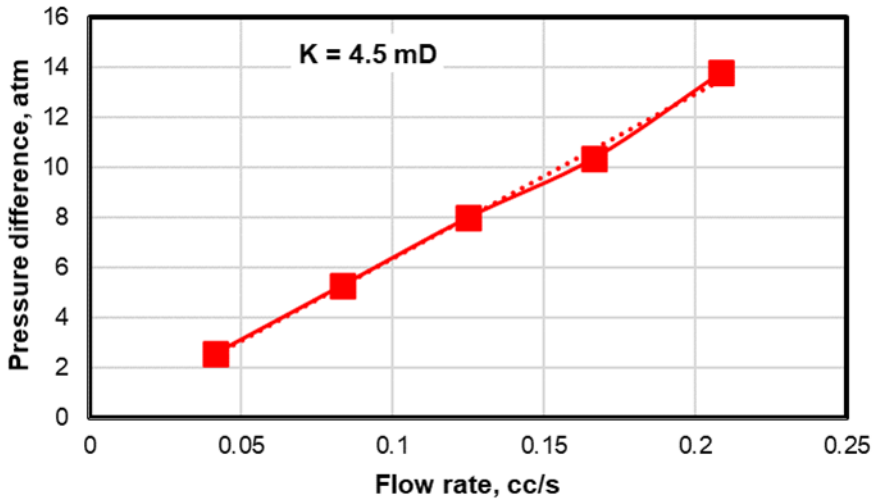

Figure 4-10. **Edwards rock class: permeability assessment for sample E14. This plot shows the detected flow rate at different levels of pressure difference applied to the core sample. 3 wt.% KCl brine is used to perform the flow experiments. Dot line is the slope which used to estimate permeability value**

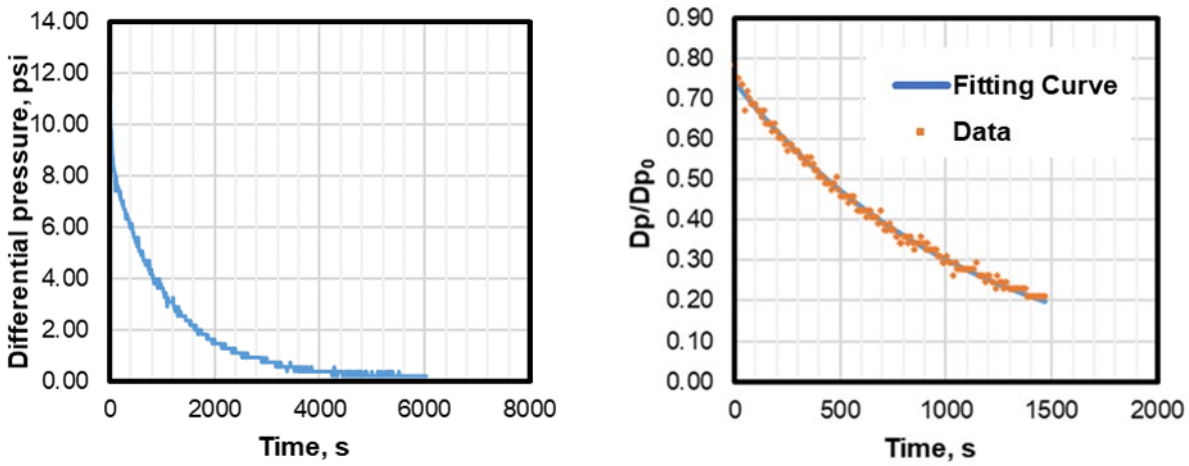

(a) (b)

Figure 4-11. **Rock class 4: (a) Differential pressure decay and (b) the normalized pressure decay as a function of time, used for permeability assessment in sample T41 via pulse-decay method. Dp is the pressure value and Dp_0 is the initial differential pressure.**

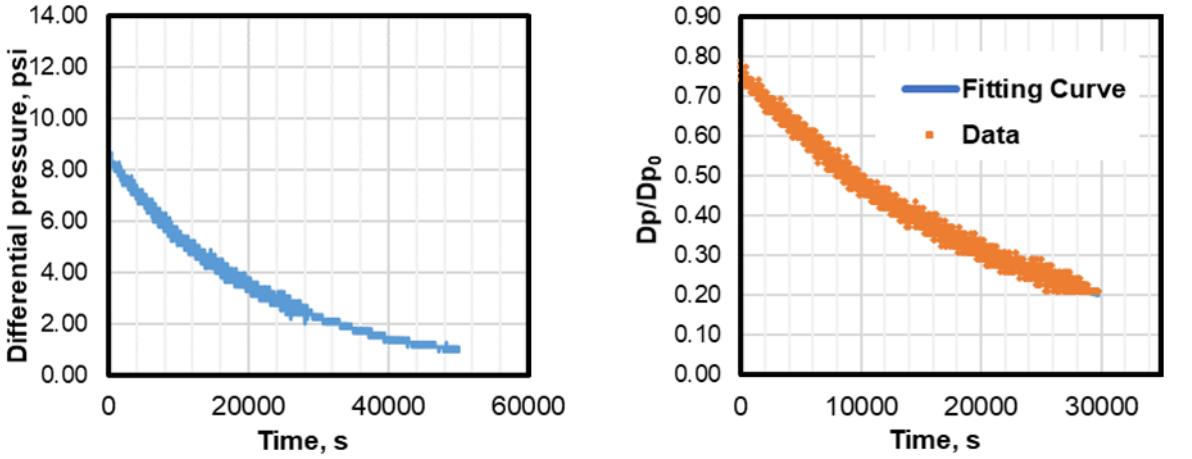

(a) (b)

Figure 4-12. Rock class 4: (a) Differential pressure decay and (b) the normalized pressure decay as a function of time, used for permeability assessment in sample T45 via pulse-decay method. Dp is the pressure value and Dp_0 is the initial differential pressure.

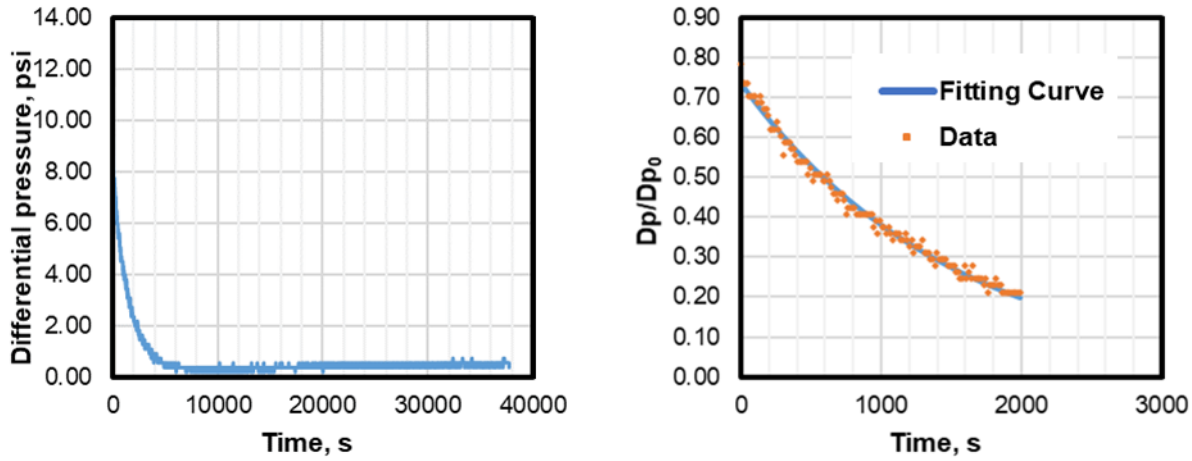

(a) (b)

Figure 4-13. Rock class 4: (a) Differential pressure decay and (b) the normalized pressure decay as a function of time, used for permeability assessment in sample T42 via pulse-decay method. Dp is the pressure value and Dp_0 is the initial differential pressure.

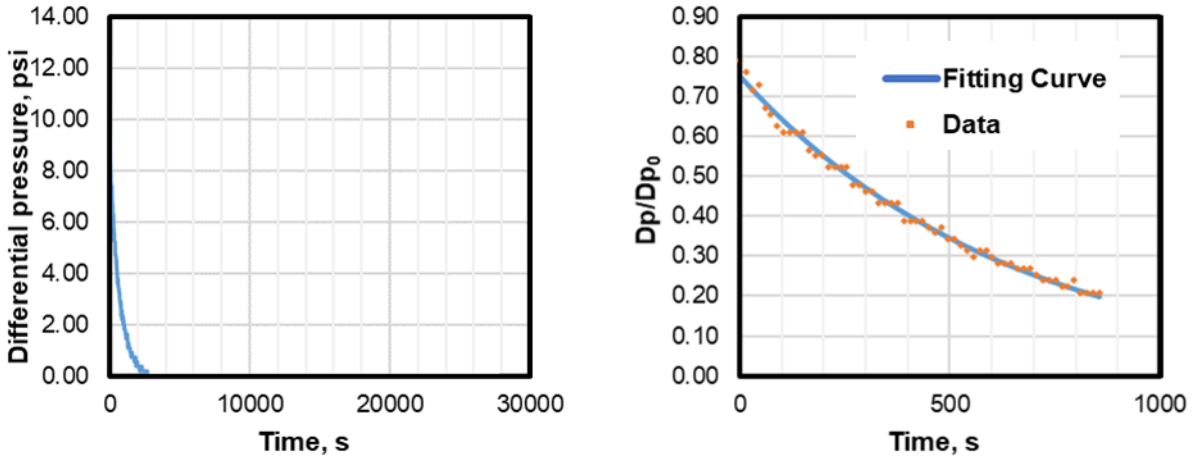

(a) (b)

Figure 4-14. Rock class 4: (a) Differential pressure decay and (b) the normalized pressure decay as a function of time, used for permeability assessment in sample T43 via pulse-decay method. Dp is the pressure value and Dp_0 is the initial differential pressure.

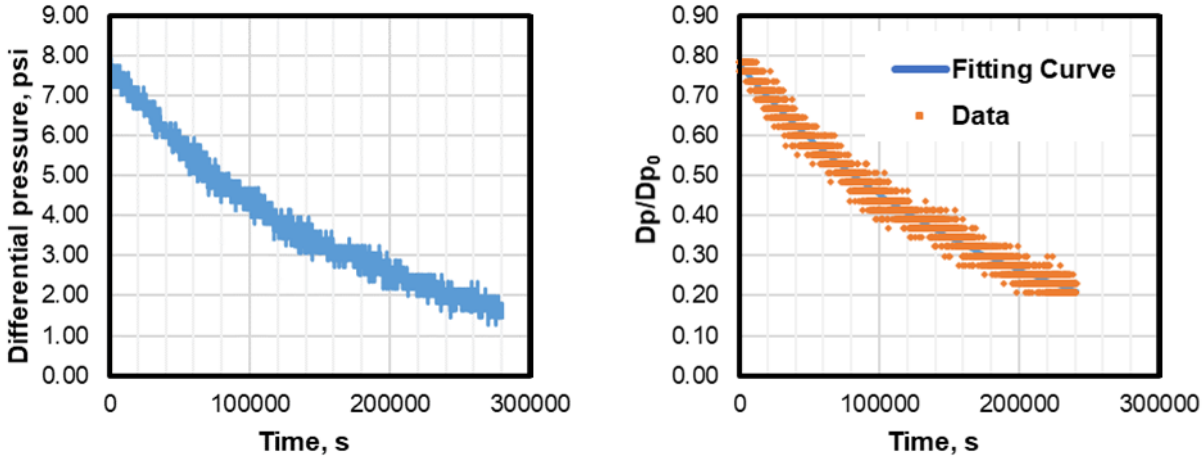

(a) (b)

Figure 4-15. Rock class 2: (a) Differential pressure decay and (b) the normalized pressure decay as a function of time, used for permeability assessment in sample T24 via pulse-decay method. Dp is the pressure value and Dp_0 is the initial differential pressure.

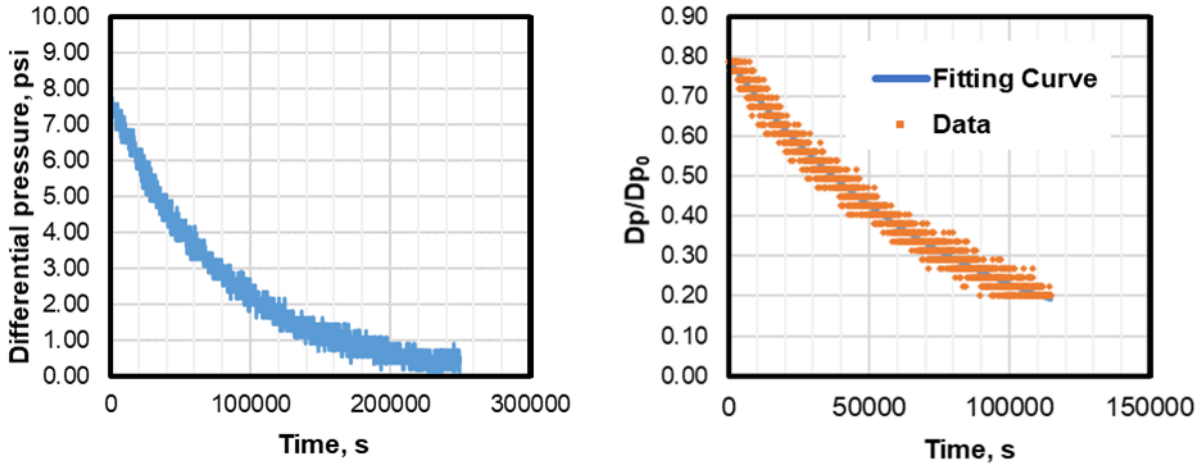

(a) (b)

Figure 4-16. Rock class 2: (a) Differential pressure decay and (b) the normalized pressure decay as a function of time, used for permeability assessment in sample T23 via pulse-decay method. Dp is the pressure value and Dp_0 is the initial differential pressure.

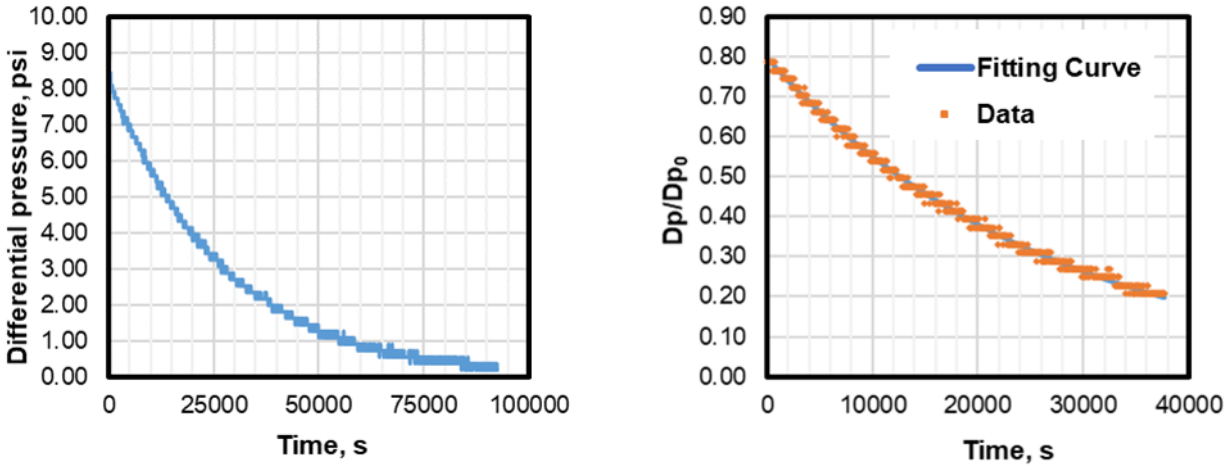

(a) (b)

Figure 4-17. Rock class 2: (a) Differential pressure decay and (b) the normalized pressure decay as a function of time, used for permeability assessment in sample T22 via pulse-decay method. Dp is the pressure value and Dp_0 is the initial differential pressure.

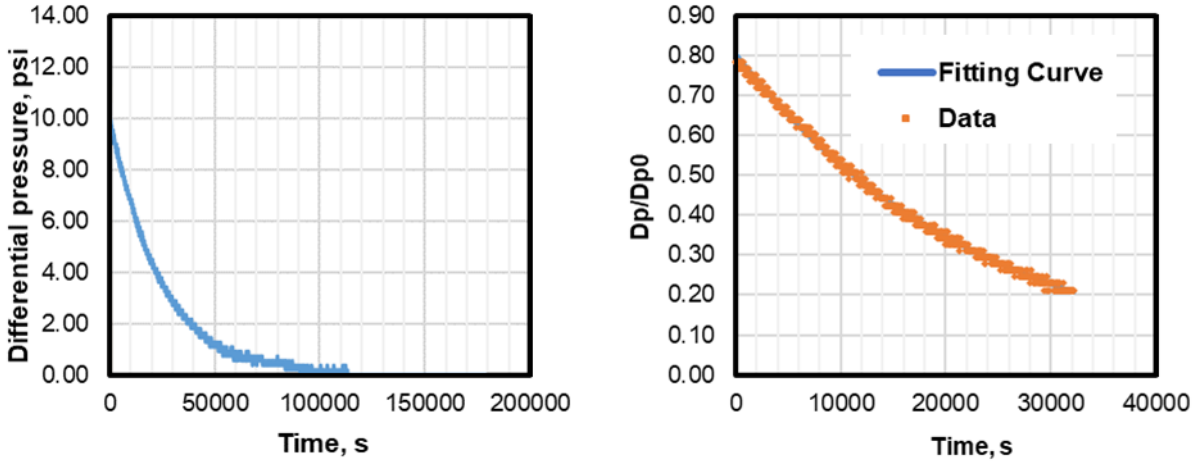

(a) (b)

Figure 4-18. Rock class 2: (a) Differential pressure decay and (b) the normalized pressure decay as a function of time, used for permeability assessment in sample T21 via pulse-decay method. Dp is the pressure value and Dp_0 is the initial differential pressure.

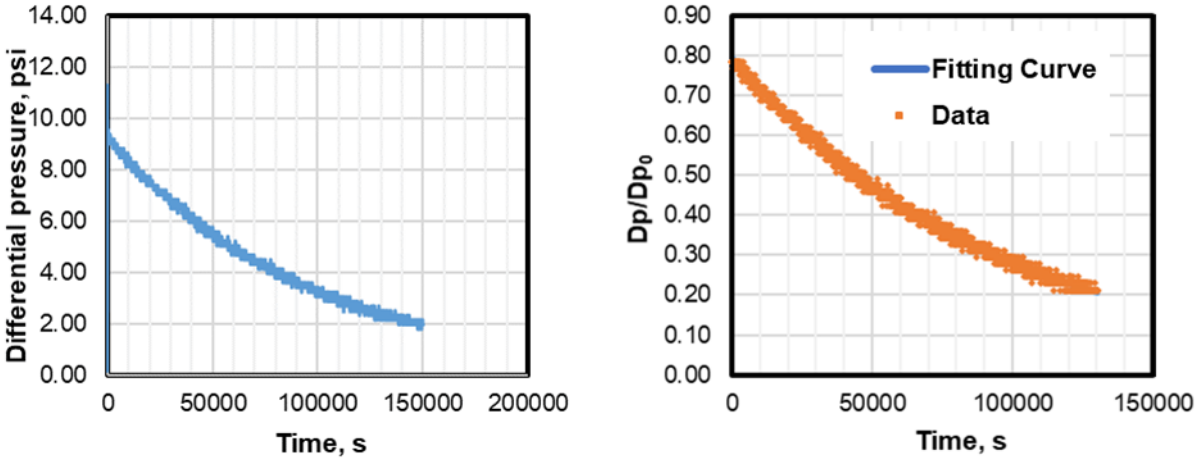

(a) (b)

Figure 4-19. Rock class 4: (a) Differential pressure decay and (b) the normalized pressure decay as a function of time, used for permeability assessment in sample T25 via pulse-decay method. Dp is the pressure value and Dp_0 is the initial differential pressure.

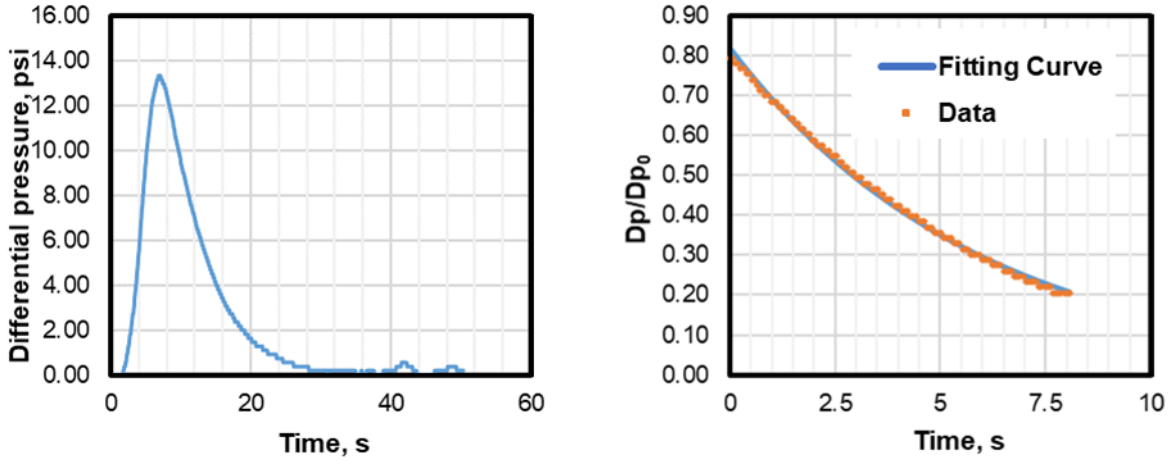

(a) (b)

Figure 4-20. Edwards rock class 4: (a) Differential pressure decay and (b) the normalized pressure decay as a function of time, used for permeability assessment in sample E11 via pulse-decay method. Dp is the pressure value and Dp_0 is the initial differential pressure.

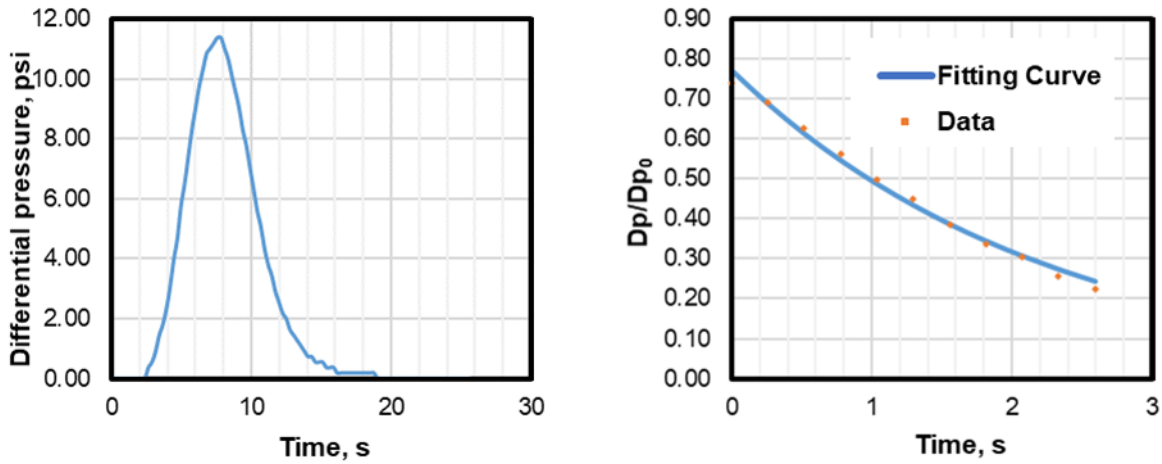

(a) (b)

Figure 4-21. Edwards rock class 4: (a) Differential pressure decay and (b) the normalized pressure decay as a function of time, used for permeability assessment in sample E12 via pulse-decay method. Dp is the pressure value and Dp_0 is the initial differential pressure.

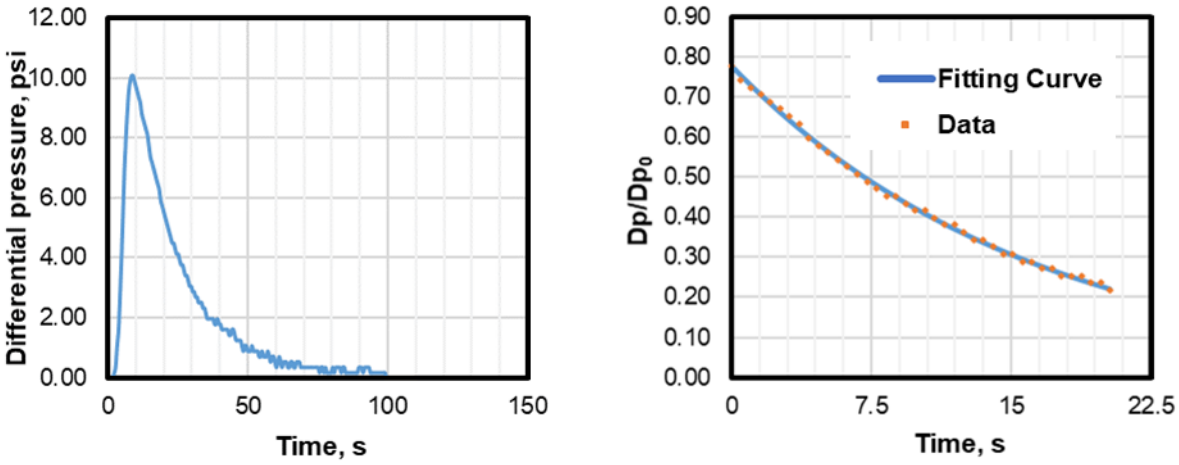

(a) (b)

Figure 4-22. Edwards rock class 4: (a) Differential pressure decay and (b) the normalized pressure decay as a function of time, used for permeability assessment in sample E13 via pulse-decay method. Dp is the pressure value and Dp_0 is the initial differential pressure.

4.2.2 NMR, electrical, and porosity measurements results

Figures 4-23 to 4-27 show NMR T_2 distribution in all the core samples as well as the corresponding magnetization decay measurements. The results of NMR measurements show a bi-modal behavior in NMR T_2 measurements in all Trinity rock classes except rock class 1. This bi-modal behavior is an indication of bi-modal pore-size distribution. rock classes 1, however, demonstrates a uni-modal pore-size distribution. It should be noted that in the case of rock class 3, although the samples were all taken from the same rock class, the clay content in the core samples vary significantly. That is the reason behind the significant difference in NMR T_2 distributions measured for rock samples taken in this rock class. It was not possible to take more core samples for analysis in this rock class.

Rock class 1 has porosity values ranging from 8% to 17%. Rock class 2 has very low porosity values ranging from 2% to 6%. Rock class 3 has porosity values ranging from 12% to 16%. Rock class 4 shows porosity values ranging from 6% to 18%, while Edwards rock class has porosity values ranging from 12% to 20%. Figure 4-28 to 4-32 show the formation factor versus porosity measurements for all rock classes. The formation factor was obtained from the electrical measurements while the porosity values were obtained from the NMR measurements on fully water-saturated rock samples. These plots are used to estimate the porosity component while Winsauer coefficient is assumed to be one. Table 4-3 lists the results of the porosity component estimates.

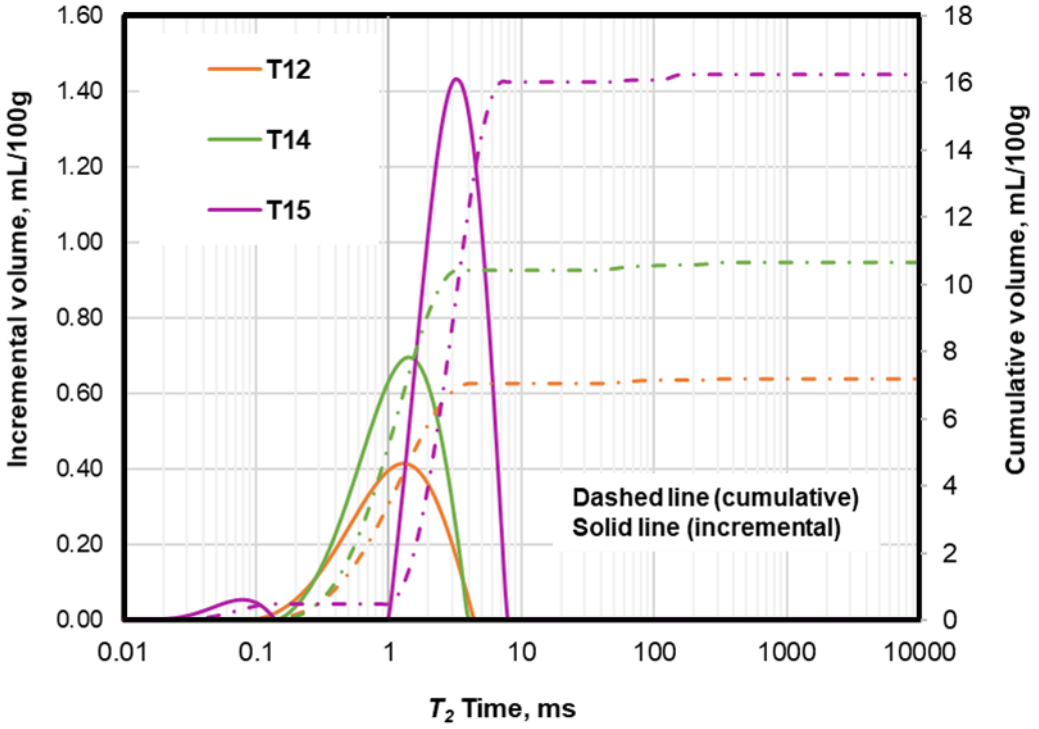

(a)

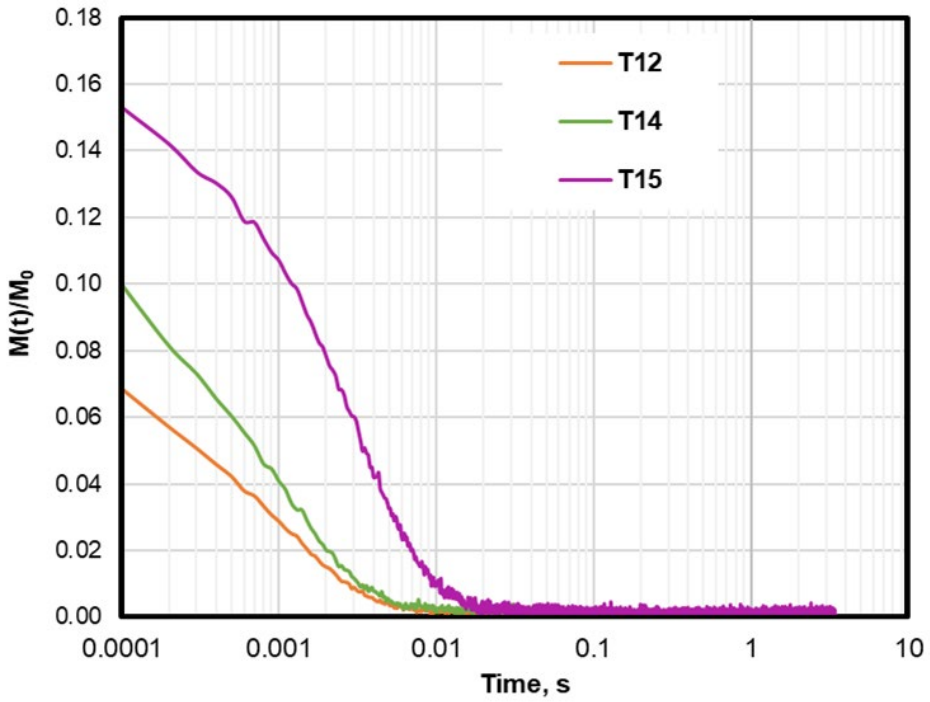

(b)

Figure 4-23. Rock class 1: (a) NMR T_2 distribution and (b) normalized magnetization decay measurements for core samples T15, T12, and T14. The rock samples are fully saturated with 3 wt.% KCl brine. Dashed and solid lines represent cumulative and incremental volume, respectively

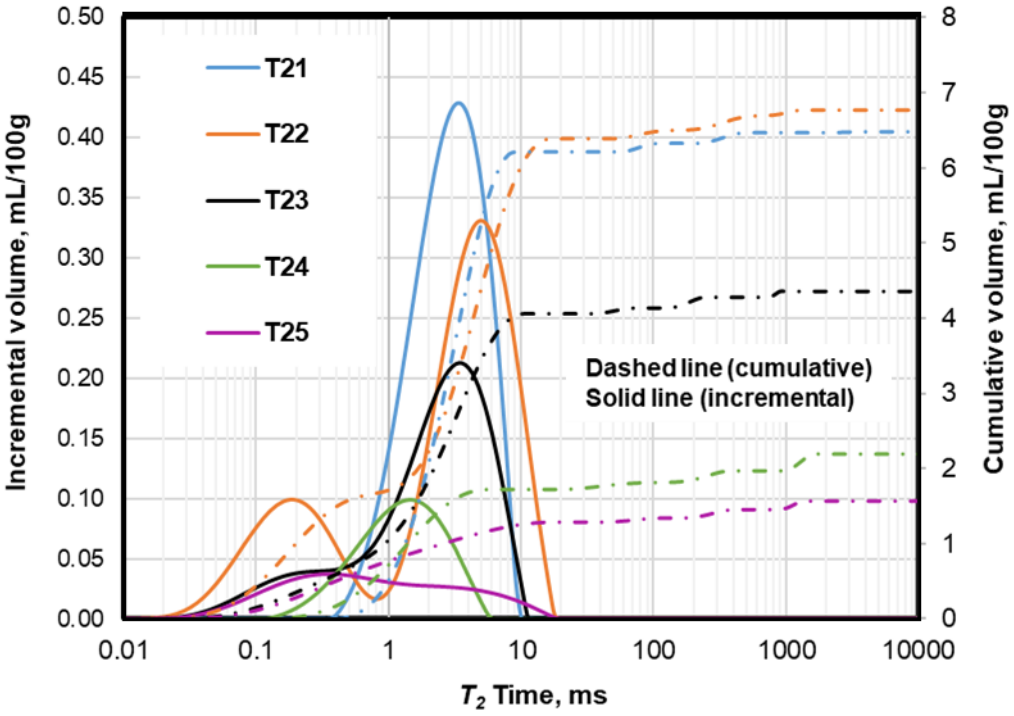

(a)

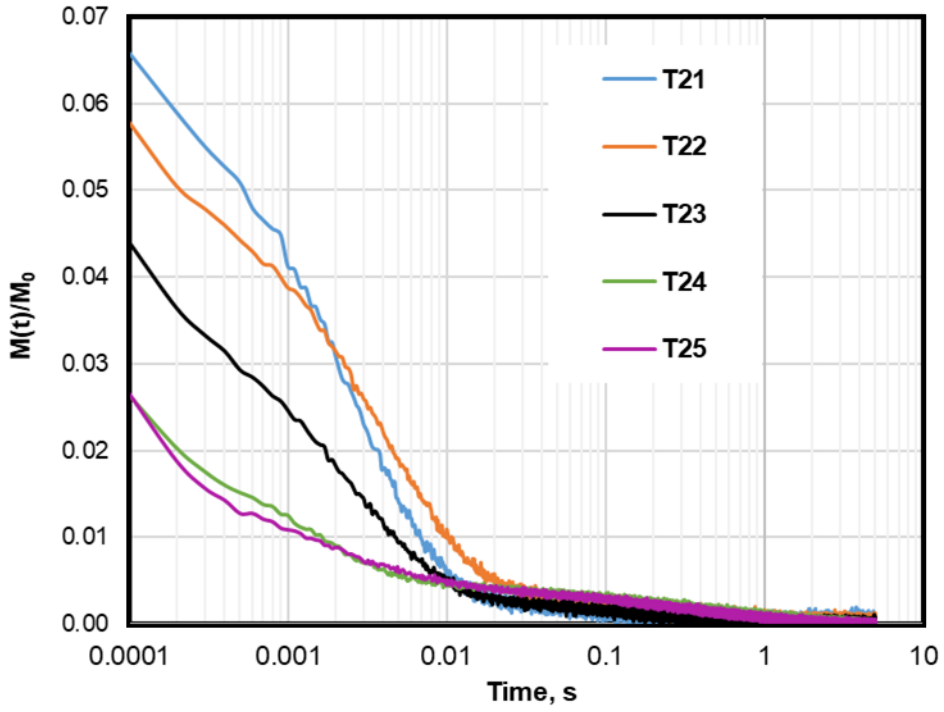

(b)

Figure 4-24. Rock class 2: (a) NMR T_2 distribution and (b) normalized magnetization decay measurements for core samples T21, T22, T23, T24 and T25. The rock samples are fully saturated with 3 wt.% KCl brine. Dashed and solid lines represent cumulative and incremental volume, respectively.

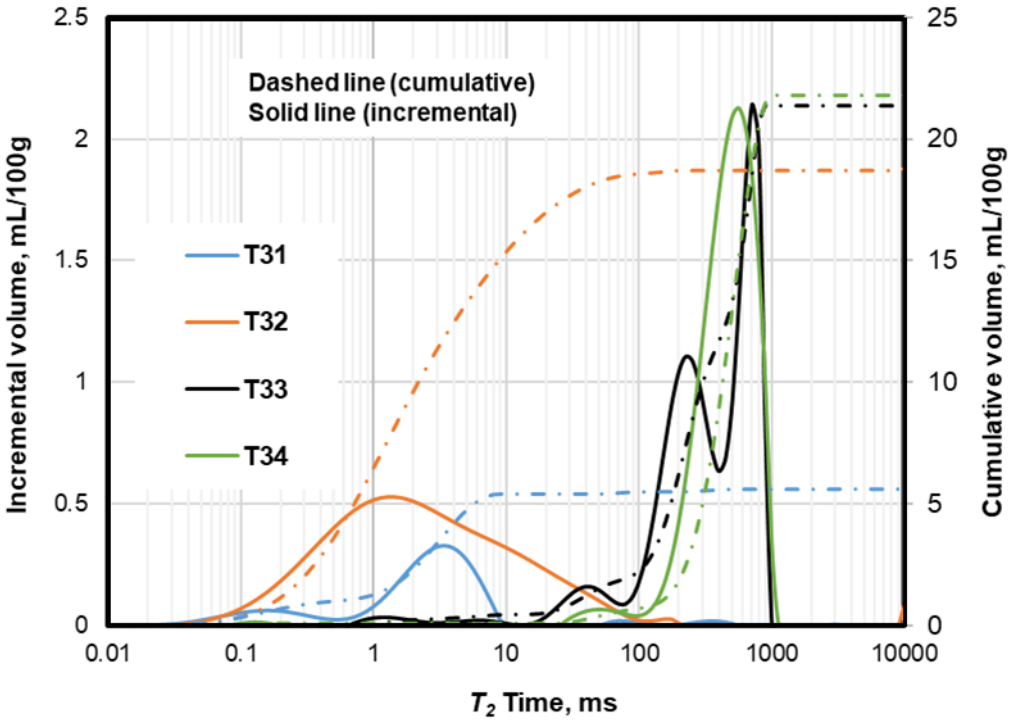

(a)

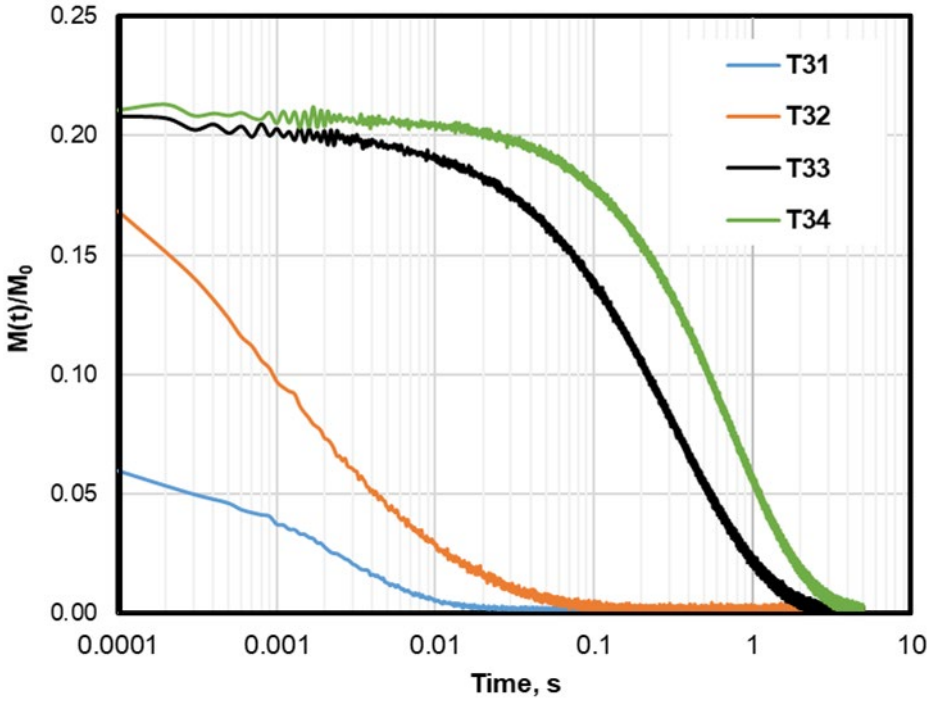

(b)

Figure 4-25. Rock class 3: (a) NMR T_2 distribution and (b) normalized magnetization decay measurements for core samples T31, T32, T33, and T34. The rock samples are fully saturated with 3 wt.% KCl brine. Dashed lines and solid lines represent cumulative and incremental volume, respectively.

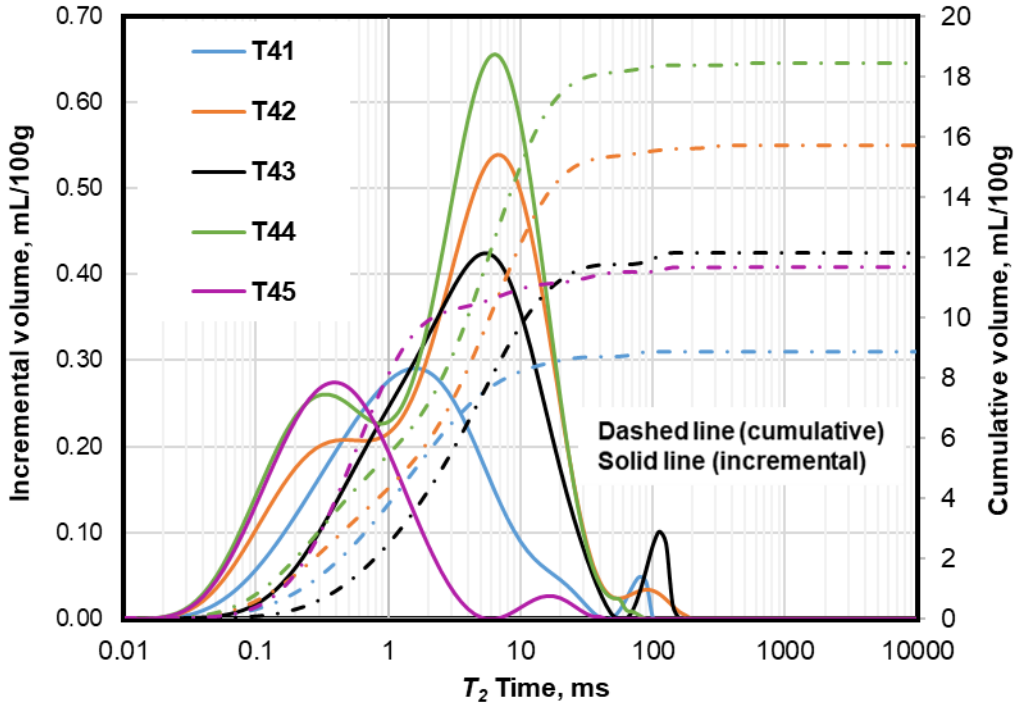

(a)

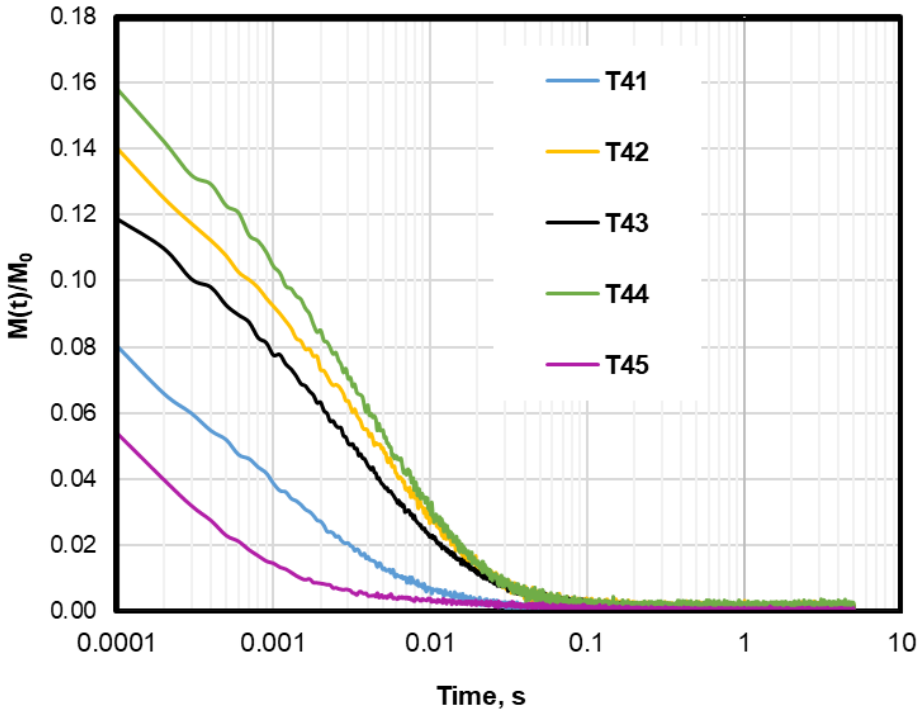

(b)

Figure 4-26. **Rock class 4: (a) NMR T_2 distribution and (b) normalized magnetization decay measurements for core samples T41, T42, T43, T44, and T45. The rock samples are fully saturated with 3 wt.% KCl brine. Dashed and solid lines represent cumulative and incremental volume, respectively.**

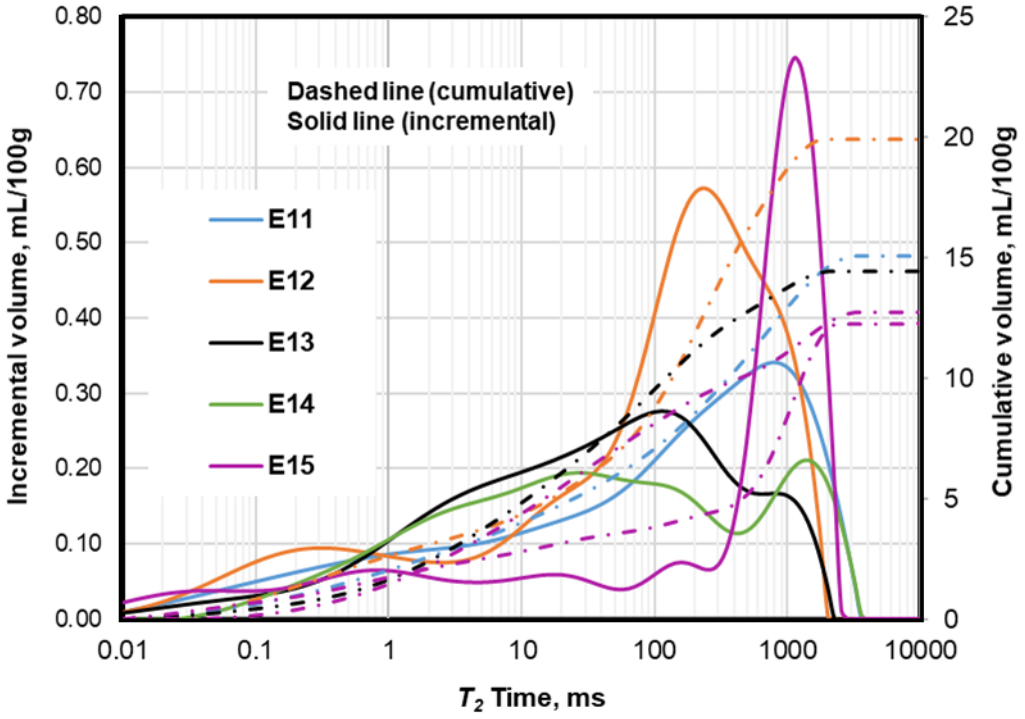

(a)

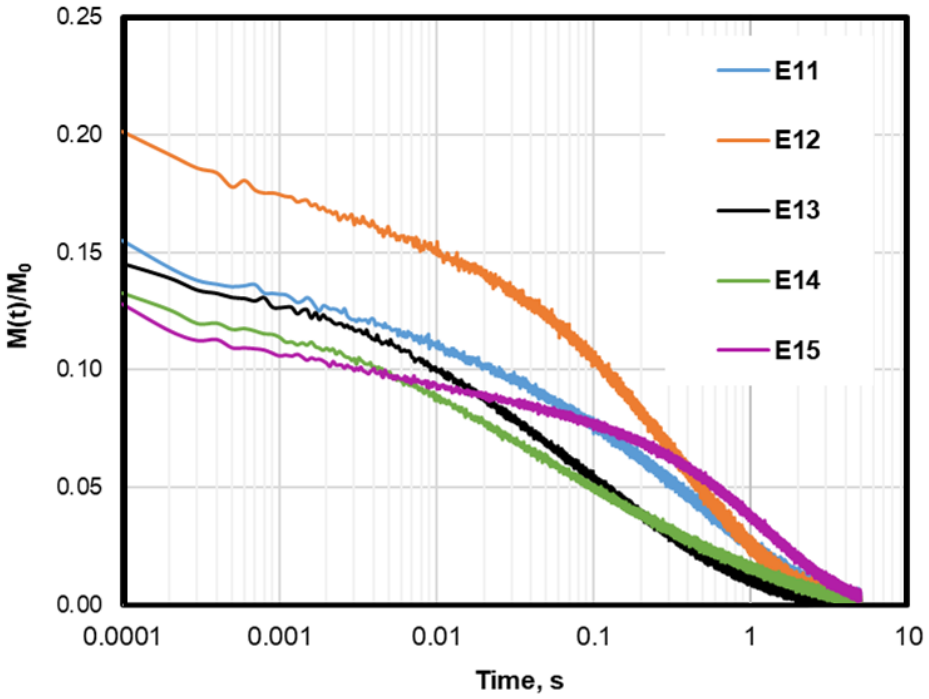

(b)

Figure 4-27. Edwards rock class: (a) NMR T_2 distribution and (b) normalized magnetization decay measurements for core samples E11, E12, T13, and E14. The rock samples are fully saturated with 3 wt.% KCl brine. Dashed and solid lines represent cumulative and incremental volume, respectively.

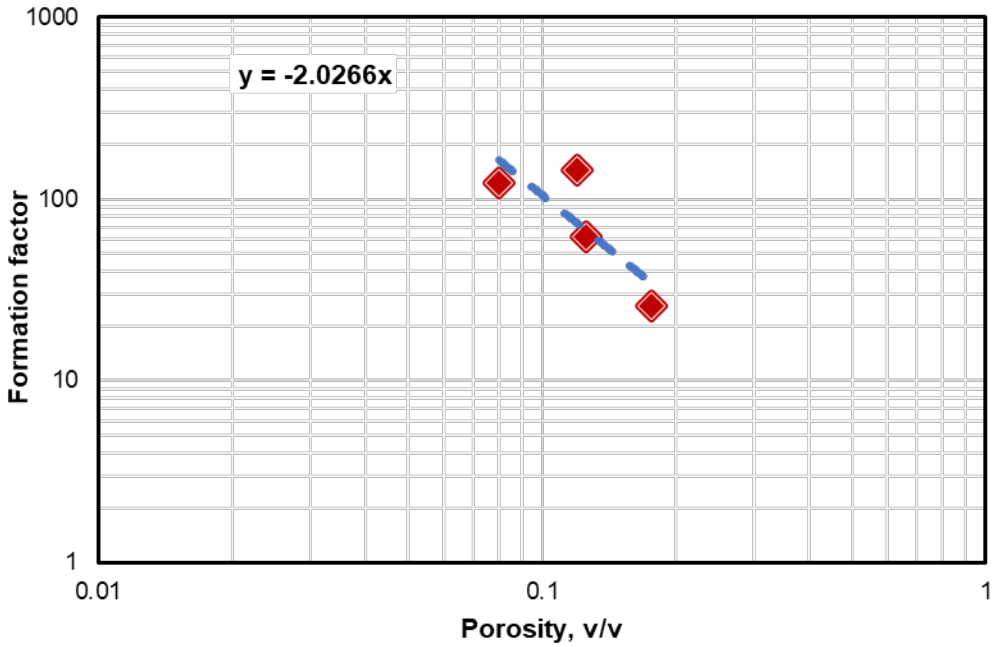

Figure 4-28. **Rock class 1: formation factor versus porosity measurements, used for assessment of porosity exponent in Archie's equation. Dot line is the slope which used to estimate porosity exponent value.**

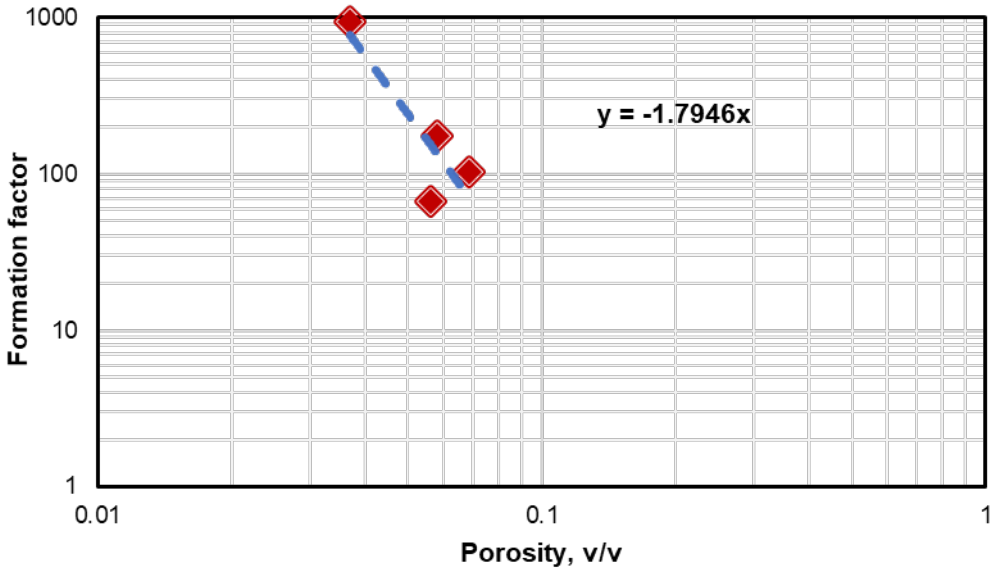

Figure 4-29. **Rock class 2: formation factor versus porosity measurements, used for assessment of porosity exponent in Archie's equation. Dot line is the slope which used to estimate porosity exponent value.**

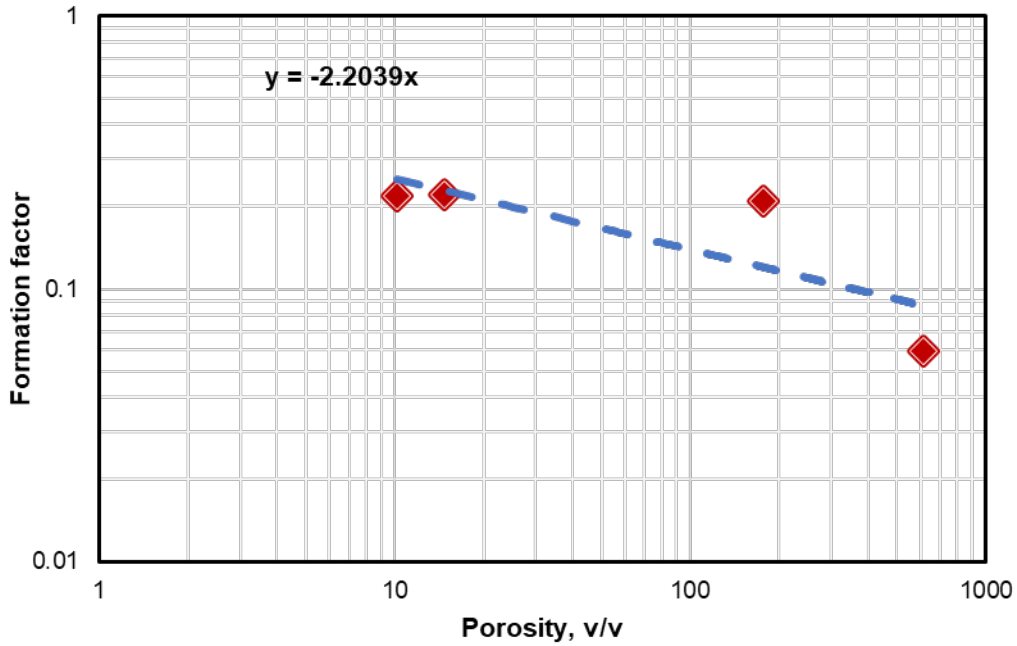

Figure 4-30. **Rock class 3: formation factor versus porosity measurements, used for assessment of porosity exponent in Archie's equation. Dot line is the slope which used to estimate porosity exponent value.**

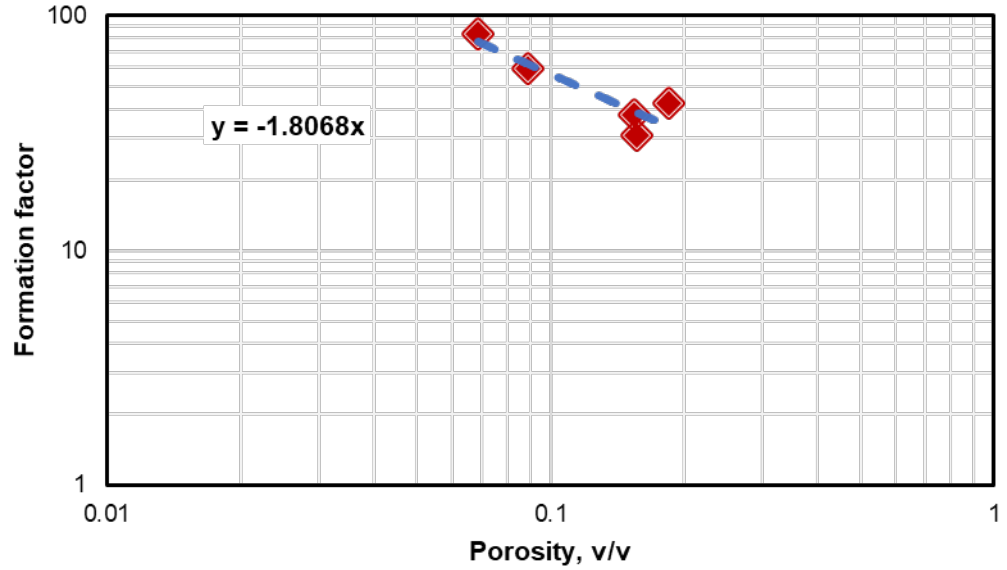

Figure 4-31. **Rock class 4: formation factor versus porosity measurements, used for assessment of porosity exponent in Archie's equation. Dot line is the slope which used to estimate porosity exponent value.**

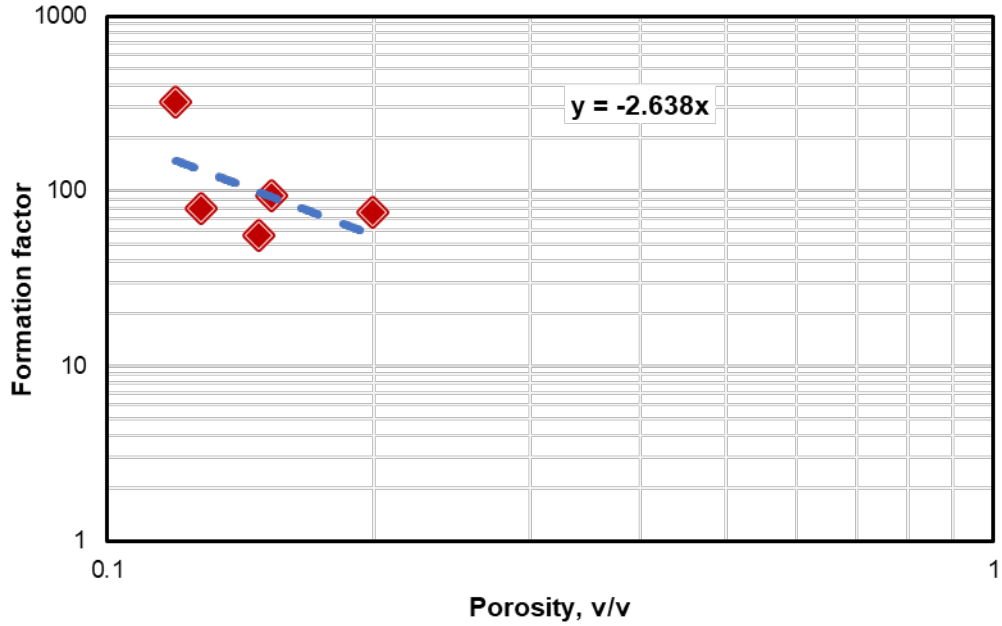

Figure 4-32. Edwards rock class: formation factor versus porosity measurements, used for assessment of porosity exponent in Archie's equation. Dot line is the slope which used to estimate porosity exponent value.

4.2.3 Summary of the Results

Table 4-3 shows a summary of the measurements obtained for all core samples for porosity, permeability, and electrical measurements.

Table 4-3. Summary of the results.

Core ID	Porosity (%)	*a*	*m*	Permeability (mD)
T11	12.0	1	2.027	damaged
T12	7.0	1	2.027	damaged
T13	12.6	1	2.027	damaged
T14	10.7	1	2.027	damaged
T15	16.2	1	2.027	damaged
T21	6.5	1	1.790	0.0021
T22	6.8	1	1.790	0.002
T23	4.4	1	1.790	0.0006
T24	2.1	1	1.790	0.082
T25	1.6	1	1.790	0.00048
T31	5.6	1	2.204	0.017
T32	18.8	1	2.204	7
T33	21.4	1	2.204	440
T34	21.8	1	2.204	1378

T41	8.9	1	1.807	0.046
T42	15.7	1	1.807	0.043
T43	15.4	1	1.807	0.096
T44	18.5	1	1.807	damaged
T45	6.9	1	1.807	0.0028
E11	15.3	1	2.638	4.59
E12	19.9	1	2.638	6.12
E13	14.8	1	2.638	1.89
E14	12.7	1	2.638	4.5
E15	11.9	1	2.638	damaged

5 Numerical simulation of well logs

This section comprises multiple synthetic models, water salinity estimation methods, total dissolved solids (TDS) correlations, and the Edwards-Trinity Plateau well logs models. The synthetic models intend to explain the methodology employed for creating the earth models and simulating the well logs. This part of the report also shows the benefits of the numerical simulation of well logs, and a sensitivity analysis for different water salinity estimation methods and electrical resistivity tools. The well logs models show the simulation results for the available well logs in the Edwards-Trinity Plateau in West Texas. These results enable the estimation of water salinity and total dissolved solids using reliable numerical simulation models.

To perform the well logs simulations, we employ UTAPWeLS, which is a numerical simulator capable of reproducing the various post-processing methods and configurations of the commercial tools used to acquire electrical logs (Voss et al., 2009). This powerful software enables the generation of multi-layer models, honoring all petrophysical properties and available measurements. These models are referred as earth models since they comprise the physics related to rock and fluid dynamics. The numerical simulator also permits modeling the mud-filtrate invasion process. Indeed, UTAPWeLS renders fully reliable petrophysical models to reproduce the well logs responses and provides a remarkable tool for formation evaluation purposes.

5.1 Water salinity estimation methods

Formation water salinity is a key parameter for formation evaluation success. However, its assessment is not trivial and its significance is often underestimated. In aquifers, formation water salinity is a crucial property for classifying and monitoring water quality. This section presents basic information for several water salinity estimation methods, such as Archie's equation, Pickett plot, resistivity ratio, and spontaneous potential (SP) log. Most of the methods focus on computing formation water electrical resistivity (R_w) as a function of salt concentration and temperature (T), assuming clean aquifers to avoid the effect of clays on conductivity. In addition, if we assume that sodium chloride (NaCl) is the only salt dissolved in the formation water, we can use equations 1 and 2 to convert the electrical

resistivity of water to salt concentration ([$NaCl_{ppm}$]).

$$R_w = \left(0.0123 + \frac{3647.5}{[NaCl_{ppm}]^{0.955}}\right)\left(\frac{81.77}{T+6.77}\right) \quad \text{..... (1)}$$

$$[NaCl_{ppm}] = 10^{\left\{\frac{3.562 - log_{10}\left[R_w\left(\frac{T+6.77}{81.77}\right) - 0.0123\right]}{0.955}\right\}} \quad \text{..... (2)}$$

5.1.1 Archie's equation

Archie's equation assumes a clean matrix and a fully saturated reservoir to calculate formation electrical resistivity (R_t) (Archie, 1942). This famous equation considers the relation between R_t, R_w, water saturation (S_w) and formation total porosity ($\emptyset$), and it uses three fitting parameters known as the tortuosity factor (a), the cementation exponent (m), and the saturation exponent (n). equation 3 presents Archie's equation for computing formation electrical resistivity.

$$R_t = R_w \left[\frac{a}{\emptyset^m}\right]\frac{1}{S_w^n} \quad \text{..... (3)}$$

Since we are dealing with aquifers, we assume a fully water saturated reservoir with $S_w = 1$; therefore, the n-exponent is not significant in our calculations. If we divide equation 3 by R_w, we obtain an expression depending on formation porosity, tortuosity and cementation. This expression, available in equation 4, is known as formation factor (F) (Archie, 1942).

$$F = \frac{R_t}{R_w} = \frac{a}{\emptyset^m} \quad \text{..... (4)}$$

Solving equation 4 for R_w, we obtain equation 5 to determine formation water resistivity as a function of total porosity and the formation factor. As mentioned, we can input the calculated R_w into equation 2 to estimate formation water salinity.

$$R_w = R_t \left[\frac{\emptyset^m}{a}\right] = \frac{R_t}{F} \quad \text{..... (5)}$$

In order to use Archie's equation to assess formation water salinity, we require to estimate R_t, $\emptyset$, a and m (Archie, 1942). Using UTAPWeLS simulator we can develop synthetic models controlling the formation electrical resistivity and the formation factor. For field cases, we can model the formation resistivity and porosity using the available well logs, and we can use the results of the core electrical measurements to determine the m-exponent. For both synthetic and field cases we assume a = 1.

5.1.2 Pickett plot

This graphical method employs the logarithmic relation of formation resistivity (log[R_t]) and porosity (log[$\emptyset$]) to linearize Archie's equation and compute R_w by fitting the slope of the line, which is equal to the m-exponent (Pickett, 1966). Equation 6 presents the

logarithmic relation of Archie's equation used by the Pickett plot method.

$$log(R_t) = log(aR_w) - mlog(\emptyset) \quad \text{..... (6)}$$

We can utilize the Picket plot method using the formation resistivity and porosity data extracted from the well logs or computed by UTAPWeLS after simulating these electrical logs. Since we are assuming a = 1, we can read the values of R_w and m (slope) directly from the graph, as shown in Figure 5-1.

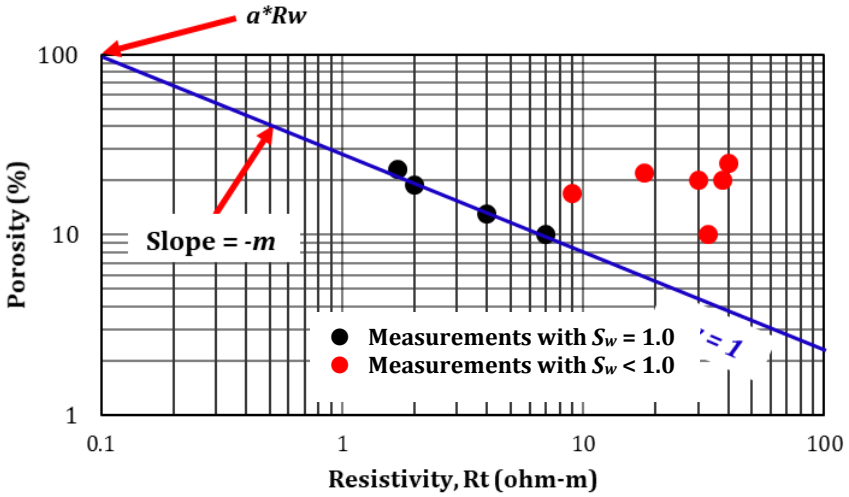

Figure 5-1. **Pickett plot method (Picket, 1966). Logarithmic plot of total porosity vs formation resistivity. The black dots show the log or core measurements in fully water saturated samples, and the red dots show the log or core measurements in samples where water saturation fraction is less than 1.0. The slope formed by the linear trend of the log or core measurements in fully water saturated samples (S_w = 1) suggests the value of the m-exponent. The extrapolation of this line towards the y-axis provides an estimation of R_w.**

5.1.3 Resistivity ratio

The resistivity ratio method serves to estimate formation water salinity for invaded formations. In permeable beds, mud-filtrate invades the near-wellbore region and changes the formation electrical resistivity of the invaded zone (R_{xo}). Resistivity tools measure the electrical resistivity of the formation at different distances from the wellbore and typically offer a deep sensing resistivity, a medium sensing resistivity and a shallow sensing resistivity. Therefore, the deep, medium, and shallow electrical resistivity logs exhibit differing values under the presence of mud-filtrate invasion. Under these circumstances it is common to assume that the deep and shallow resistivities provide reliable values for R_t and R_{xo} because the deep resistivity log senses only the virgin formation resistivity and the shallow resistivity log senses the fully invaded formation resistivity. Nevertheless, the complexity of mud-filtrate invasion mechanisms renders a challenging characterization of the invaded region and uncertainties in water salinity estimations.

In order to implement the resistivity ratio method, Archie's equation could be modified to estimate the electrical resistivity of the invaded zone using the following equations.

$$R_{xo} = R_{mf}\left[\frac{a}{\emptyset^m}\right]\frac{1}{S_{xo}^n} \quad \text{..... (7)}$$

$$F = \frac{R_t}{R_w} = \frac{a}{\emptyset^m} = \frac{R_{xo}}{R_{mf}} \quad \text{..... (8)}$$

where R_{mf} is the mud-filtrate electrical resistivity and S_{xo} is the water saturation of the invaded region, which is assumed as 1 for water-base mud-filtrate invading an aquifer. Solving for R_w in equation 8 and using the concept of formation factor, we obtain an expression for formation water resistivity using the deep sensing and the shallow sensing resistivities and the mud-filtrate resistivity at formation temperature.

$$R_w = \frac{R_t}{R_{xo}} R_{mf} \quad \text{..... (9)}$$

5.1.4 Spontaneous potential (SP) log

The spontaneous potential log measures the electrical potential generated from the salinity contrast between formation water and water-base mud-filtrate. This log is useful to estimate water salinity under the adequate circumstances, which are permeable and clean formations with notable differences in salt concentration between drilling mud-filtrate and formation water.

The SP method utilizes equations 10 to 12 to directly estimate the formation water salinity from SP log measurements. First, the permeable bed is located with the deflection of the SP log from a constant SP value encounter in pure shales. The SP value for pure shales represents the shale baseline, denoted as SP_{shale}. The SP value at the center of the permeable bed can be used as the input SP_{log} in equation 10 to calculate the static spontaneous potential (*SSP*).

$$S\text{SP} = \text{SP}_{log} - SP_{shale} \quad \text{..... (10)}$$

Similarly, an experimental equation defines the *SSP* as a function of formation water and mud filtrate salt concentrations at reservoir temperature. These salt concentrations are denoted as C_w and C_{mf}, respectively. Equation 11 presents the experimental expression for *SSP*, showing a relation with salt concentration in formation water and mud-filtrate and using a constant (K_{SP}) that depends on ion mobility and temperature. The empirical constant K_{SP} is approximately 71 mV. Equation 11 allows solving for C_w and computing the formation water salinity using equation 12.

$$SSP = -K_{SP} log_{10}\left(\frac{C_w}{C_{mf}}\right) \quad \text{..... (11)}$$

$$C_w = C_{mf} 10^{-SSP/K_{SP}} \quad \text{..... (12)}$$

5.2 Synthetic models: Base case

Using UTAPWeLS, we construct various multi-layer models to visually demonstrate the capabilities of the numerical simulations of well logs for different lithologies and formation water salinities. We select limestone, dolomite and sandstone as the aquifer lithologies for these synthetic examples because they are the dominant lithologies in the Edwards-Trinity Plateau aquifers. Shoulder-bed effects and mud-filtrate invasion alter the response of electrical resistivity logs. A set of synthetic cases enable the estimation of water salinity using the methods explained in the previous section and the comparison of induction and laterolog resistivity tools.

5.2.1 Assumptions

The synthetic models are clean, isotropic, and fully water saturated reservoirs. The borehole diameter is 12.25 in (wellbore radius = 0.5104 ft). Table 5-1 summarizes the input parameters for the synthetic model base case. Archie's equation serves to calculate electrical resistivities, assuming a and m have a value of 1 and 2, respectively. We assume that NaCl is the only salt dissolved in the formation water. The mud-filtrate salinity is 3,000 ppm NaCl. We simulate mud-filtrate invasion with an overbalance pressure of 400 psi at 750 ft for a period of 3 days. Mudcake porosity, permeability, and thickness are 0.35, 0.03 md, and 0.4 in, respectively. For invasion simulation purposes, we employ a radial grid with 30 blocks evenly distributed with a geometric expansion to reproduce a reservoir with an external radius of 200 ft.

The previously described assumptions serve as input parameters for the base case model. The base case enables a sensitivity analysis using alternative synthetic cases developed to investigate the effects of mud-filtrate invasion radius and formation factor uncertainties in the estimation of formation water salinity. For these cases, we assume variable invasion time to obtain a variable invasion radius and electrical resistivity profile in the invaded zone. We assess formation factor varying total porosity and m-exponent. In their corresponding sections, we provide further details for the assumptions and changes applied on these synthetic cases.

Table 5-1. Input parameters for the synthetic model base case.

Layer	Depth (ft)	Lithology	k (md)[a]	ϕ[b]	T (°F)[c]	Salinity (ppm NaCl)[d, e]
1	500	Shale	0.001	0.25	79.23	100,000
2	525	Dolomite	300	0.15	80.03	1,000
3	575	Shale	0.001	0.25	80.47	100,000
4	600	Sandstone	300	0.15	80.91	3,000
5	650	Shale	0.001	0.25	81.34	100,000
6	675	Limestone	300	0.15	81.71	9,000
7	725	Shale	0.001	0.25	82.14	100,000

Note: All depths are top-layer's depth. We consider a normal geothermal gradient of 0.95 °F/100ft, similar to the temperatures encounter in West Texas wells and aquifers evaluated in the simulation studies, and in agreement with the geothermal gradients reported by Blanchard (1970). The range of formation water salinity responds to the observations and results encounter in the well logs simulations for the Edwards-Trinity Plateau.

[a] k = formation permeability.

[b] $\emptyset$ = total porosity.
[c] T = reservoir temperature.
[d] ppm = parts per million.
[e] NaCl = sodium chloride.

5.2.2 Model initialization

We construct the earth model using three aquifers of dolomite, sandstone, and limestone located in layers 2, 4, and 6, respectively, and bounded by sealing shales in layers 1, 3, 5, and 7, respectively. We input the parameters described in Table 5-1, using variable formation water salinities for the three synthetic aquifers and computing formation temperature using a geothermal gradient of 0.95 °F/100ft analogous to the temperature gradient of West Texas aquifers in the study area and in agreement with Blanchard (1970). These information enables the calculation of bulk nuclear properties and electrical resistivities using Archie's equation. Since porosity and the m-exponent are constant, the formation resistivity depends exclusively on formation water salinity.

After computing key petrophysical properties in the earth model, we simulate triple combo well logs. For electrical resistivities, we simulate induction and laterolog tools responses. Figure 5-2 shows the base case synthetic model results before invasion, which serves to illustrate the methodology for simulating all well logs in the project using UTAPWeLS.

Using the base case synthetic data, we apply Archie's equation to estimate formation water salinity. We read the values from the center of the deep resistivity curve. Table 5-2 compares the simulation results with the Archie's equation method for induction log (IL) and laterolog (LL). We can infer that the reliability of both resistivity tools increases as formation water salinity increases. However, induction log offers less uncertainty in the electrical resistivity measurements than laterolog. Since we are not considering mud-filtrate invasion and mud-filtrate properties, we cannot implement the resistivity ratio and SP methods during this model initialization. In addition, a constant porosity halts the application of the Pickett plot, where a wide range of porosity values and multiple data points is required to properly employ this graphical method.

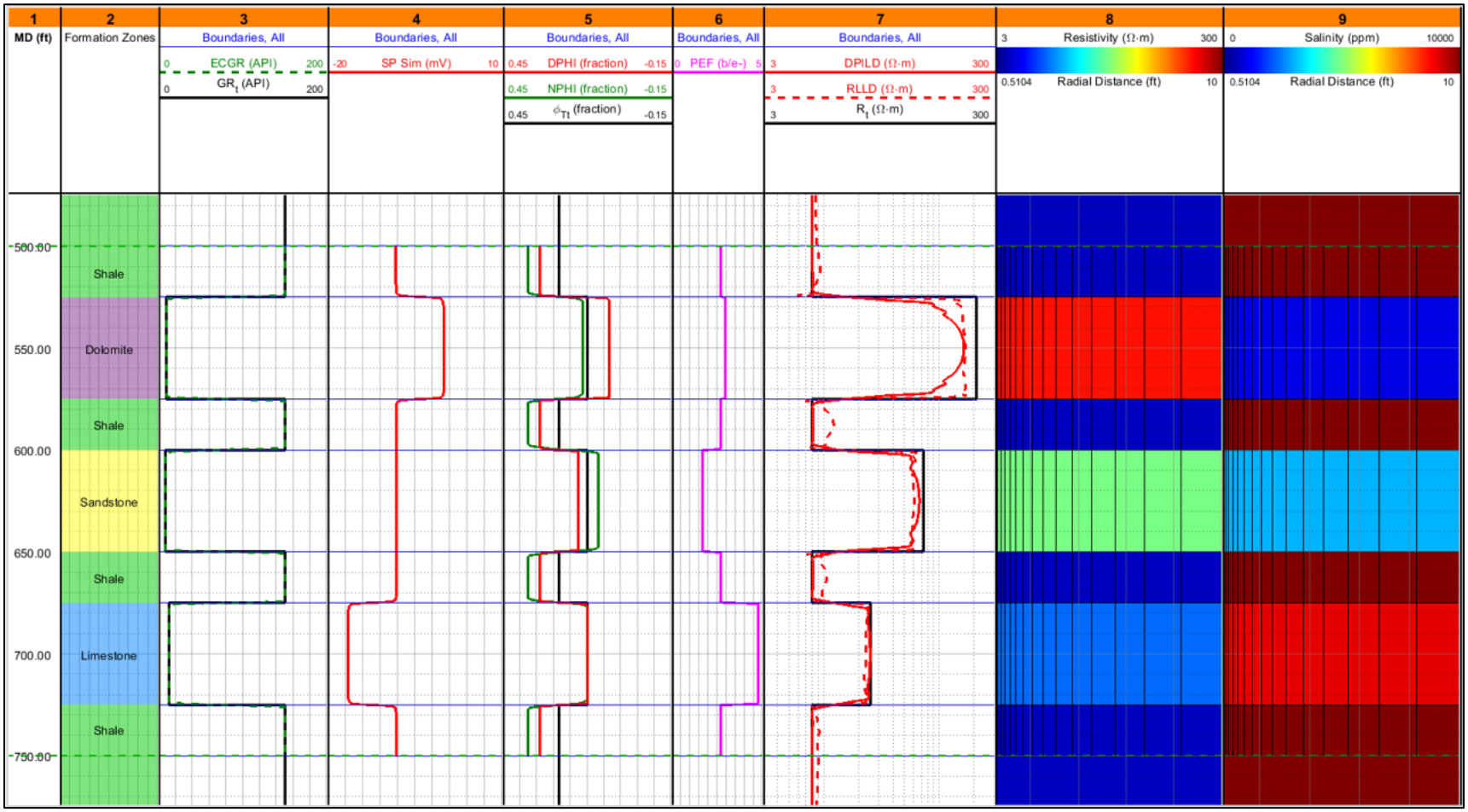

Figure 5-2. **Synthetic model initialization and base case results without mud-filtrate invasion. Track 1 presents the measured depth in ft. Track 2 presents the formation lithology with shale in green, dolomite in purple, sandstone in yellow and limestone in light blue. Track 3 presents the gamma ray curves for the earth model in black and the simulated log in dash green. Track 4 presents the spontaneous potential simulated log in red. Track 5 presents the earth model total porosity in black, the simulated density log in red, and the neutron simulated log in green. Track 6 presents the photoelectric factor simulated log in magenta. Track 7 presents the earth model formation resistivity in black, the deep induction simulated log in red, and the deep laterolog simulation in dash red. Tracks 8 and 9 present the vertical cross-section color map for formation resistivity and formation water salinity. The blue horizontal lines in tracks 2 to 7 represent the layer boundaries.**

Table 5-2. Results for various formation water salinity estimation methods for the base case before simulating mud-filtrate invasion.

Method	T (°F) [a]	R_w [b]	Salinity (ppm NaCl) [c, d]	Error (%)
Simulation	80.03	4.7005	1,000	0.0
	80.91	1.6372	3,000	0.0
	81.71	0.5756	9,000	0.0
Archie's Equation IL [e]	80.03	3.7125	1,281	28.1
	80.91	1,5075	3,273	9.1
	81.71	0.5625	9,224	2.5
Archie's Equation LL [f]	80.03	3.7800	1,257	25.7
	80.91	1.3725	3,614	20.5
	81.71	0.5175	10,084	12.0

Note: Error calculation assumes input formation water salinity as the true formation water salinity. Archie's equation method assumes total porosity, *a* and *m* exponents as constants according to information available in Table 5-1, and it uses the deep resistivities readings from the center of the curve of the simulated logs.

[a] T = reservoir temperature.

[b] R_w = Formation water resistivity.

[c] ppm = parts per million.

[d] NaCl = sodium chloride.

[e] IL = induction resistivity log.

[f] LL = laterolog electrical resistivity.

5.2.3 Base case results

Figure 5-3 displays the base case results. Table 5-3 presents the data for comparing various methods to estimate water salinity and the effects of invasion in induction and laterolog resistivity tools. Since we are simulating mud-filtrate invasion, we can implement all the methods explained in the previous section, except for the Pickett plot graphical method due to the lack of synthetic data and porosity variations.

Under the effects of mud-filtrate invasion, we observe a considerable increase in the error estimating formation water salinity with Archie's equation. Interestingly, the error is higher for the resistivity ratio and Archie's equation methods in the low water salinity scenario of layer 2, which is generally the case for Edwards-Trinity aquifers. On the other hand, the error decreases in all methods for the scenario of layer 4 where formation water salinity is equal to the mud-filtrate salinity rendering negligible salinity contrast.

The base case results with mud-filtrate invasion confirms the observations of the initial model without invasion, where the induction tool provides higher reliability than laterolog tools for measuring electrical resistivity in low-salinity aquifers. The differences in the error estimation for both tools increases when the formation water salinity increases and the formation resistivity decreases. Indeed, laterolog tools require a high formation resistivity compared with the borehole resistivity to obtain satisfactory results (Schlumberger, 1972; Griffiths et al., 2000; Crary et al., 2001), which is not normally the case for Edwards-Trinity Plateau aquifers.

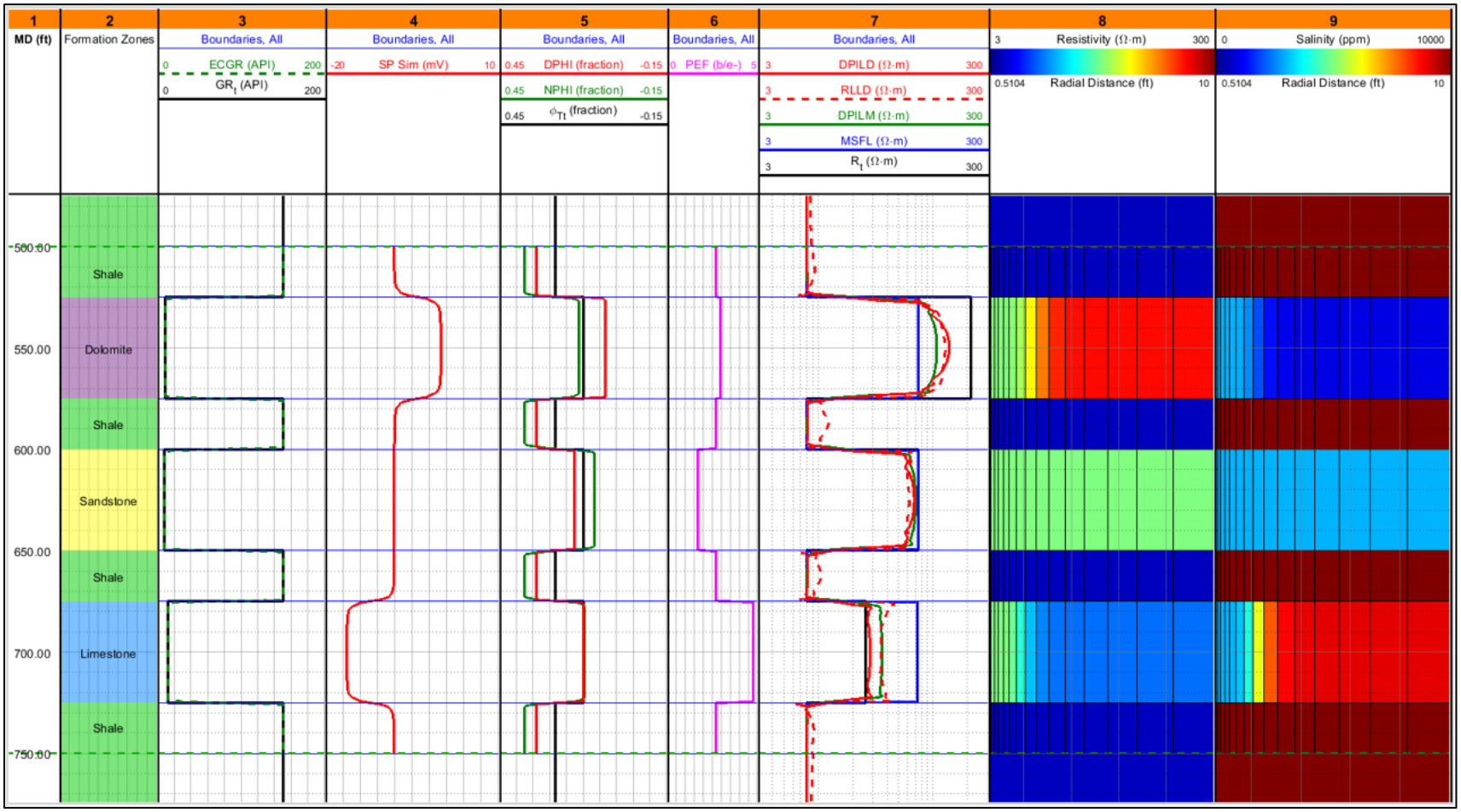

Figure 5-3. **Base case synthetic model results. Track 1 presents the measured depth in ft. Track 2 presents the formation lithology with shale in green, dolomite in purple, sandstone in yellow and limestone in light blue. Track 3 presents the gamma ray curves for the earth model in black and the simulated log in dash green. Track 4 presents the spontaneous potential simulated log in red. Track 5 presents the earth model total porosity in black, the simulated density log in red, and the neutron simulated log in green. Track 6 presents the photoelectric factor simulated log in magenta. Track 7 presents the earth model formation resistivity in black, the deep induction simulated log in red, and the deep laterolog simulation in dash red. Tracks 8 and 9 present the vertical cross-section color map for formation resistivity and formation water salinity. The blue horizontal lines in tracks 2 to 7 represent the layer boundaries.**

Table 5-3. Results for various formation water salinity estimation methods for the base case.

Layer	T (°F)[a]	R_{mf}[b]	R_w[c]	Salinity (ppm NaCl)[d, e]	Method	Error (%)
			4.7005	1,000	Simulation	0.0
			3.1275	1,534	Archie's Equation IL[f]	53.4
2	80.03	1.654	3.0650	1,567	Resistivity Ratio IL[f]	56.7
			2.8800	1,673	Archie's Equation LL[g]	67.3
			2.8224	1,709	Resistivity Ratio LL[g]	70.9
			6.0188	771	Spontaneous Potential	22.9
			1.6372	3,000	Simulation	0.0
			1.5525	3,173	Archie's Equation IL[f]	5.8
4	80.91	1.637	1.5265	3,230	Resistivity Ratio IL[f]	7.7
			1.3950	3,552	Archie's Equation LL[g]	18.4
			1.3717	3,616	Resistivity Ratio LL[g]	20.5
			1.6122	3,049	Spontaneous Potential	1.6
			0.5756	9,000	Simulation	0.0
			0.6300	8,173	Archie's Equation IL[f]	9.2
6	81.71	1.622	0.6139	8,402	Resistivity Ratio IL[f]	6.6
			0.8100	6,255	Archie's Equation LL[g]	30.5
			0.7893	6,430	Resistivity Ratio LL[g]	28.6
			0.4518	11,666	Spontaneous Potential	29.6

Note: Error calculation assumes input formation water salinity as the true formation water salinity. Archie's equation method assumes total porosity, *a* and *m* exponents as constants according to information available in Table 5-1, and it uses the deep resistivities readings from the simulated logs. Resistivity ratio method uses the estimated R_{mf} at formation temperature and the deep and shallow resistivities readings from the simulated logs. Electrical resistivity measurements are obtained from the center of the curves (peak). Spontaneous potential method assumes the mud-filtrate salinity of 3,000 ppm NaCl and estimates the static spontaneous potential (SSP) using the simulated SP log to obtain the shale baseline and the formation SP.

[a] T = reservoir temperature.

[b] R_{mf} = mud-filtrate resistivity.

[c] R_w = formation water resistivity.

[d] ppm = parts per million.

[e] NaCl = sodium chloride.

[f] IL = induction resistivity log.

[g] LL = laterolog electrical resistivity.

5.3 Synthetic models: Sensitivity analysis

The base case permits the development of a sensitivity analysis to explore the impact of invasion radius and formation factor uncertainties in the estimation of salt concentration in formation water. The synthetic cases assume variable invasion time rendering a variable invasion radius and an electrical resistivity profile in the invaded region. In addition, we modify the formation factor varying total porosity and *m*-exponent in the synthetic models to generate synthetic cases for these Archie's parameters.

5.3.1 Invasion radius

The synthetic models developed to test the effects of invasion radius comprise a scenario for shallow invasion with a mud-filtrate invasion time of 1 day (three times lower than the

base case invasion time), and a deep invasion case with an invasion time of 9 days (three times higher than the base case invasion time). Figure 5-4 and Figure 5-5 illustrate the results for shallow invasion radius and deep invasion, respectively. The invasion radius for the shallow invasion case is around 1 ft and the invasion radius for the deep invasion case is about 5 ft. these invasion radii depend on the mud-filtrate invasion input parameters of the model varying invasion time as explained above.

From Table 5-4, we observe that in general the errors in the estimation of formation water salinity decrease if invasion is shallower. In other words, the lower the invasion radius the better the reliability of the water estimation methods. However, the errors are still considerable in the low salt concentration case (layer 2). Induction resistivity tools show around 20% less error than laterolog tools for these types of reservoirs and conditions, offering excellent reliability in high-salinity aquifers with errors below 2% when formation water salinity is above 9,000 ppm NaCl. The SP method does not change at shallower invasion radius since the difference in salt concentration between the mud-filtrate and the formation water is the same as the base case.

On the other hand, a deep invaded region significantly affects the reliability of Archie's equation and resistivity ratio methods to compute formation water salinity. On Figure 5-5 and Table 5-5, we encounter that induction log and laterolog overlap at low salinities in layer 2. Both resistivity logs provide a highly uncertain resistivity measurement, which escalates in errors above 90% in the estimation of salt concentration for the resistivity-based methods. Similarly, at high water salinities the error is above 20% for both resistivity-based methods and both resistivity tools. These results demonstrate the effect of deep mud-filtrate invasion on resistivity measurements with electrical logs, as exposed by Semmelbeck and Holditch (1988), and the impact on the estimation of salt concentration in formation water for geohydrology applications. Conventional methods and resistivity dependent methods clearly pose high uncertainty in deeply invaded aquifers.

For the spontaneous potential method, the SP log response is not affected by variations in invasion radius because the salinity contrast remains constant. If invasion occurs, despite it is deep or shallow, it is an indication of permeable beds and the SP log values will depend exclusively on the salinity contrast of filtrate and formation water. Consequently, under adequate conditions, the salt concentration calculated with the SP log could be useful to estimate the formation factor (F). This approach is very useful for geohydrology, where lack of well logs data and geological information is limited. In multiple occasions, especially in wells drilled decades ago, the only available logs are SP and resistivity logs. Indeed, we assess formation factor using these two basic electrical logs along with equations 1 and 4 presented in the previous section. Moreover, if we have information about formation porosity, we can infer the cementation exponent (m). Likewise, if we have information about m, we can estimate total porosity thanks to Archie's equation and the formation factor concept.

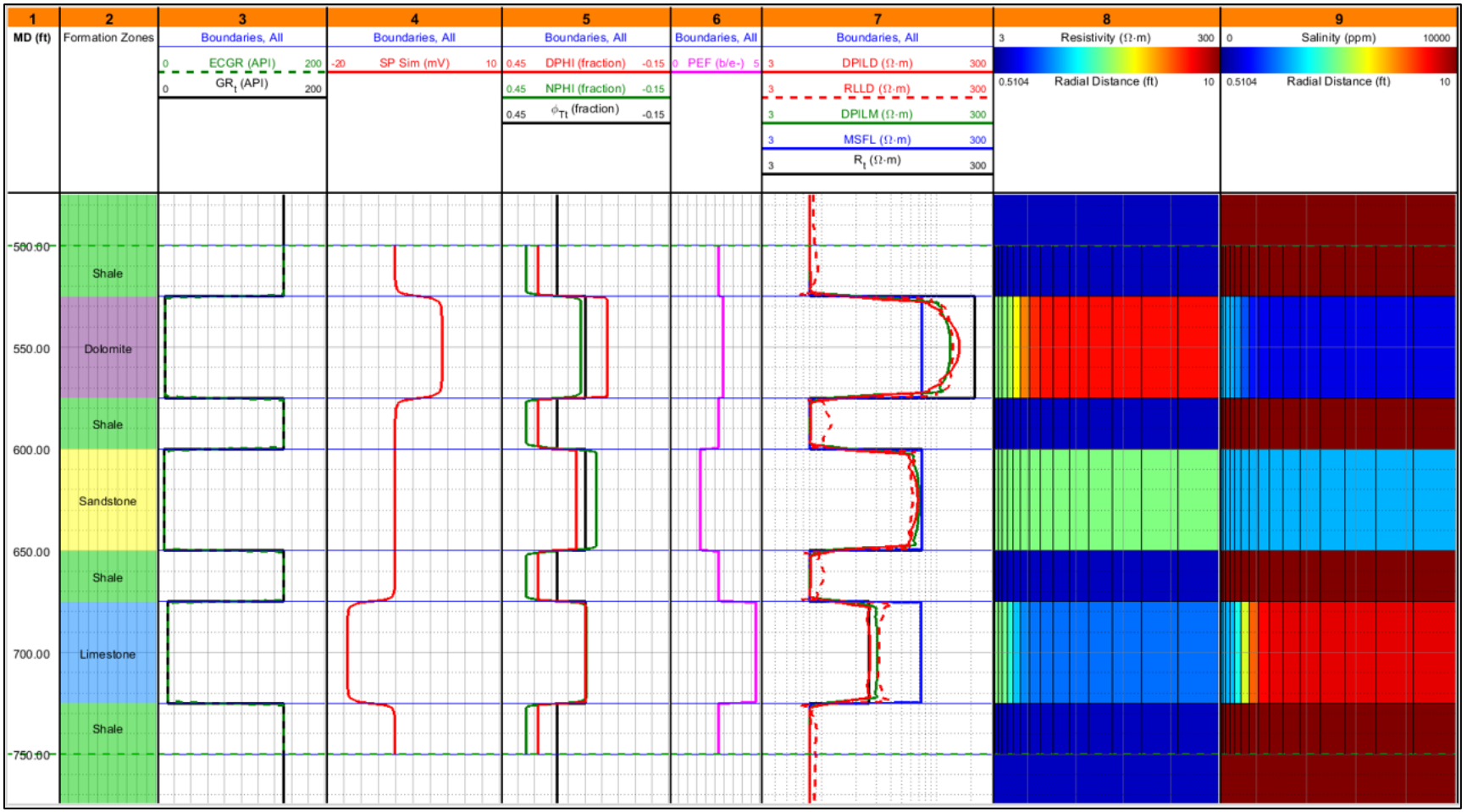

Figure 5-4. **Shallow invasion case results. Track 1 presents the measured depth in ft. Track 2 presents the formation lithology with shale in green, dolomite in purple, sandstone in yellow and limestone in light blue. Track 3 presents the gamma ray curves for the earth model in black and the simulated log in dash green. Track 4 presents the spontaneous potential simulated log in red. Track 5 presents the earth model total porosity in black, the simulated density log in red, and the neutron simulated log in green. Track 6 presents the photoelectric factor simulated log in magenta. Track 7 presents the earth model formation resistivity in black, the deep induction simulated log in red, and the deep laterolog simulation in dash red. Tracks 8 and 9 present the vertical cross-section color map for formation resistivity and formation water salinity. The blue horizontal lines in tracks 2 to 7 represent the layer boundaries.**

Table 5-4. Results for various formation water salinity estimation methods for the shallow invasion case.

Layer	T[a] (°F)	R_{mf}[b] (ohm.m)	R_w[c] (ohm.m)	Salinity (ppm NaCl)[d, e]	Method	Error (%)	Δ Error[f] (%)
			4.7005	1,000	Simulation	0.0	0.0
			3.5550	1,341	Archie's Equation IL[g]	34.1	-19.3
2	80.03	1.654	3.4839	1,370	Resistivity Ratio IL[g]	37.0	-19.7
			3.1275	1,534	Archie's Equation LL[h]	53.4	-13.9
			3.0650	1,567	Resistivity Ratio LL[h]	56.7	-14.2
			6.0188	771	Spontaneous Potential	22.9	0.0
			1.6372	3,000	Simulation	0.0	0.0
			1.5525	3,173	Archie's Equation IL[g]	5.8	0.0
4	80.91	1.637	1.5265	3,230	Resistivity Ratio IL[g]	7.7	0.0
			1.3950	3,552	Archie's Equation LL[h]	18.4	0.0
			1.3717	3,616	Resistivity Ratio LL[h]	20.5	0.0
			1.6122	3,049	Spontaneous Potential	1.6	0.0
			0.5756	9,000	Simulation	0.0	0.0
			0.5850	8,845	Archie's Equation IL[g]	1.7	-7.5
6	81.71	1.622	0.5700	9,094	Resistivity Ratio IL[g]	1.0	-5.6
			0.7200	7,089	Archie's Equation LL[h]	21.2	-9.3
			0.7016	7,288	Resistivity Ratio LL[h]	19.0	-9.5
			0.4518	11,666	Spontaneous Potential	29.6	0.0

Note: Error calculation assumes input formation water salinity as the true formation water salinity. Archie's equation method assumes total porosity, *a* and *m* exponents as constants according to information available in Table 5-1, and it uses the deep resistivities readings from the simulated logs. Resistivity ratio method uses the estimated R_{mf} at formation temperature and the deep and shallow resistivities readings from the simulated logs. Electrical resistivity measurements are obtained from the center of the curves (peak). Spontaneous potential method assumes the mud-filtrate salinity of 3,000 ppm NaCl and estimates the static spontaneous potential (SSP) using the simulated SP log to obtain the shale baseline and the formation SP.

[a] T = reservoir temperature.

[b] R_{mf} = mud-filtrate resistivity.

[c] R_w = formation water resistivity.

[d] ppm = parts per million.

[e] NaCl = sodium chloride.

[f] Δ = delta error.

[g] IL = induction resistivity log.

[h] LL = laterolog electrical resistivity.

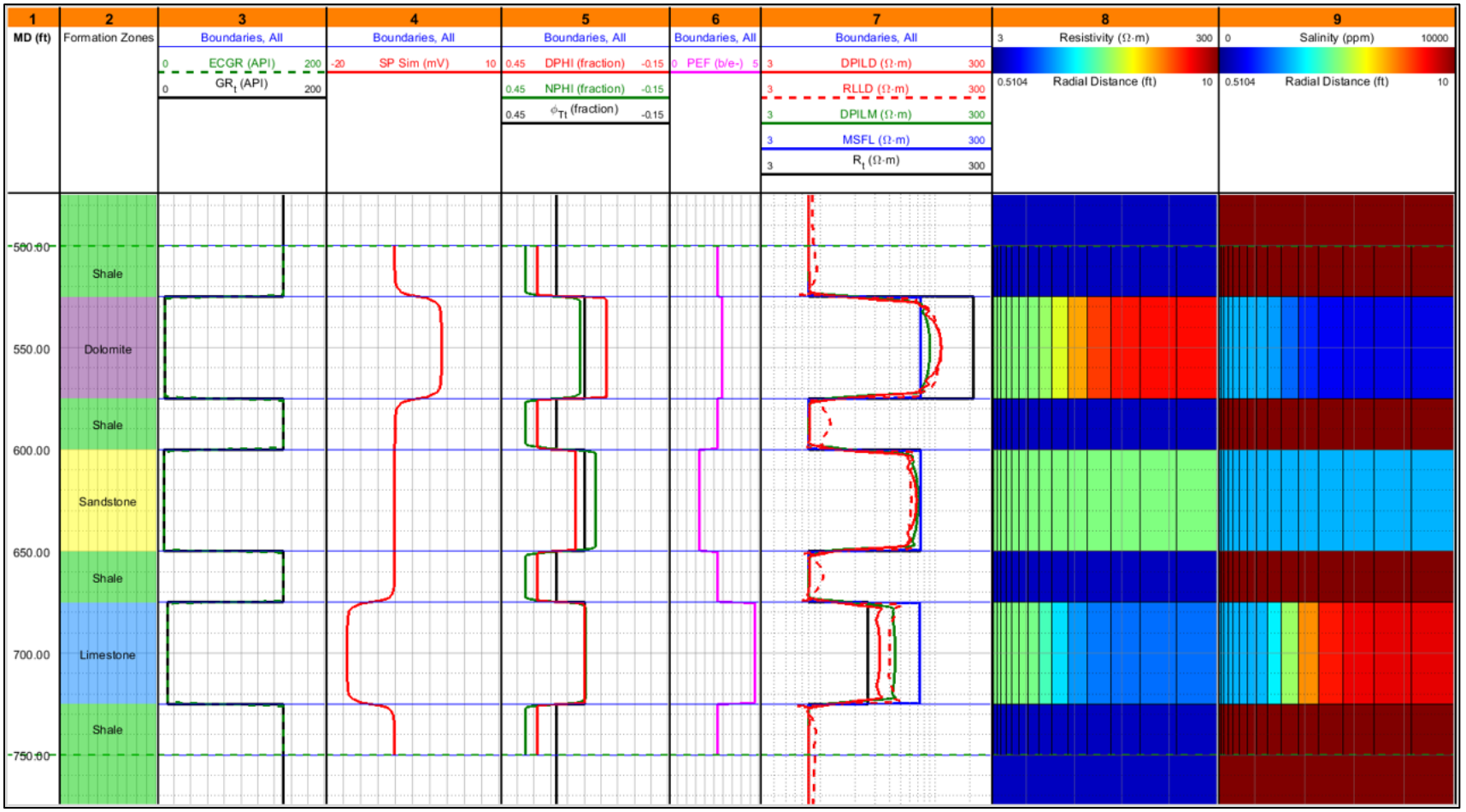

Figure 5-5. **Deep invasion case results. Track 1 presents the measured depth in ft. Track 2 presents the formation lithology with shale in green, dolomite in purple, sandstone in yellow and limestone in light blue. Track 3 presents the gamma ray curves for the earth model in black and the simulated log in dash green. Track 4 presents the spontaneous potential simulated log in red. Track 5 presents the earth model total porosity in black, the simulated density log in red, and the neutron simulated log in green. Track 6 presents the photoelectric factor simulated log in magenta. Track 7 presents the earth model formation resistivity in black, the deep induction simulated log in red, and the deep laterolog simulation in dash red. Tracks 8 and 9 present the vertical cross-section color map for formation resistivity and formation water salinity. The blue horizontal lines in tracks 2 to 7 represent the layer boundaries.**

Table 5-5. Results for various formation water salinity estimation methods for the deep invasion case.

Layer	T[a] (°F)	R_{mf}[b] (ohm.m)	R_w[c] (ohm.m)	Salinity (ppm NaCl)[d, e]	Method	Error (%)	Δ Error[f] (%)
2	80.03	1.654	4.7005	1,000	Simulation	0.0	0.0
			2.5200	1,925	Archie's Equation IL[g]	92.5	39.1
			2.4696	1,967	Resistivity Ratio IL[g]	96.7	40.0
			2.5200	1,925	Archie's Equation LL[h]	92.5	25.2
			2.4696	1,967	Resistivity Ratio LL[h]	96.7	25.8
			6.0188	771	Spontaneous Potential	22.9	0.0
4	80.91	1.637	1.6372	3,000	Simulation	0.0	0.0
			1.5525	3,173	Archie's Equation IL[g]	5.8	0.0
			1.5265	3,230	Resistivity Ratio IL[g]	7.7	0.0
			1.3950	3,552	Archie's Equation LL[h]	18.4	0.0
			1.3717	3,616	Resistivity Ratio LL[h]	20.5	0.0
			1.6122	3,049	Spontaneous Potential	1.6	0.0
6	81.71	1.622	0.5756	9,000	Simulation	0.0	0.0
			0.7425	6,861	Archie's Equation IL[g]	23.8	14.6
			0.7235	7,053	Resistivity Ratio IL[g]	21.6	15.0
			0.9000	5,593	Archie's Equation LL[h]	37.9	7.4
			0.8770	5,749	Resistivity Ratio LL[h]	36.1	7.6
			0.4518	11,666	Spontaneous Potential	29.6	0.0

Note: Error calculation assumes input formation water salinity as the true formation water salinity. Archie's equation method assumes total porosity, *a* and *m* exponents as constants according to information available in Table 5-1, and it uses the deep resistivities readings from the simulated logs. Resistivity ratio method uses the estimated R_{mf} at formation temperature and the deep and shallow resistivities readings from the simulated logs. Electrical resistivity measurements are obtained from the center of the curves (peak). Spontaneous potential method assumes the mud-filtrate salinity of 3,000 ppm NaCl and estimates the static spontaneous potential (SSP) using the simulated SP log to obtain the shale baseline and the formation SP.

[a] T = reservoir temperature.

[b] R_{mf} = mud-filtrate resistivity.

[c] R_w = formation water resistivity.

[d] ppm = parts per million.

[e] NaCl = sodium chloride.

[f] Δ = delta

[g] IL = induction resistivity log.

[h] LL = laterolog electrical resistivity

5.3.2 Formation Factor

Formation factor is an extremely useful and significant concept for assessing salt concentration of groundwater. This factor directly relates changes in porosity and cementation with formation resistivity, which translates in a direct relation with the petrophysical and geological conditions of the reservoir. For this reason, we prepare two synthetic cases varying the parameters of the formation factor equation assuming a constant tortuosity of $a = 1$.

Formation factor models present sensitivity cases for the cementation exponent and total porosity. We modify the *m*-exponent values for the carbonate lithologies in layers 2 and 6

with m = 2.5 and m = 3.0, respectively. Figure 5-6 illustrates the simulation model for the variable m-exponent case and Table 5-6 presents its results comparing the water salinity estimation methods.

Since m value increases from 2 to 2.5 in layer 2, the formation resistivity increases in comparison to the base case. For this layer we can observe that the error in the induction logs increases considerably, whereas the error for laterolog tool remains almost invariable. As mentioned before in this report, the laterolog resistivity tool improves its performance when formation resistivity is high compared with the borehole resistivity (Schlumberger, 1972; Griffiths et al., 2000; Crary et al., 2001). Despite large errors on the estimation of formation water salinity for both resistivity-based methods, the laterolog outcomes indicate that the tool reliability improves on high-resistivity formations. This is an important fact to consider for the petrophysical evaluation of aquifers and the reliability of the analysis in field data and the numerical simulation of well logs.

In addition to the cementation exponent sensitivity case, we develop a synthetic case to reproduce the effect of a variable porosity. We increase the total porosity of the dolomite layer to 0.20, and we decrease the total porosity of the limestone layer to 0.10. Figure 5-7 displays the total porosity synthetic case and Table 5-7 compares the results of the water salinity estimation methods.

For this case, we note that porosity directly impacts mud-filtrate invasion radius. During early-time invasion, formation permeability tends to control the invasion mechanisms and the mud-filtrate invasion rate. During this period of time, the mudcake builds up until the mudcake properties take control over invasion. At this late-time period, where the invasion rate is practically constant, total formation porosity controls the invasion radius. The higher the porosity the shallower the invasion. We observe a decrease in the error of the resistivity-based methods in layer 2 because the porosity increased from 15% in the base case to 20% for this particular case. This error performance is very similar to the one observed in the shallow invasion synthetic case (see result for layer 2 on Table 5-4). On the other hand, layer 6 has a slightly higher error because the lower porosity of 10% causes a deeper invaded region and a higher uncertainty in the estimation of formation water salt concentration.

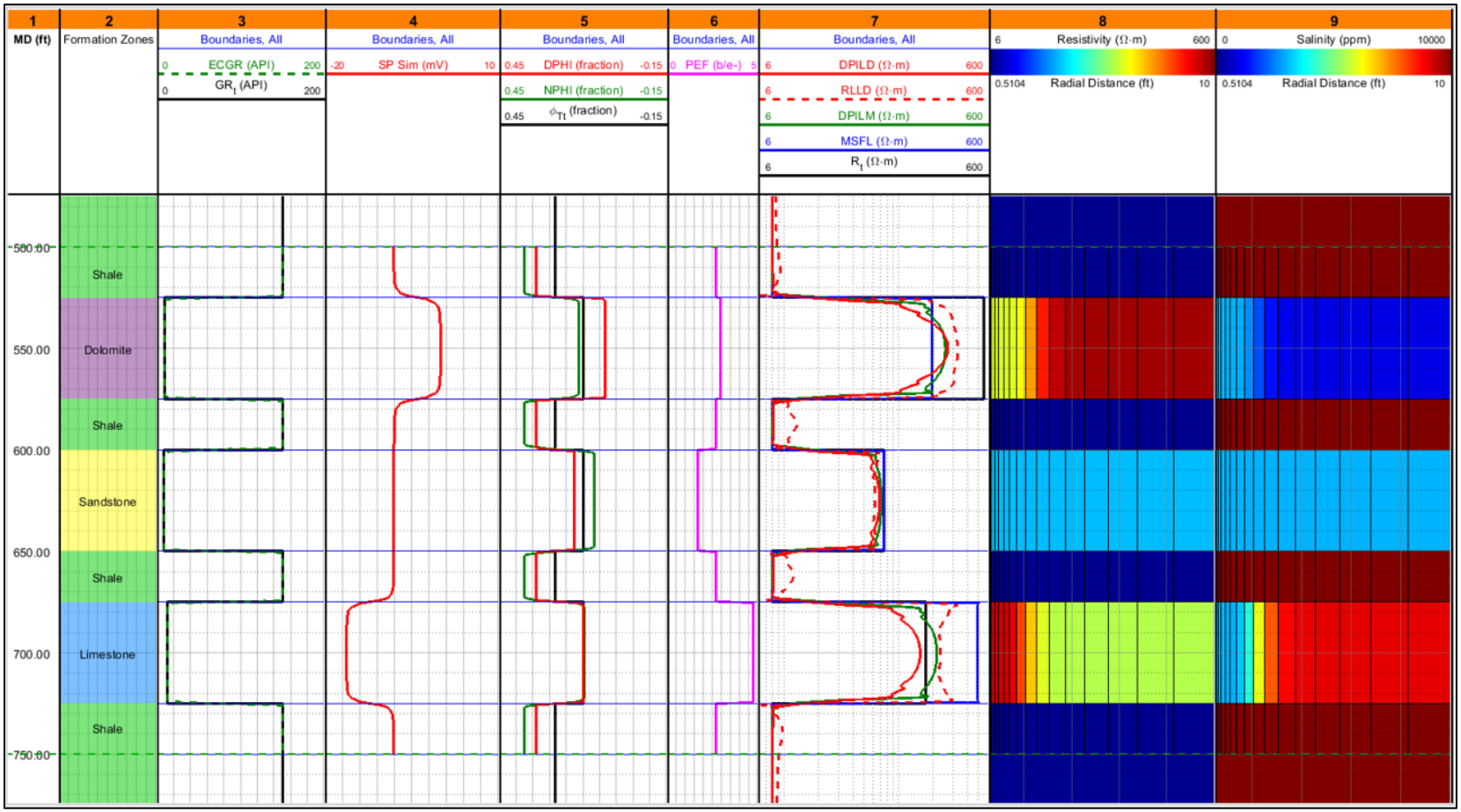

Figure 5-6. **Cementation exponent case results. Track 1 presents the measured depth in ft. Track 2 presents the formation lithology with shale in green, dolomite in purple, sandstone in yellow and limestone in light blue. Track 3 presents the gamma ray curves for the earth model in black and the simulated log in dash green. Track 4 presents the spontaneous potential simulated log in red. Track 5 presents the earth model total porosity in black, the simulated density log in red, and the neutron simulated log in green. Track 6 presents the photoelectric factor simulated log in magenta. Track 7 presents the earth model formation resistivity in black, the deep induction simulated log in red, and the deep laterolog simulation in dash red. Tracks 8 and 9 present the vertical cross-section color map for formation resistivity and formation water salinity. The blue horizontal lines in tracks 2 to 7 represent the layer boundaries. *Note:* the cementation exponent value *m* for layer 2 (dolomite) is 2.5, for layer 4 (sandstone) is 2.0, and for layer 6 (limestone) is 3.0.**

Table 5-6. Results for various formation water salinity estimation methods for the cementation exponent case.

Layer	T[a] (°F)	R_{mf}[b] (ohm.m)	R_w[c] (ohm.m)	Salinity (ppm NaCl)[d, e]	Method	Error (%)	Δ Error[f] (%)
2	80.03	1.654	4.7005	1,000	Simulation	0.0	0.0
			2.5794	1,879	Archie's Equation IL[g]	87.9	34.4
			2.5233	1,923	Resistivity Ratio IL[g]	92.3	35.6
			2.8495	1,692	Archie's Equation LL[h]	69.2	1.9
			2.7875	1,731	Resistivity Ratio LL[h]	73.1	2.2
			6.0188	771	Spontaneous Potential	22.9	0.0
4	80.91	1.637	1.6372	3,000	Simulation	0.0	0.0
			1.5525	3,173	Archie's Equation IL[g]	5.8	0.0
			1.5265	3,230	Resistivity Ratio IL[g]	7.7	0.0
			1.3950	3,552	Archie's Equation LL[h]	18.4	0.0
			1.3717	3,616	Resistivity Ratio LL[h]	20.5	0.0
			1.6122	3,049	Spontaneous Potential	1.6	0.0
6	81.71	1.622	0.5756	9,000	Simulation	0.0	0.0
			0.5198	10,038	Archie's Equation IL g	11.5	2.3
			0.5088	10,268	Resistivity Ratio IL g	14.1	7.4
			0.7796	6,514	Archie's Equation LL h	27.6	-2.9
			0.7633	6,663	Resistivity Ratio LL h	26.0	-2.6
			0.4518	11,666	Spontaneous Potential	29.6	0.0

Note: The cementation exponent m value used for layer 2 (dolomite) is 2.5, for layer 4 (sandstone) is 2.0, and for layer 6 (limestone) is 3.0. Error calculation assumes input formation water salinity as the true formation water salinity. Archie's equation method assumes total porosity and tortuosity factor a as constants according to information available in Table 5-1, and it uses the deep resistivities readings from the simulated logs. Resistivity ratio method uses the estimated R_{mf} at formation temperature and the deep and shallow resistivities readings from the simulated logs. Electrical resistivity measurements are obtained from the center of the curves (peak). Spontaneous potential method assumes the mud-filtrate salinity of 3,000 ppm NaCl and estimates the static spontaneous potential (SSP) using the simulated SP log to obtain the shale baseline and the formation SP.

[a] T = reservoir temperature.

[b] R_{mf} = mud-filtrate resistivity.

[c] R_w = formation water resistivity.

[d] ppm = parts per million.

[e] NaCl = sodium chloride.

[f] Δ = delta

[g] IL = induction resistivity log.

[h] LL = laterolog electrical resistivity

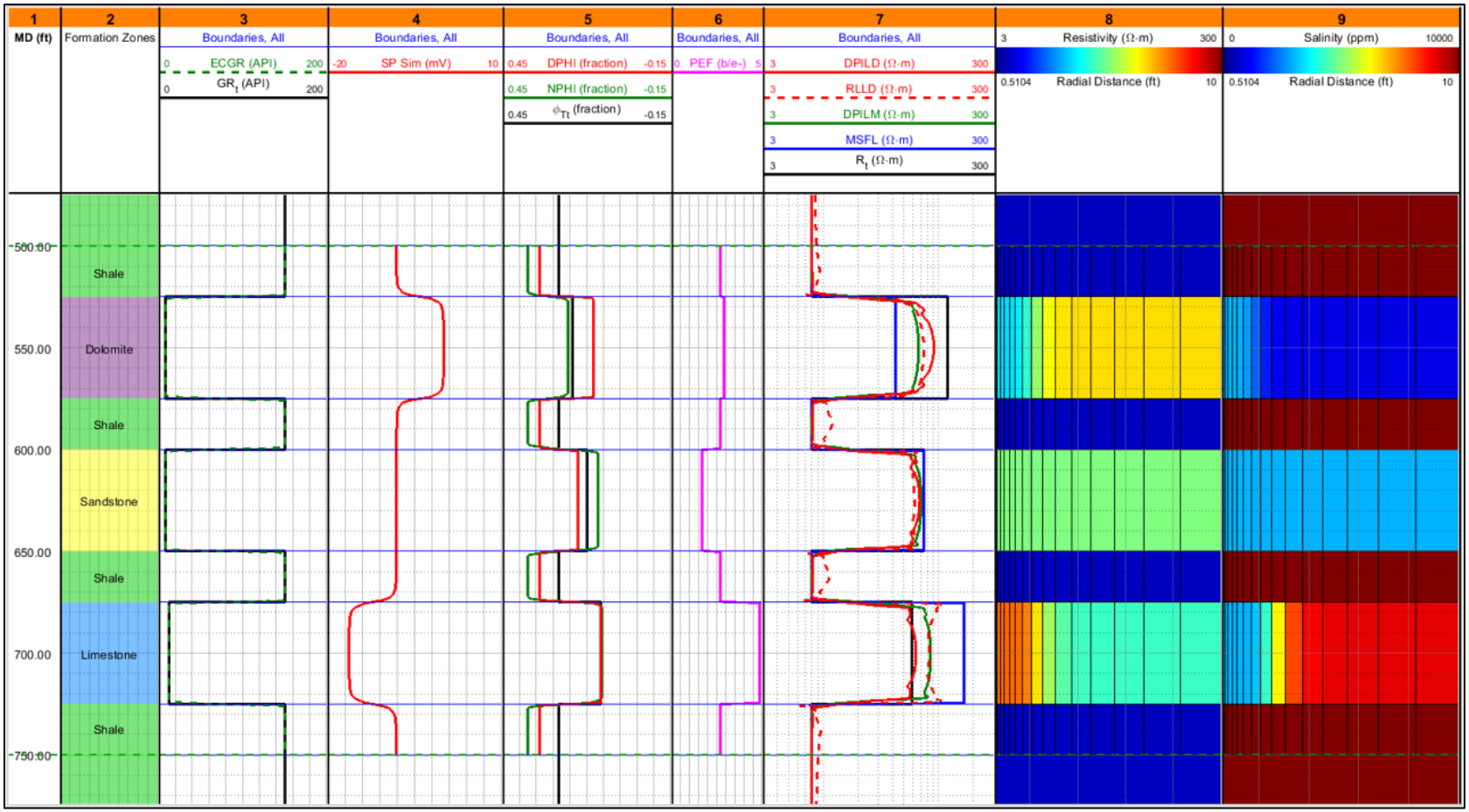

Figure 5-7. **Total porosity case results. Track 1 presents the measured depth in ft. Track 2 presents the formation lithology with shale in green, dolomite in purple, sandstone in yellow and limestone in light blue. Track 3 presents the gamma ray curves for the earth model in black and the simulated log in dash green. Track 4 presents the spontaneous potential simulated log in red. Track 5 presents the earth model total porosity in black, the simulated density log in red, and the neutron simulated log in green. Track 6 presents the photoelectric factor simulated log in magenta. Track 7 presents the earth model formation resistivity in black, the deep induction simulated log in red, and the deep laterolog simulation in dash red. Tracks 8 and 9 present the vertical cross-section color map for formation resistivity and formation water salinity. The blue horizontal lines in tracks 2 to 7 represent the layer boundaries. *Note:* Total porosity fraction for layer 2 (dolomite) is 0.20, for layer 4 (sandstone) is 0.15, and for layer 6 (limestone) is 0.10.**

Table 5-7. Results for various formation water salinity estimation methods for the total porosity case.

Layer	T[a] (°F)	R_{mf}[b] (ohm.m)	R_w[c] (ohm.m)	Salinity (ppm NaCl)[d, e]	Method	Error (%)	Δ Error[f] (%)
2	80.03	1.654	4.7005	1,000	Simulation	0.0	0.0
			3.6400	1,308	Archie's Equation IL[g]	30.8	-22.6
			3.5831	1,330	Resistivity Ratio IL[g]	33.0	-23.7
			3.0000	1,603	Archie's Equation LL[h]	60.3	-7.0
			2.9531	1,629	Resistivity Ratio LL[h]	62.9	-7.9
			6.0188	771	Spontaneous Potential	22.9	0.0
4	80.91	1.637	1.6372	3,000	Simulation	0.0	0.0
			1.5525	3,173	Archie's Equation IL[g]	5.8	0.0
			1.5265	3,230	Resistivity Ratio IL[g]	7.7	0.0
			1.3950	3,552	Archie's Equation LL[h]	18.4	0.0
			1.3717	3,616	Resistivity Ratio LL[h]	20.5	0.0
			1.6122	3,049	Spontaneous Potential	1.6	0.0
6	81.71	1.622	0.5756	9,000	Simulation	0.0	0.0
			0.6400	8,037	Archie's Equation IL[g]	10.7	1.5
			0.6255	8,236	Resistivity Ratio IL[g]	8.5	1.8
			0.8300	6,095	Archie's Equation LL[h]	32.3	1.8
			0.8112	6,245	Resistivity Ratio LL[h]	30.6	2.0
			0.4518	11,666	Spontaneous Potential	29.6	0.0

Note: Error calculation assumes input formation water salinity as the true formation water salinity. Archie's equation method assumes *a* and *m* exponents as constants according to information available in Table 5-1, and it uses the deep resistivities readings from the simulated logs. Total porosity fraction is 0.20 for layer 2 (dolomite), 0.15 for layer 4 (sandstone), and 0.10 for layer 6 (limestone). Resistivity ratio method uses the estimated R_{mf} at formation temperature and the deep and shallow resistivities readings from the simulated logs. Electrical resistivity measurements are obtained from the center of the curves (peak). Spontaneous potential method assumes the mud-filtrate salinity of 3,000 ppm NaCl and estimates the static spontaneous potential (SSP) using the simulated SP log to obtain the shale baseline and the formation SP.

[a] T = reservoir temperature.

[b] R_{mf} = mud-filtrate resistivity.

[c] R_w = formation water resistivity.

[d] ppm = parts per million.

[e] NaCl = sodium chloride.

[f] Δ = delta

[g] IL = induction resistivity log.

[h] LL = laterolog electrical resistivity

5.4 Edwards-Trinity Plateau well log simulations

The TWDB provided a total of 7 well logs datasets acquired in West Texas wells. These wells were drilled across the hydrogeologic units of Edwards and Trinity. We digitize the well logs data and use their information as input for the numerical simulator UTAPWeLS. After a careful review and quality control of the datasets, we construct the earth models and simulate the well logs to match their responses. The earth models include all petrophysical properties for rocks and fluids and their interactions as a synthetic model to reproduce the available well logs.

The map on Figure 5-8 shows the study area and the location of the wells with available logs to perform numerical simulations. Five of these simulation wells are successfully modeled and reported. Table 5-8 provides supplementary information with respect to the available well logs and the expected depths to encounter the hydrogeologic units of the Edwards-Trinity Plateau aquifers.

The well Earl Vest #1, which is highlighted in red in Figure 5-8, only has SP log and laterolog resistivity. Unfortunately, laterolog response does not provide a consistent result for the formation salinity in Reeves county. In addition, the absence of gamma ray (GR) log to identify shale beds render the SP log unreliable due to the uncertainty of the value of a shale baseline. However, we use this well to back calculate formation water salinity of Reeves-State #1 and to generate a synthetic case to explain the inconsistency of the results and the impact of laterolog tools in Reeves County. Likewise, in Figure 5-8 we highlight in red the well Hurt #1, which is not simulated due to poor quality logs, cropped curves and highly noisy resistivity measurements. These issues in the well logs' quality pose limitations for the estimation of formation water salinity using conventional methods and numerical simulations.

In order to determine the simulation water-salinity assessment, we simulate all available logs for the wells highlighted in green in Figure 5-8 by adjusting various earth model petrophysical parameters, including formation water salinity. In addition, we simulate mud-filtrate invasion to properly consider its effects in the electrical resistivity logs and the estimation of salt concentration in formation water. Once we match the logs using the adequate formation water salinity, we assume its salt concentration as the true value for the comparison of our results with other conventional methods, as shown in the synthetic cases. To estimate formation water salinity from the numerical simulation, we use the model petrophysical properties as inputs for the Archie's equation and/or resistivity ratio methods.

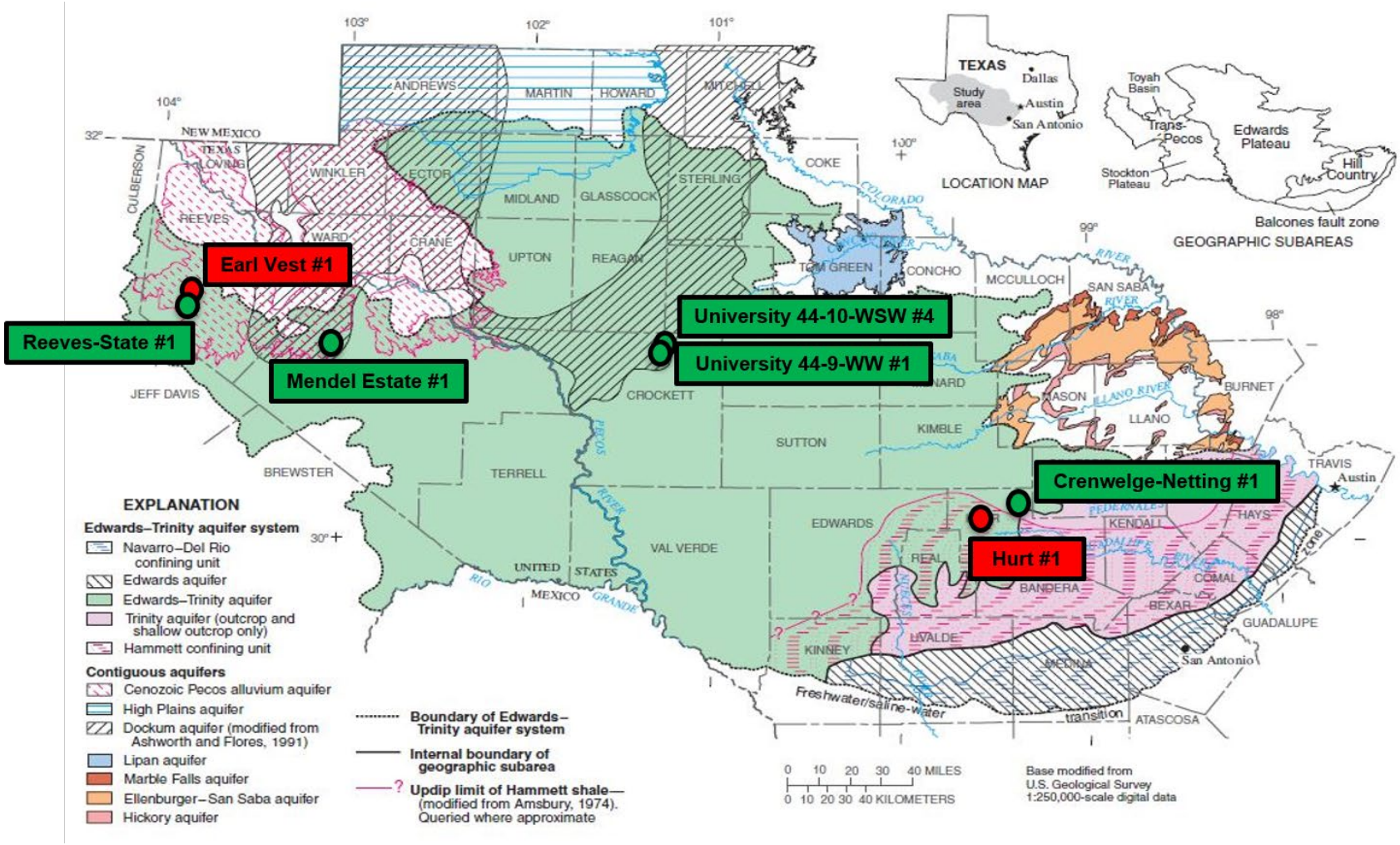

Figure 5-8. Wells locations map. In green are the wells that were successfully modeled, and in red are the wells not modeled due to lack of reliability in laterolog measurements and/or poor quality well logs. Modified from Kuniansky and Ardis (2004).

Table 5-8. Wells available for simulation.

Well	County	BRACS ID	Well Logs	Depths of Interest (ft)
Crenwelge-Netting # 1	Kerr	6693	GR [a], SP [b], RES [c] (Dual Induction, SFL [d]), DEN [e], NEU [f], PEF [g]	100 – 1,050
Hurt # 1	Kerr	6457	GR [a], SP [b], RES [c] (Dual Induction, SFL [d])	80 – 1,150
University 44-10-WSW # 4	Crockett	56209	GR [a], SP [b], RES [c] (Dual Induction), DEN [e], NEU [f], PEF [g]	350 - 750
University 44-9-WW # 1	Crockett	56206	GR [a], SP [b], RES [c] (Dual Induction), DEN [e], NEU [f]	330 - 740
Reeves-State # 1	Reeves	36667	GR [a], SP [b], RES [c] (Dual Induction), NEU [f]	740 – 1,320
Earl Vest # 1	Reeves	2688	SP [b], RES [c] (Laterolog)	350 – 1,500
Mendel Estate # 1	Pecos	21069	GR [a], RES [c] (Dual Induction)	58 - 700

Note: Depth of interest is a range provided by the TWDB for the expected location of the Edwards-Trinity aquifers.

[a] GR = gamma ray log.

[b] SP = spontaneous potential log.

[c] RES = electrical resistivity logs.

[d] SFL = spherical resistivity log.

[e] DEN = density log.

[f] NEU = neutron log.

[g] PEF = photoelectric effect log.

5.4.1 Crenwelge Netting #1

This well is located to the southeast of the Edwards Plateau in the limit with the Hill Country geographic subarea. Figure 5-9 displays the stratigraphic and hydrogeologic units of the Edwards Plateau, indicating the stratigraphic section encountered by the well logs of Crenwelge Netting #1.

Crenwelge Netting #1 has triple-combo well logs, which offers sufficient inputs to model and simulate the well logs response. Figure 5-10 presents the stratigraphic section and the triple combo logs for the Trinity aquifers. We observe sufficient separation of resistivity logs in Glen Rose Limestone (GRL) and Cow Creek Limestone (CCL), which indicates the presence of permeable beds and potential aquifers in these geological formations. Consequently, we developed an earth model for each formation in order to simulate them independently and estimate their formation water salinity.

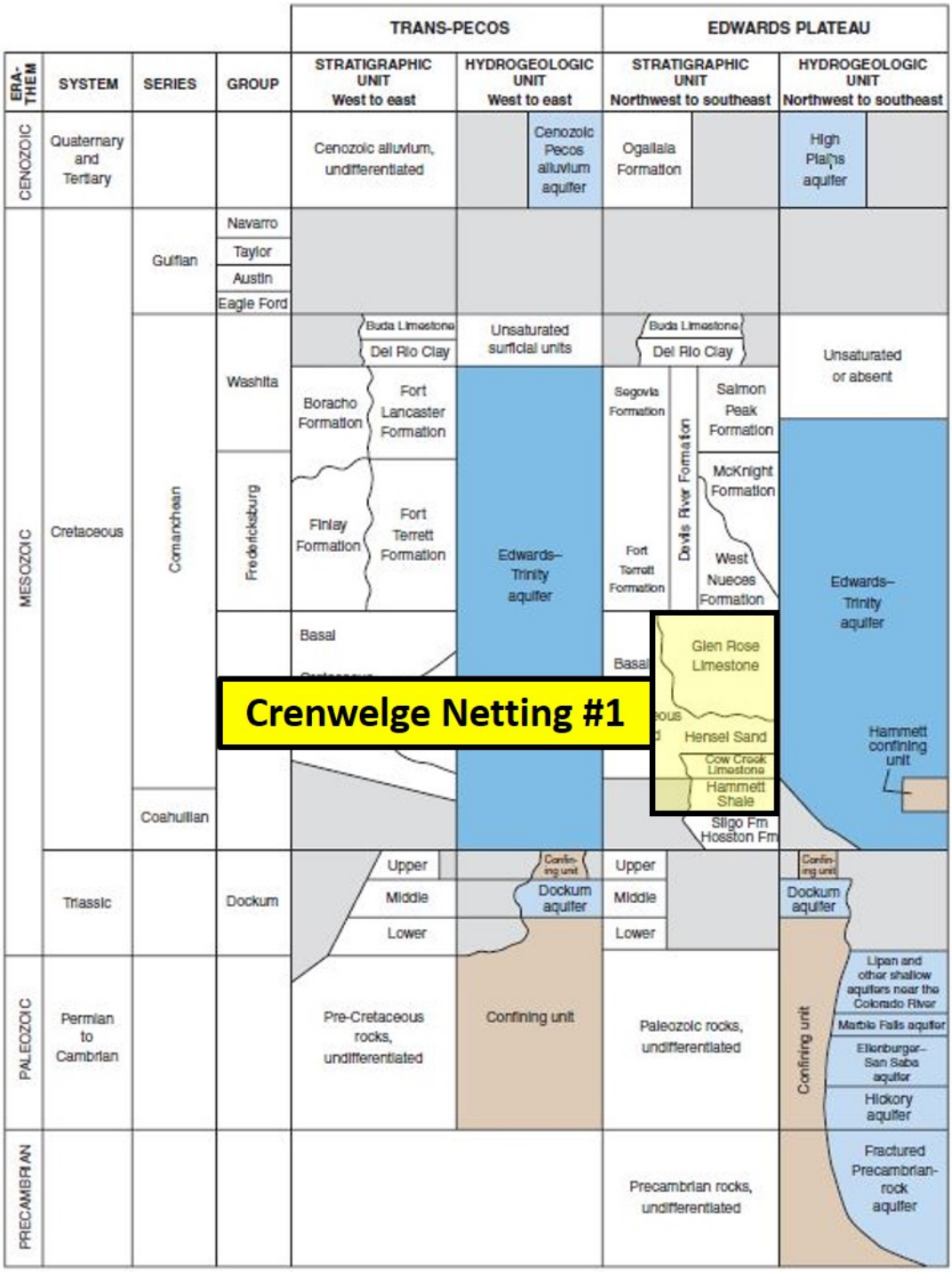

Figure 5-9. Crenwelge Netting #1 stratigraphy. Edwards-Trinity Plateau stratigraphic and hydrogeologic units available in the Trans-Pecos and Edwards Plateau geographic subareas. Crenwelge Netting #1 stratigraphy is highlighted in yellow. Modified from Kuniansky and Ardis (2004).

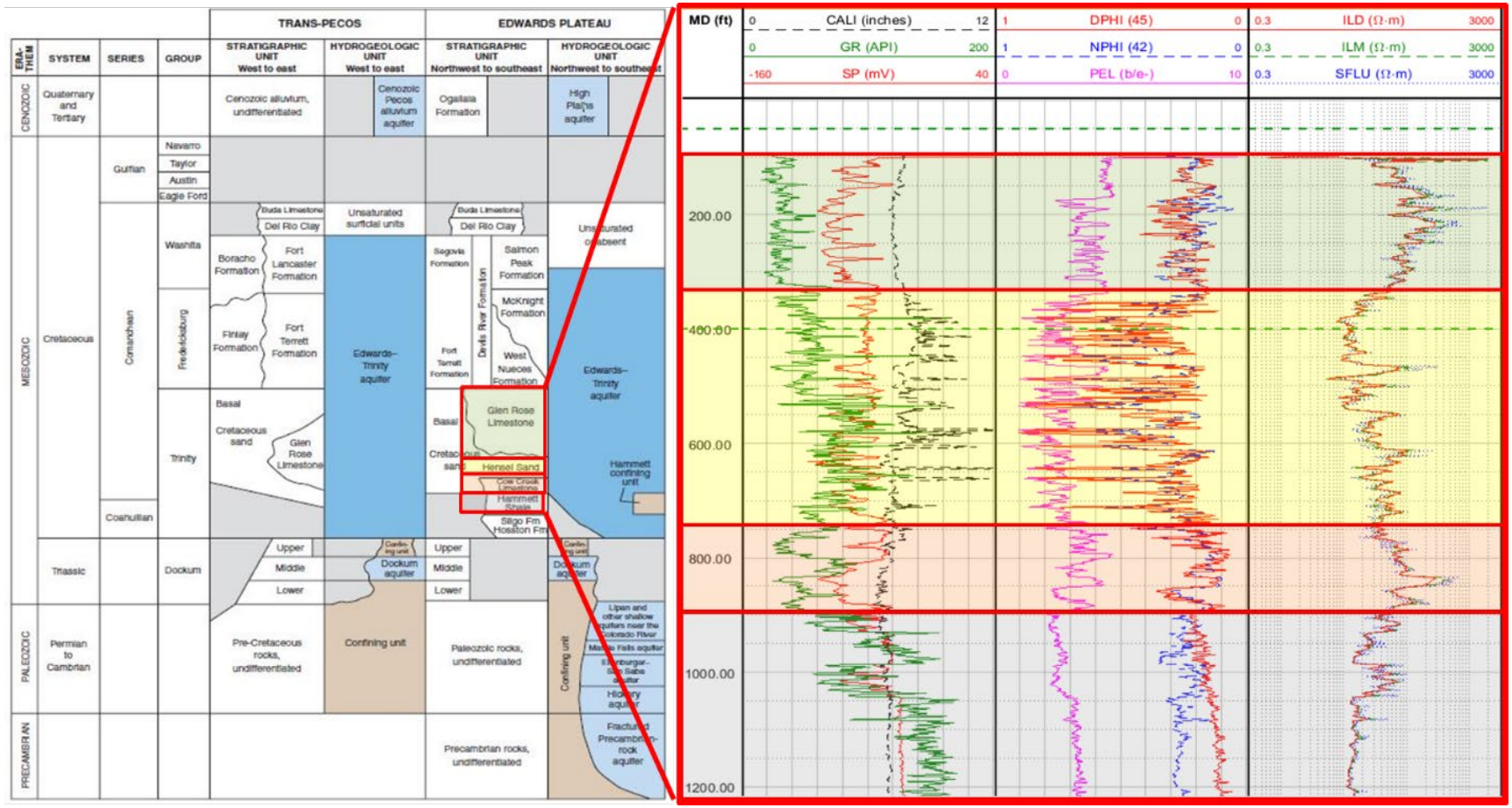

Figure 5-10. Crenwelge Netting #1 geological formations stratigraphy and well logs. Modified from Kuniansky and Ardis (2004). Glen Rose Limestone formation is highlighted in light green, Hensel Sand is highlighted in light yellow, Cow Creek Limestone formation is highlighted in light red, and Hammett Shale is highlighted in light gray.

Glen Rose Limestone

Figure 5-11 exhibits the stratigraphic section and well logs for the Glen Rose Limestone section. From the well logs, we can identify the formation bottom around 340 ft MD. Upper and lower GRL presents a lithology dominated by pure calcite, whereas mid-GRL shows variations in the photoelectric factor (PEF) log due to presence of dolomite. We model the lithology of these layers accordingly. In addition, we observe separation of resistivity log in the section from 150 ft MD to 250 ft MD, which is the zone that we select for modeling. To avoid shoulder bed effects and numerical instabilities, we expand the modeling region from 50 ft MD to 400 ft MD to allow sufficient space between our modeling limits and the zone-of-interest limits. We consider clean matrix for our model since gamma ray (GR) log is low and fairly flat.

For continuing building the model for GRL, we intend to properly assess formation factor (F) using the Pickett plot. We interpret total porosity from the density and neutron logs and, we generate logarithmic plots of electrical resistivity log versus the interpreted porosity. Since we have not estimated any water resistivity yet, we perform a sensitivity analysis varying the m-exponent from 2 to 3. We also perform a linear regression of the data assuming all the reservoir is 100% water saturated, and the tortuosity factor a is equal to 1. Figure 5-12 shows the scenarios for m equal to 2, 2.5, and 3, and the regression-calculated m-exponent equal to 2.97.

In order to continue the estimation of the m-exponent and to validate the sensitivity observations, we perform another linear regression for the invaded zone. We utilize the SFL electrical resistivity log to account for R_{xo} instead of R_t, and we calculate R_{mf} using the well-header data provided for the mud-filtrate resistivity at surface conditions and the respective temperature correction using the geothermal gradient available also in the well-header. Since we have a known measurement for R_{mf}, we can compute the m-exponent from the Pickett plot. Figure 5-13 displays the comparison of the Pickett plot method for the invaded and the uninvaded zones. Indeed, the m value obtained from the regression of the invaded zone data and the fixed R_{mf} is equal to the m obtained from the regression of the uninvaded zone (m = 2.97). Therefore, we can use this m-exponent as input for the GRL formation factor in our model. From these observations we can also infer that the resistivity logs are reliable to estimate formation water salinity since the invasion effects might not affect the deep sensing resistivity.

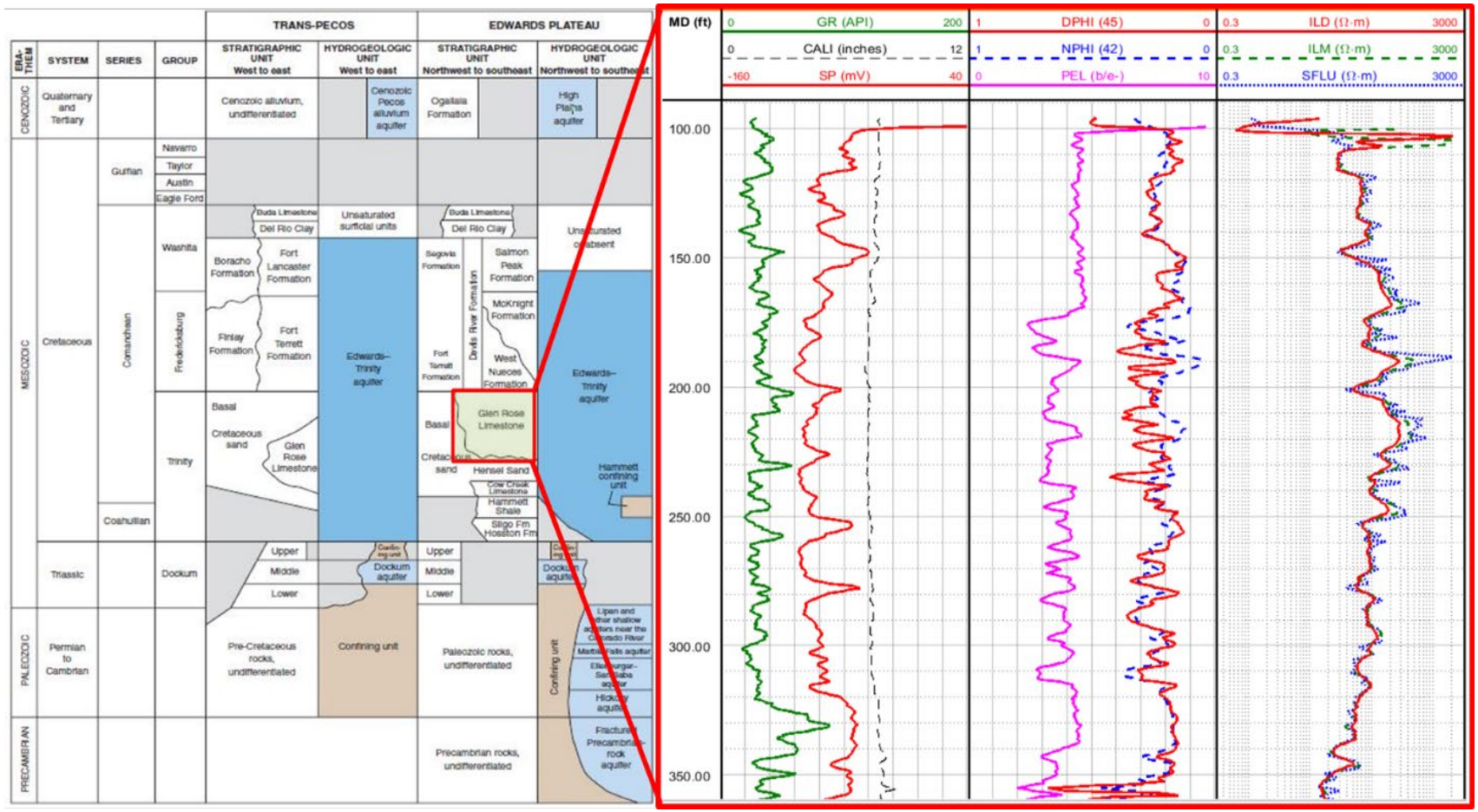

Figure 5-11. Crenwelge Netting #1 geological formations stratigraphy and well logs for Glen Rose Limestone section. Modified from Kuniansky and Ardis (2004).

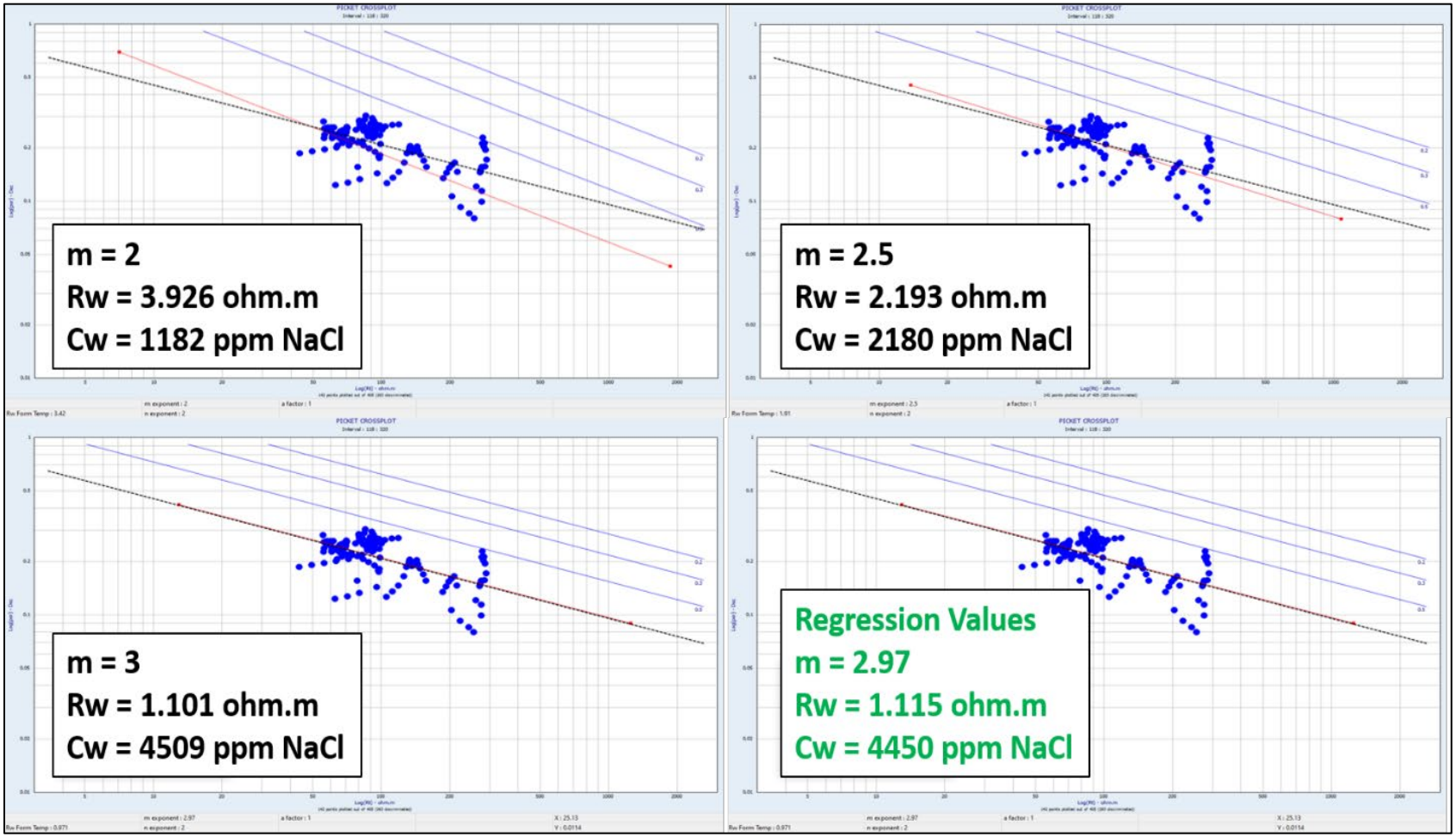

Figure 5-12. **Picket plot sensitivity results for the Crenwelge Netting #1 well logs in the Glen Rose Limestone for the estimation of formation water salinity. Sensitivity performed for the *m*-exponent from 2 to 3. Log-log plot of electrical resistivity (x-axis) and total porosity (y-axis). Formation resistivity is obtained from the deep sensing electrical resistivity log. Total porosity is interpreted from density and neutron logs. Red regression line indicates a S_w = 1.0. Blue regression lines indicate S_w of 0.20, 0.30 and 0.50. Black regression line indicates the linear regression of the well data points (blue dots).**

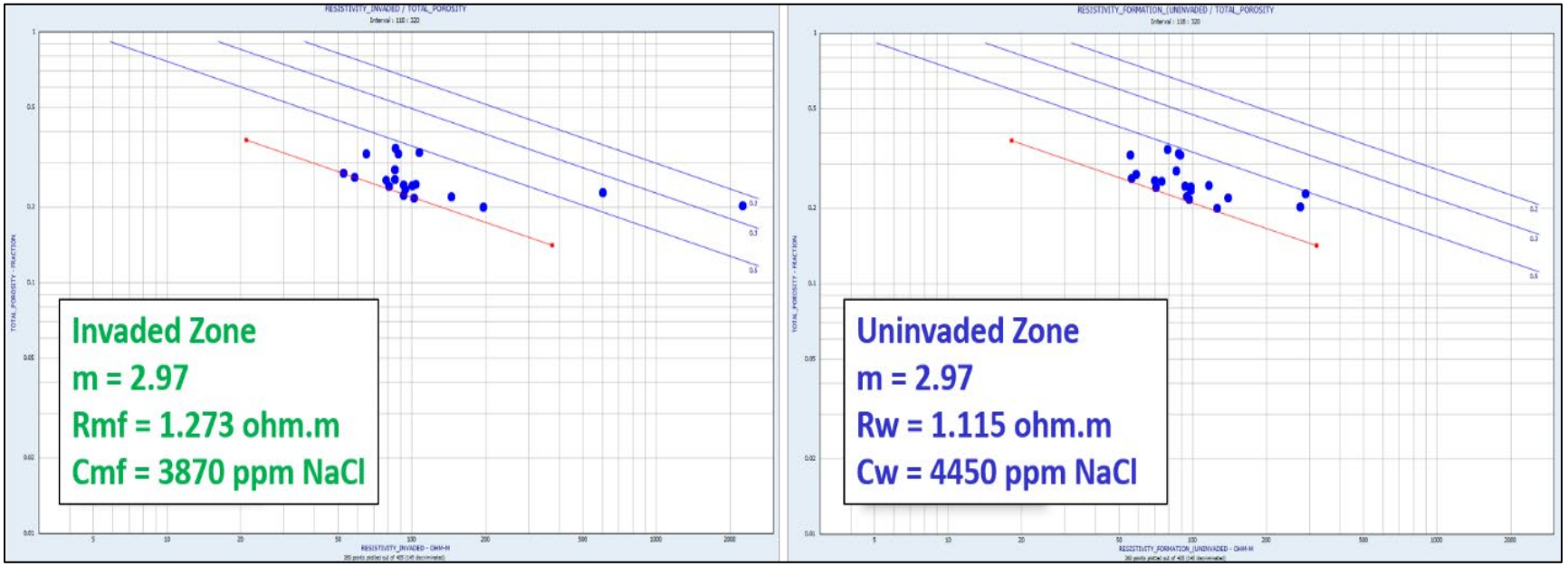

Figure 5-13. **Comparison between invaded and uninvaded zones using Picket plot results for the Crenwelge Netting #1 well logs in the Glen Rose Limestone formation. Log-log plot of electrical resistivity (x-axis) and total porosity (y-axis). Formation resistivity is obtained from the deep sensing electrical resistivity log. Total porosity is interpreted from density and neutron logs. Red regression line indicates a S_w = 1.0. Blue regression lines indicate S_w of 0.20, 0.30 and 0.50. Black regression line indicates the linear regression of the well data points (blue dots).**

From the mud-filtrate resistivity and temperature extracted from the well-header and using equation 2, we can compute the mud-filtrate salinity, which is 3,869 ppm NaCl. We simulate mud-filtrate invasion with an overbalance pressure of 250 psi at 400 ft MD for a period of 10 days. The excessively extended invasion time intends to review the invasion front for extended times and obtain the best invasion profile at any time lower than the maximum invasion time. Invasion time and overbalance pressure are unknown for our model, and we assume one constant (overbalance pressure) and the other (invasion time) variable in order to observe the movement of the invasion front. We find good invasion results and match after two days of invasion at constant overbalance pressure. Likewise, mudcake porosity, mudcake permeability, and mudcake thickness are 0.35, 0.03 md, and 0.4 in, respectively. We utilize a radial grid with 30 blocks evenly distributed with a geometric expansion to reproduce a reservoir with an external radius of 200 ft.

Once we complete all these previous model-construction steps, we are ready to simulate and match the electrical logs. Figure 5-14 illustrates the numerical simulation match of the gamma ray log, porosity logs and resistivity logs, along with a vertical cross section of the invaded zone in the near-wellbore.

Table 5-9 summarizes the results of the formation water salinity estimation methods. Crenwelge Netting #1 is the only well where we apply all methods presented in previous sections, including Pickett plot. This is possible because of the variations of porosity in Glen Rose Limestone and the availability of sufficient data offered by the density, neutron and PEF logs.

The salt concentration in the Edwards-Trinity Plateau aquifer is not composed exclusively by sodium chloride. Since UTAPWeLS assumes that the formation water salinity contains NaCl only, we need to convert the salinity outcome of the simulator to total dissolved solids. The TWDB developed certain correlations depending on the wells location and formations based on laboratory measurements received from different wells located in the study area. We use these correlations to convert our results to TDS and offer consistent results to compare with their experimental data. The empirical correlation between water resistivity and TDS for Crenwelge Netting #1 obeys the following expression:

$$TDS = 0.5801\left(\frac{10{,}000}{R_w\frac{T}{75}}\right) + 1{,}826.5 \quad \text{.......} \quad (13)$$

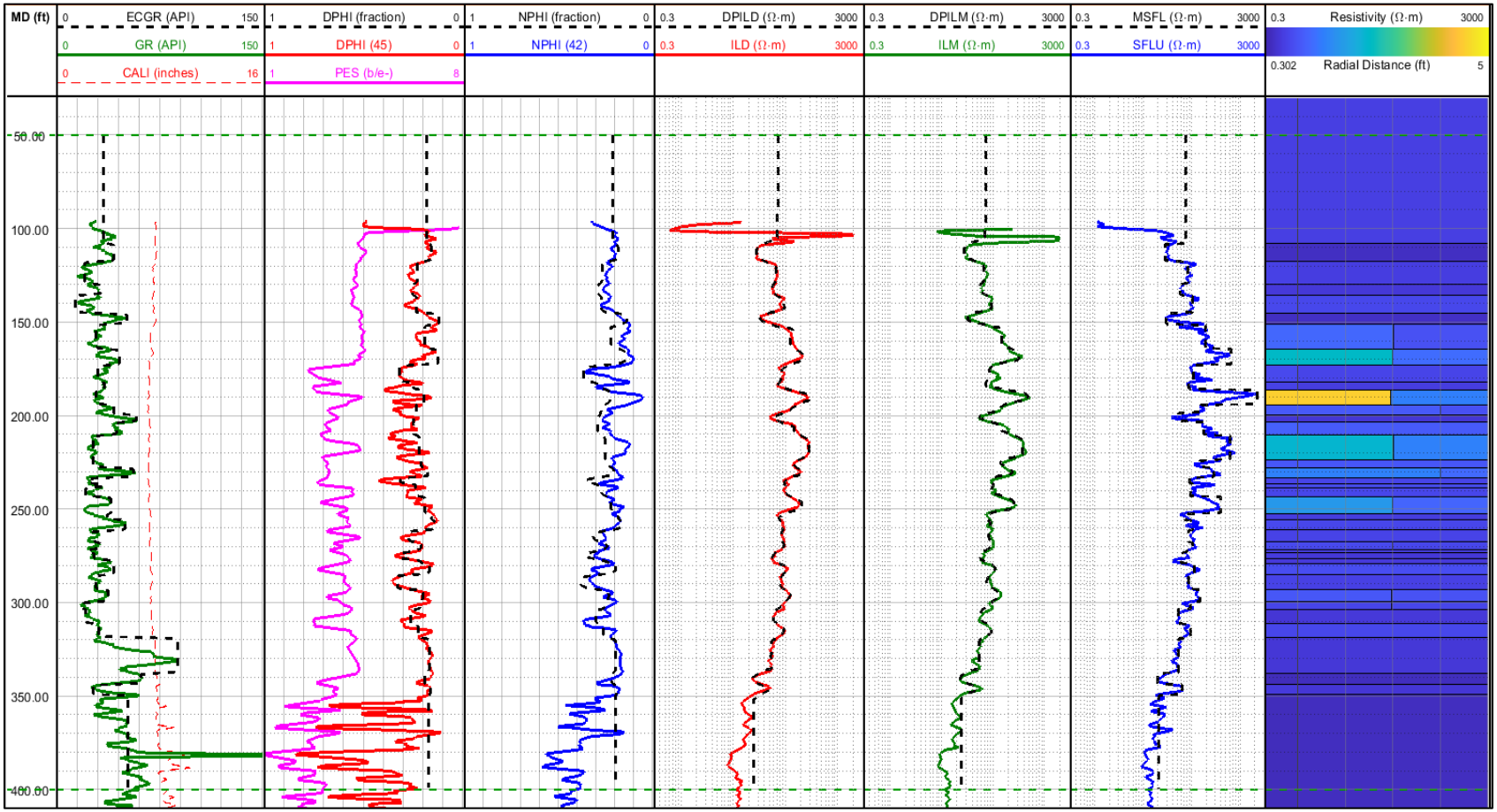

Figure 5-14. Numerical simulation results for Crenwelge Netting #1 well logs in Glen Rose Limestone geological formation. Black dashed line in each track represents the numerical simulation of the respective log.

Table 5-9. Summary of water salinity estimations from the numerical simulation results for the Crenwelge Netting #1 well logs in the Glen Rose Limestone geological formation.

Depth (ft)	R_{mf} [a] (ohm.m)	R_w [b] (ohm.m)	C_{mf} [c] (ppm)	C_w [d] (ppm)[e]	TDS [f] (mg/L)	Method	Error (%)
		1.1647		4,250	6,391	Simulation	0.2
		1.1930		4,142	6,281	Archie's Equation	1.7
190	1.273	1.1040	3,869	4,495	6,639	Resistivity Ratio	3.9
		1.1150		4,450	6,593	Pickett Plot	3.2
		0.9369		5,351	7,500	Spontaneous Potential	17.4

Note: Error calculation assumes input formation water salinity as the true formation water salinity. We use the earth model computed values as inputs to calculate the simulation results using the Archie's equation method. The estimated temperature at the reported depth is 81.85 F. This temperature is used to compute salt concentration and electrical resistivity of mud-filtrate and formation water.
[a] R_{mf} = mud-filtrate resistivity.
[b] R_w = formation water resistivity.
[c] C_{mf} = mud-filtrate salinity.
[d] C_w = formation water salinity.
[e] ppm = parts per million.
[f] TDS = total dissolved solids.

Simulations results and resistivity-based methods offer excellent results for the estimation of formation water salinity. These results are also possible due to the low salinity contrast between the mud-filtrate and the formation water. On the other hand, the SP log shows a higher error. We infer this larger error is caused by the difficulty to assess a proper shale baseline in this rather clean formation.

Cow Creek Limestone

Figure 5-15 displays the stratigraphic section and well logs for the Cow Creek Limestone section. Similarly, Figure 5-16 shows the numerical simulation match of triple-combo well logs, including SP log and PEF log. We follow the same procedure as explained for the GRL simulation. Mud-filtrate invasion modeling is performed between 830 ft MD to 850 ft MD to reproduce the invasion process in this limestone permeable bed. Tracks 10 and 11 in Figure 5-16 exhibit the invaded zone profile for formation resistivity and formation water salinity, respectively.

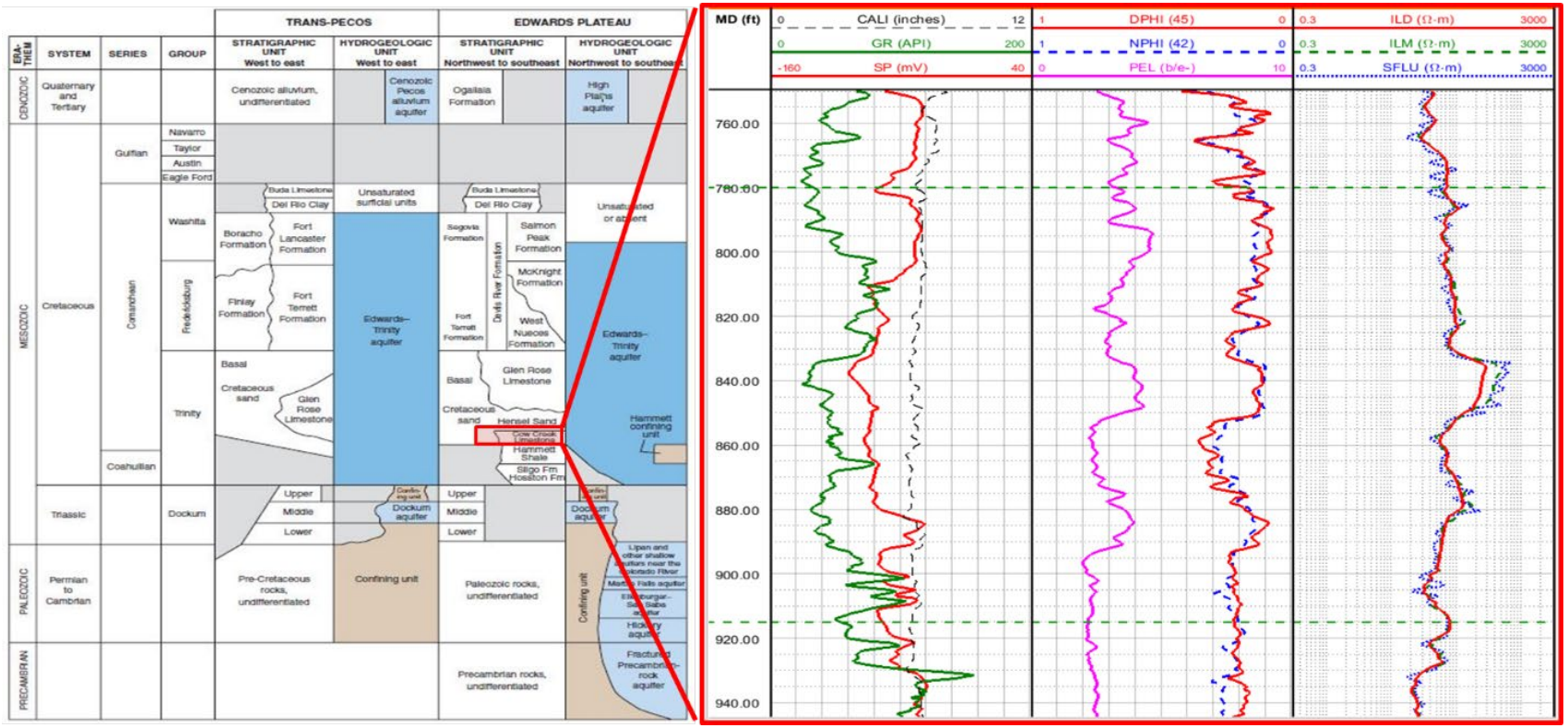

Figure 5-15. Crenwelge Netting #1 geological formations stratigraphy and well logs for Cow Creek Limestone section.

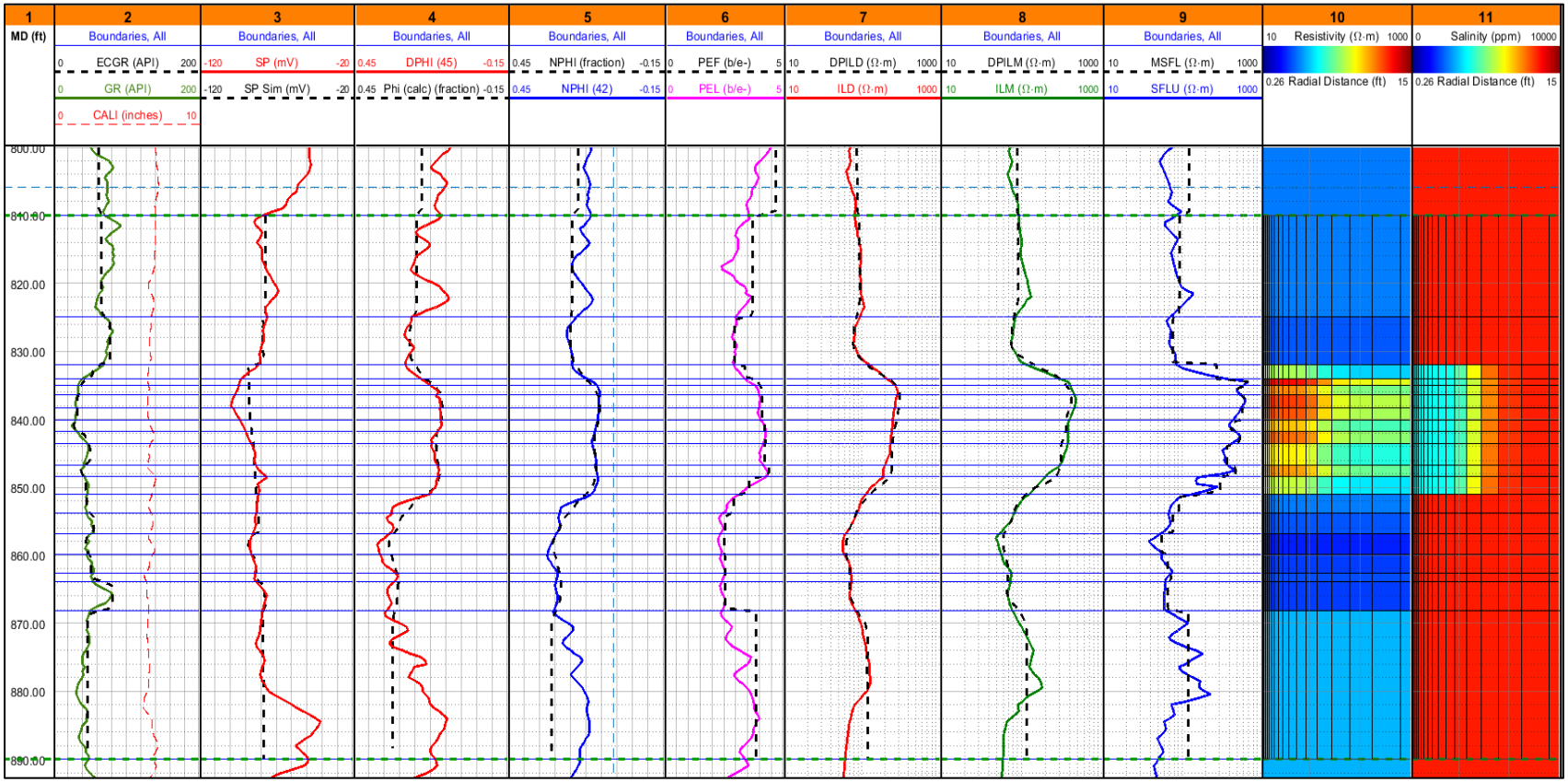

Figure 5-16. Numerical simulation results for Crenwelge Netting #1 well logs in the Cow Creek Limestone geological formation. Black dashed line in each track represents the numerical simulation of the respective log.

Table 5-10 shows the results for CCL formation. Formation water salinity is high with TDS around 10,000 mg/L. CCL model presents a scenario of high salt concentration and high salinity contrast between in-situ water and mud-filtrate. Consistently with the synthetic cases observations, all methods present low errors below 10% and provide good reliability to assess formation water salinity using a complete petrophysical interpretation and well logs simulations. Unfortunately, we cannot implement the Pickett plot method in this section since the porosity is fairly constant.

Table 5-10. Summary of water salinity estimations from the numerical simulation results for the Crenwelge Netting #1 well logs in the Cow Creek Limestone geological formation.

Depth (ft)	R_{mf} [a] (ohm.m)	R_w [b] (ohm.m)	C_{mf} [c] (ppm)	C_w [d] (ppm)[e]	TDS [f] (mg/L)	Method	Error (%)
835	1.180	0.562	3,869	8,500	10,541	Simulation	0.1
		0.587		8,113	10,169	Archie's Equation	3.5
		0.604		7,879	9,943	Resistivity Ratio	5.7
		0.510		10,236	11,441	Spontaneous Potential	8.5

Note: Error calculation assumes input formation water salinity as the true formation water salinity. We use the earth model computed values as inputs to calculate the simulation results using the Archie's equation method. The estimated temperature at the reported depth is 88.82 F. This temperature is used to compute salt concentration and electrical resistivity of mud-filtrate and formation water.
[a] R_{mf} = mud-filtrate resistivity.
[b] R_w = formation water resistivity.
[c] C_{mf} = mud-filtrate salinity.
[d] C_w = formation water salinity.
[e] ppm = parts per million.
[f] TDS = total dissolved solids.

5.4.2 University 44-9-WW #1

The two University wells, University 44-9-WW #1 and University 44-10-WSW #1, are located in Crocket County, in the northwest of the Edwards Plateau geographic subarea. Figure 5-17 displays the stratigraphic and hydrogeologic units of the Edwards Plateau, indicating the stratigraphic section and the geological formations encountered by the well logs of both University wells in the Trinity hydrogeologic unit. In Crockett County, the Trinity hydrogeologic unit is composed mainly of Maxon sands formation, which are basal cretaceous sands. Therefore, we encounter Edwards unit and then we have Maxon sands at the top of Trinity formation. In Figure 5-18 we show a geological correlation for both University wells with their respective sections and formations in Edward's unit. At the top of both wells we find an invaded section in the Segovia formation. Below, we observe two invaded sections in the Fort Terrett carbonates for well University 44-10-WSW#1 and only the upper bed of Fort Terrett formation in well University 44-9-WW#4. This report includes the simulations for Segovia formation and Fort Terrett formation for both University wells.

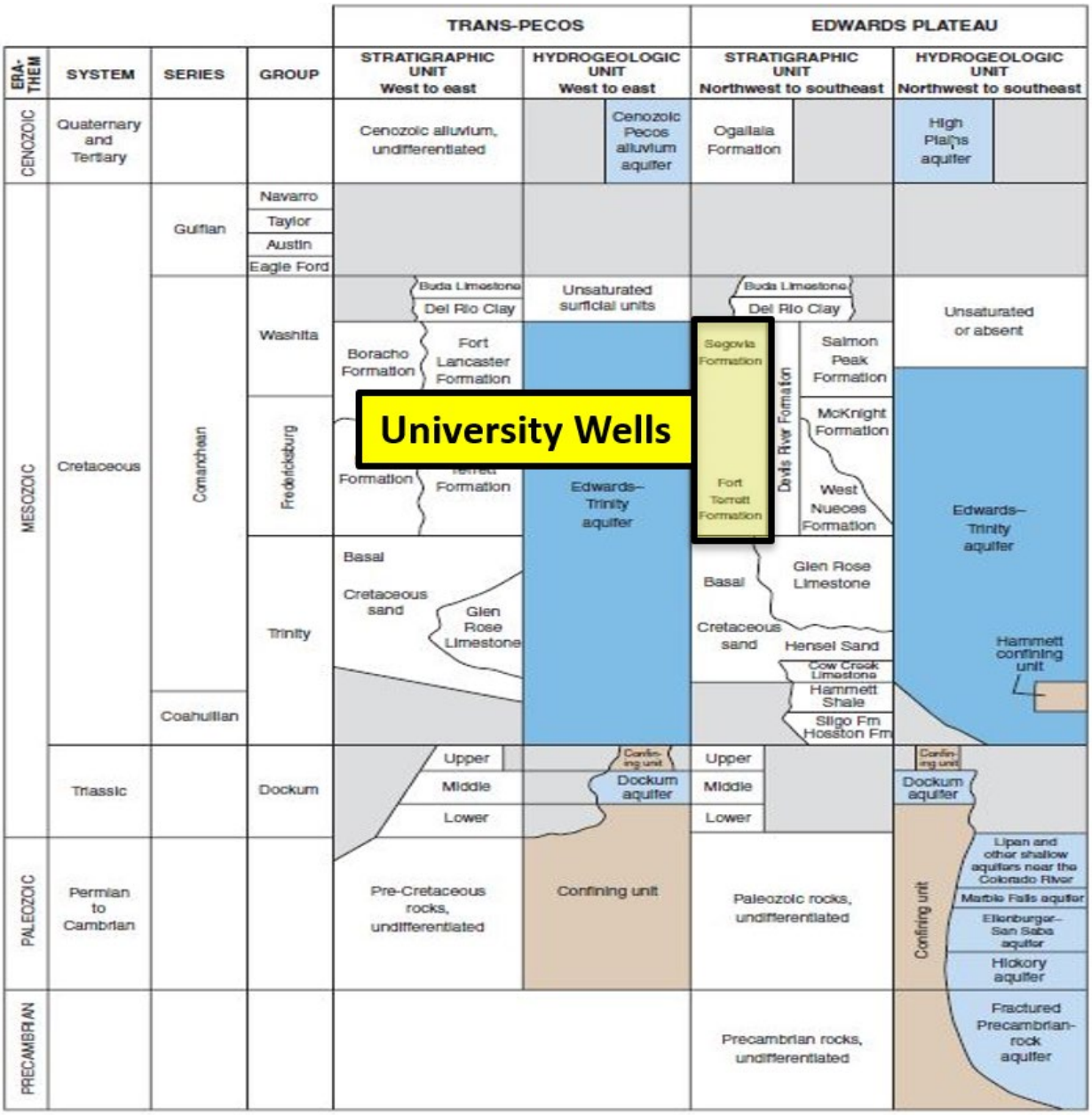

Figure 5-17. University wells stratigraphy. Edwards-Trinity Plateau stratigraphic and hydrogeologic units available in the Trans-Pecos and Edwards Plateau geographic subareas. University wells stratigraphy is highlighted in yellow.

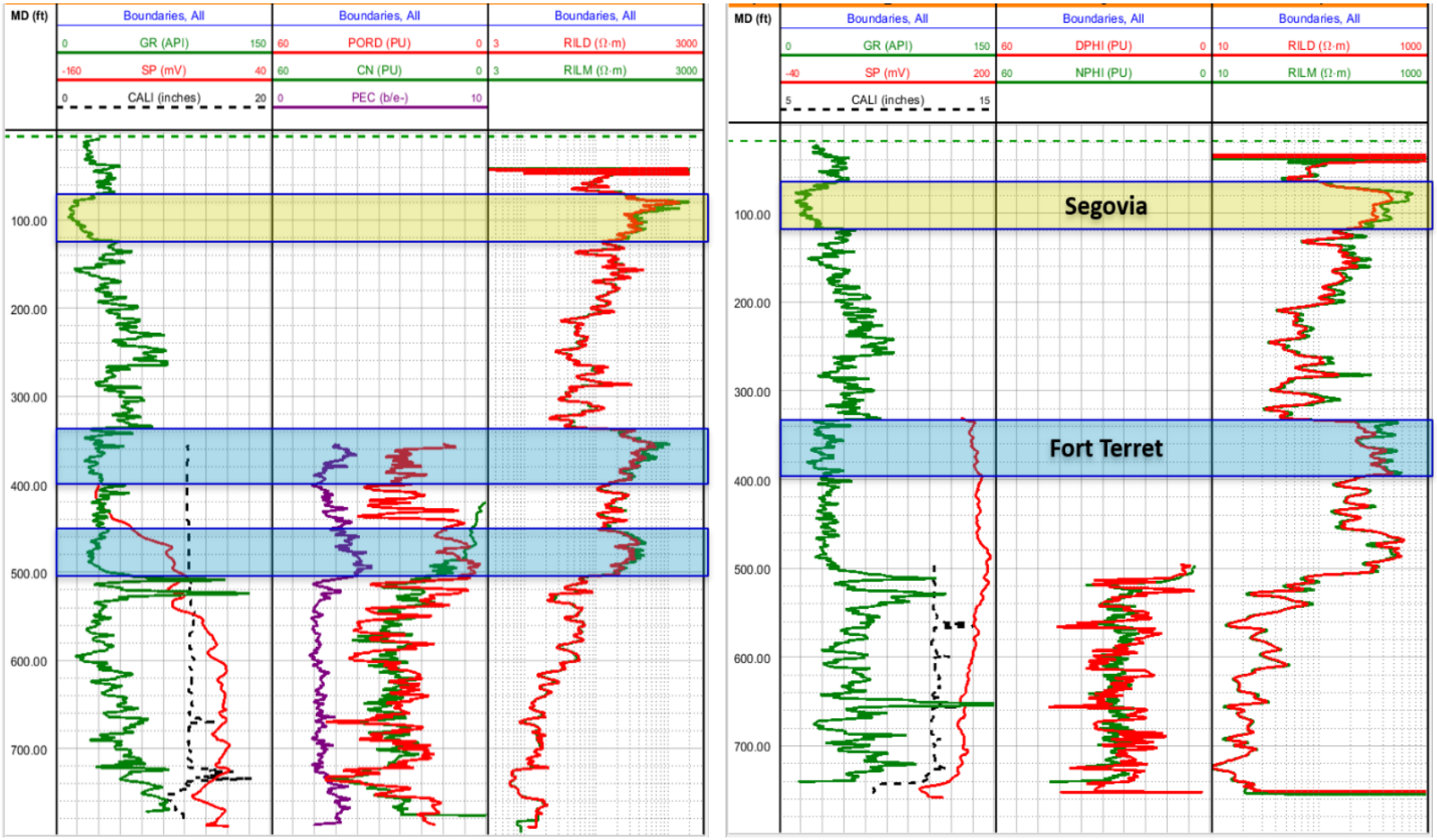

Figure 5-18. **Geological context for the University wells formations and well logs. On the left we present the well logs for University 44-10-WSW#1, and on the right we show the well logs for University 44-9-WW#4. Permeable beds in the Segovia formation are highlighted in light yellow, and the permeable beds in the Fort Terrett formation are highlighted in light blue.**

Segovia

This well's dataset does not include porosity logs or SP log for this section. The Segovia formation comprises three rock classes: upper light-gray limestone, medium brownish-gray dolomite, and lower light-yellowish-gray limestone. Consequently, we use three different m values, which are: m = 3.1 for the upper limestone, m = 2.5 for the medium dolomite, and m = 2.2 for the lower limestone. We estimate these m values with a match and iterations of total porosity and m-exponent as variables in Archie's equation for the invaded zone, assuming S_w = 1, a = 1, and R_{xo} as the medium sensing resistivity log RILM. There are no spherical resistivity log (SFL) available for this well. R_{mf} is obtained from the well log header for both wells. The m value found for the dolomitic limestone rock class measured and reported in Task 4 was 2.638, which is consistent with our medium dolomite m-exponent of 2.5.

We apply this procedure in all sections where porosity logs are not available and there is no SFL. In sections where the SFL is available, we use its electrical resistivity measurements to estimate R_{xo} for the invaded zone. Figure 5-19 shows the numerical simulation results for the well University 44-9-WW #1 in the Segovia formation, and Table 5-11 presents the estimations of formation water salinity using Archie's equation and the simulation model. The resistivity ratio method and the spontaneous potential method are not computed for this section of the well since we do not have a shallow resistivity log and a SP log available. The empirical correlation between water resistivity and TDS for the University wells is shown in equation 14.

$$TDS = 0.66\left(\frac{10{,}000}{R_w\frac{T}{75}}\right) + 58.502 \qquad \text{..... (14)}$$

From Figure 5-19, we observe a complex and variable invasion profile, which translates in high error of the Archie's equation method. In addition, low salt concentration and lack of reliable porosity data increase the uncertainty of the conventional estimations. We circumvent these issues with an adequate simulation of the invasion profile and a match of the available well logs to reduce the uncertainty in our calculations and reduce the error in the assessment of formation water salinity.

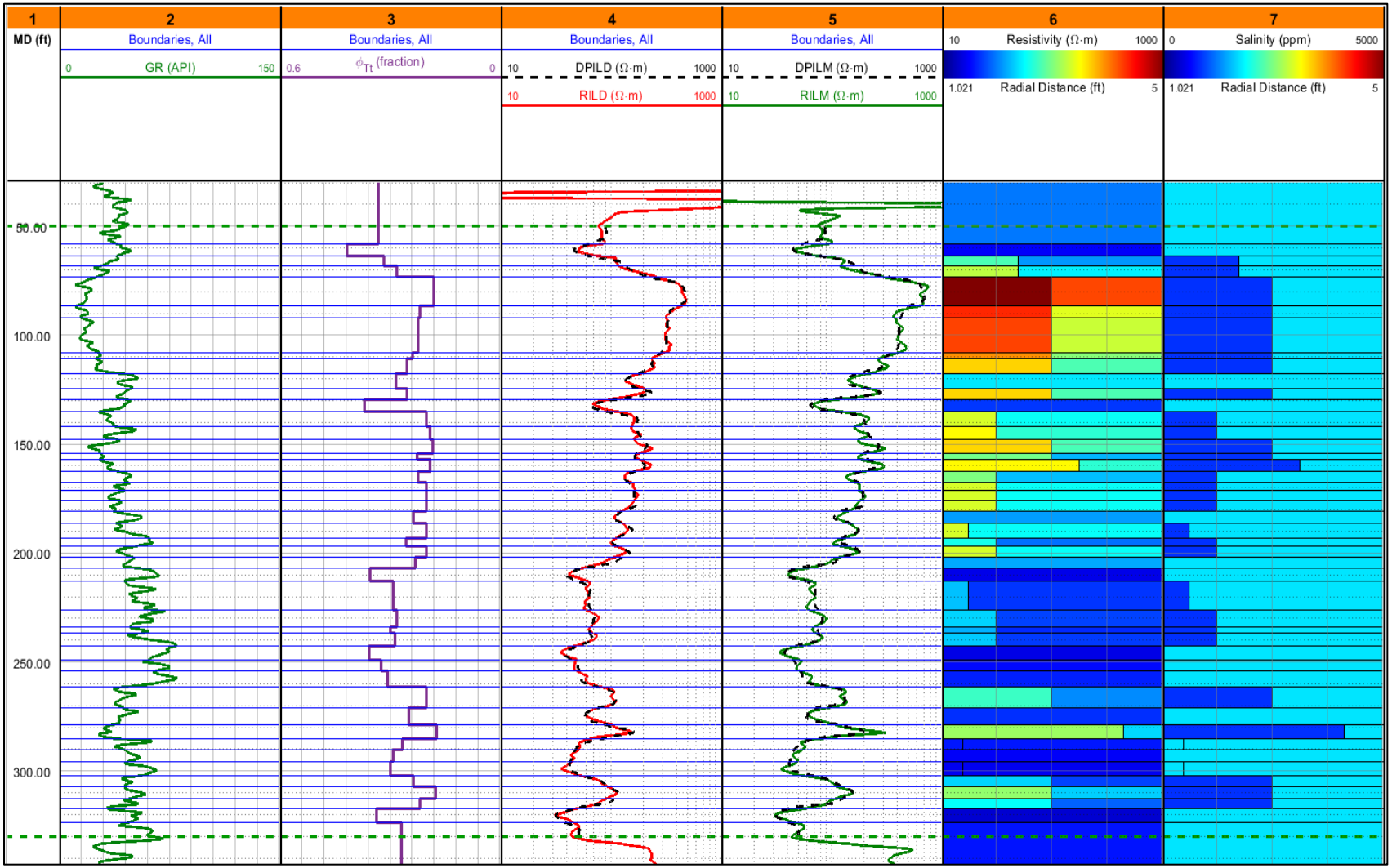

Figure 5-19. Numerical simulation results for the University 44-9-WW#1 well logs in the Segovia geological formation. Black dashed line in each track represents the numerical simulation of the respective log.

Table 5-11. Summary of water salinity estimations from the numerical simulation results for the University 44-9-WW#1 well logs in the Segovia geological formation.

Depth (ft)	R_{mf} [a] (ohm.m)	R_w [b] (ohm.m)	C_{mf} [c] (ppm)	C_w [d] (ppm)[e]	TDS [f] (mg/L)	Method	Error (%)
73	5.846	2.9772	861	1,749	2,313	Simulation	0.1
		2.1136		2,508	3,234	Archie's Equation	39.7

Note: Error calculation assumes input formation water salinity as the true formation water salinity. We use the earth model computed values as inputs to calculate the simulation results using the Archie's equation method. The estimated temperature at the reported depth is 73.74 F. This temperature is used to compute salt concentration and electrical resistivity of mud-filtrate and formation water.
[a] R_{mf} = mud-filtrate resistivity.
[b] R_w = formation water resistivity.
[c] C_{mf} = mud-filtrate salinity.
[d] C_w = formation water salinity.
[e] ppm = parts per million.
[f] TDS = total dissolved solids.

Fort Terrett

This section does not have porosity logs either, but it does have SP and SFL logs. Similar to the Segovia formation rock classes, the Fort Terrett formation comprises three rock classes, which includes an upper limestone, a mid-dolomite, and a lower limestone with gypsum content. However, for this well the only section with separation of resistivity logs is the upper limestone section. We employ an *m*-exponent equal to 3.4. Figure 5-20 displays the well logs match for the well University 44-9-WW #1 in the Fort Terrett formation located at the bottom of the Edwards hydrogeologic unit.

Table 5-12 indicates the results for R_w, water salinity in ppm NaCl, and TDS in ppm estimated with the resistivity-based methods. SP log data is available from the top of Fort Terrett section and it does not provide a SP measurement for the shale baseline. Consequently, the SP log was not investigated for this section, but it was simulated to match the bottom portion of this formation, and to corroborate the estimations of total porosity and the *m*-exponent.

Formation water salinity of both Fort Terrett and Segovia formations are very similar. However, the error in the estimation of Fort Terrett is significantly decreased due to the availability of a more robust well logs dataset. The addition of shallow resistivity logs and SP log positively impacts the accuracy in the assessment of salt concentration.

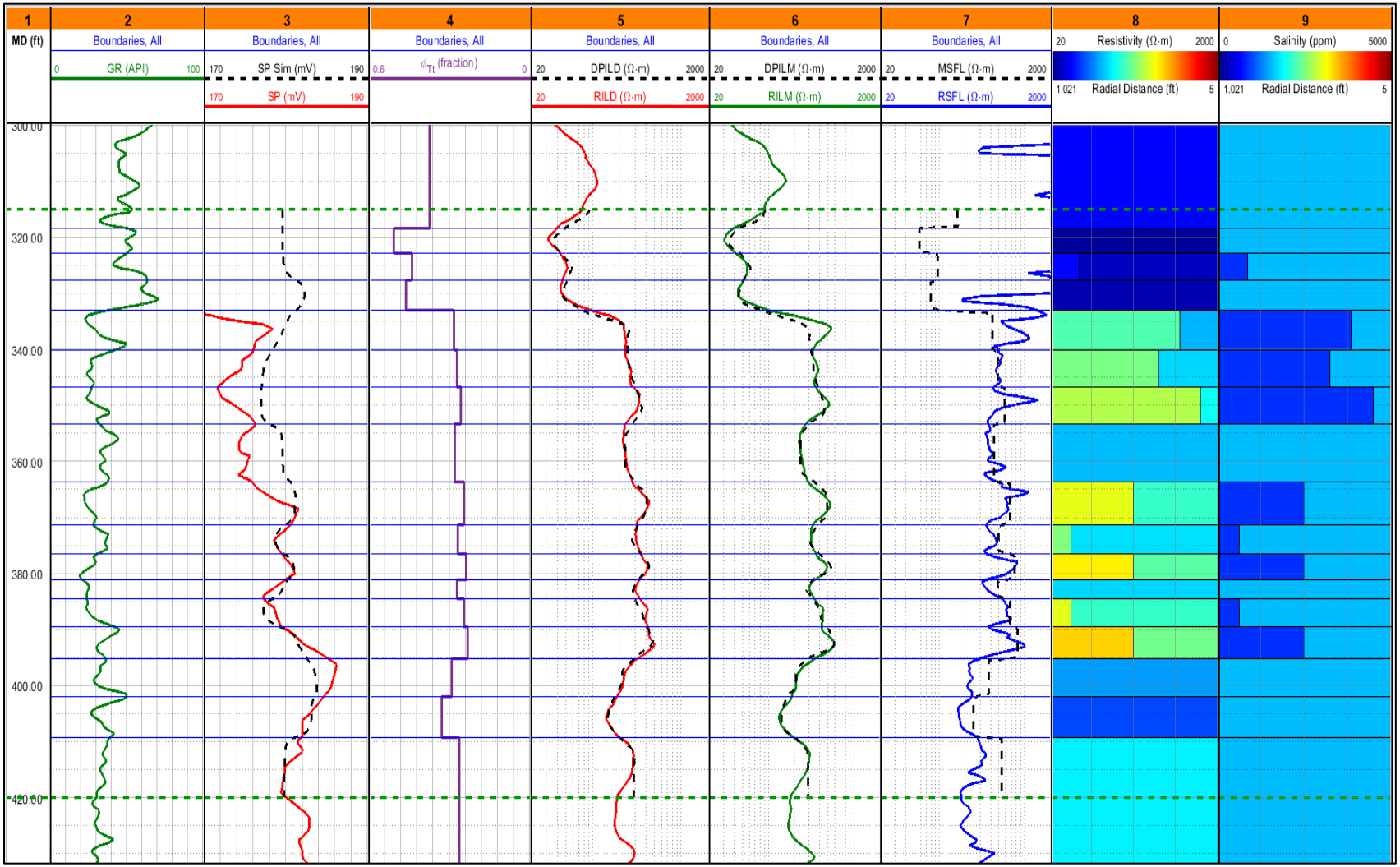

Figure 5-20. Numerical simulation results for the University 44-9-WW#1 well logs in the Fort Terrett geological formation. Black dashed line in each track represents the numerical simulation of the respective log.

Table 5-12. Summary of water salinity estimations from the numerical simulation results for the University 44-9-WW#1 well logs in the Fort Terrett geological formation.

Depth (ft)	R_{mf} [a] (ohm.m)	R_w [b] (ohm.m)	C_{mf} [c] (ppm)	C_w [d] (ppm)[e]	TDS [f] (mg/L)	Method	Error (%)
		3.2409		1,545	2,057	Simulation	0.3
368	5.657	3.6262	861	1,373	1,845	Archie's Equation	10.6
		3.8484		1,290	1,742	Resistivity Ratio	15.6

Note: Error calculation assumes input formation water salinity as the true formation water salinity. We use the earth model computed values as inputs to calculate the simulation results using the Archie's equation method. The estimated temperature at the reported depth is 76.42 F. This temperature is used to compute salt concentration and electrical resistivity of mud-filtrate and formation water.
[a] R_{mf} = mud-filtrate resistivity.
[b] R_w = formation water resistivity.
[c] C_{mf} = mud-filtrate salinity.
[d] C_w = formation water salinity.
[e] ppm = parts per million.
[f] TDS = total dissolved solids.

5.4.3 University 44-10-WSW #4

The left-side well logs on Figure 5-18 illustrates the geological interpretation and context of the well University 44-10-WSW #4. As observed, the electrical resistivity logs separate at the top of the Segovia formation and at the top and bottom sections of the Fort Terrett formation. We simulate these two formations to estimate the water salinity in these aquifers.

Segovia

Similar to the previous University well, the simulation section in the Segovia formation do not have porosity logs, SP log, and spherical resistivity log. We simulate the upper section of the Segovia formation with an estimated m = 3.1 (same as previous well). Figure 5-21 shows the simulation model for this well section, and Table 5-13 presents the results for Archie's equation. Again, the other methods cannot be implemented because of the lack of well logs curves.

Similar to the Segovia formation in well University 44-9-WW#1, the error in the determination of salt concentration is considerably high for the Archie's equation method. A complex invasion profile and insufficient well logs and petrophysical data originate this large error.

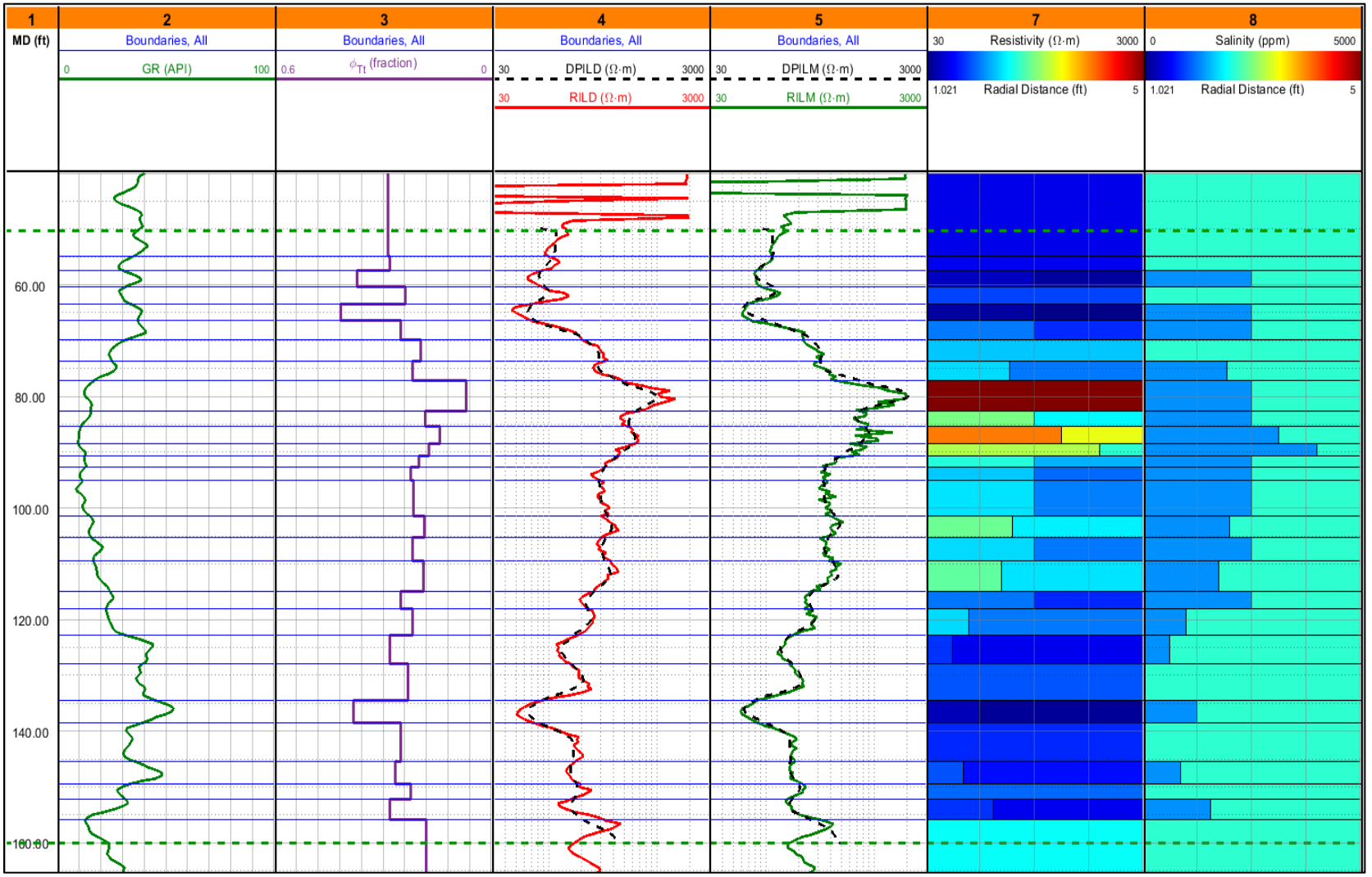

Figure 5-21. Numerical simulation results for the University 44-10-WSW#4 well logs in the Segovia geological formation. Black dashed line in each track represents the numerical simulation of the respective log.

Table 5-13. Summary of water salinity estimations from the numerical simulation results for the University 44-10-WSW#4 well logs in the Segovia geological formation.

Depth (ft)	R_{mf} [a] (ohm.m)	R_w [b] (ohm.m)	C_{mf} [c] (ppm)	C_w [d] (ppm)[e]	TDS [f] (mg/L)	Method	Error (%)
85	3.744	2.4443	1,342	2,102	2,739	Simulation	0.1
		1.6277		3,226	4,083	Archie's Equation	49.2

Note: Error calculation assumes input formation water salinity as the true formation water salinity. We use the earth model computed values as inputs to calculate the simulation results using the Archie's equation method. The estimated temperature at the reported depth is 75.56 F. This temperature is used to compute salt concentration and electrical resistivity of mud-filtrate and formation water.
[a] R_{mf} = mud-filtrate resistivity.
[b] R_w = formation water resistivity.
[c] C_{mf} = mud-filtrate salinity.
[d] C_w = formation water salinity.
[e] ppm = parts per million.
[f] TDS = total dissolved solids.

Fort Terrett

This well section comprises a full dataset of acquired triple-combo logs, rendering the most complete dataset of the four well logs sections evaluated for the University wells. We simulate the complete Fort Terret formation, and we encounter three distinct rock classes according to the observations of the core samples reported in Task 2. In order to account for these rock classes, we use three different *m*-exponent values, which are $m = 3.4$ for the upper limestone, $m = 2.3$ for the dolomitic limestone rock class, and $m = 1.7$ for the lower carbonates with gypsum content. The estimated water salinity is 2000 ppm NaCl. Figure 5-22 displays the simulation results and the invasion profile after matching the available well logs.

Table 5-14 compare the results in the assessment of formation water salinity for the resistivity-based methods. Even though we have a more robust well logs dataset, the SP log and the shallow resistivity logs are available only for the bottom portion of the Fort Terrett formation, below 400 ft MD. Consequently, the SP method cannot be implemented because it is not available to define a shale baseline and a variation in the spontaneous potential of the aquifer section. On the other hand, the availability of the shallow resistivity log permits to estimate a more reliable water salinity using the resistivity ratio method.

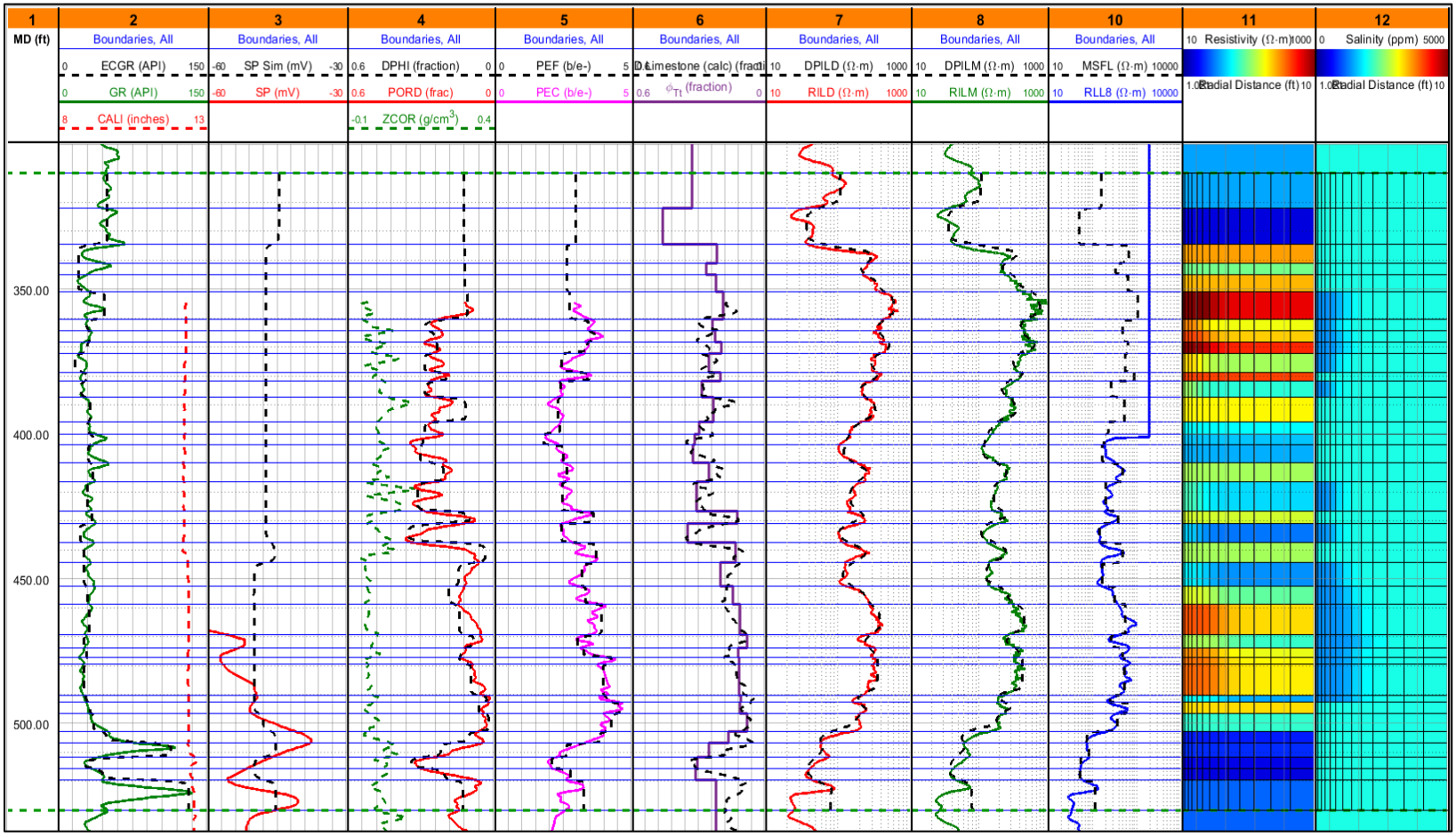

Figure 5-22. Numerical simulation results for the University 44-10-WSW#4 well logs in the Fort Terrett geological formation. Black dashed line in each track represents the numerical simulation of the respective log.

Table 5-14. Summary of water salinity estimations from the numerical simulation results for University 44-10-WSW#4 well logs in the Fort Terrett geological formation.

Depth (ft)	R_{mf} [a] (ohm.m)	R_w [b] (ohm.m)	C_{mf} [c] (ppm)	C_w [d] (ppm)[e]	TDS [f] (mg/L)	Method	Error (%)
		2.4853		2,000	2,608	Simulation	0.0
479	3.632	2.1730	1,342	2,304	2,975	Archie's Equation	14.0
		2.2945		2,175	2,820	Resistivity Ratio	8.1

Note: Error calculation assumes input formation water salinity as the true formation water salinity. We use the earth model computed values as inputs to calculate the simulation results using the Archie's equation method. The estimated temperature at the reported depth is 78.11 F. This temperature is used to compute salt concentration and electrical resistivity of mud-filtrate and formation water.
[a] R_{mf} = mud-filtrate resistivity.
[b] R_w = formation water resistivity.
[c] C_{mf} = mud-filtrate salinity.
[d] C_w = formation water salinity.
[e] ppm = parts per million.
[f] TDS = total dissolved solids.

5.4.4 Reeves-State #1

This well is located in Reeves County, in the Trans-Pecos region to the northwest sector of our study area. Figure 5-23 shows the stratigraphic and hydrogeologic units of the Edwards Plateau, indicating the stratigraphic section and the geological formations encountered by Reeves-State #1. Within the Trinity hydrogeologic unit, we encounter the Lower Cretaceous sands, which are clean sandstones with a rock composition varying from quartz to calcareous material. Likewise, Figure 5-24 illustrates the digitized triple combo logs with additional interpretations for porosity, NaCl salinity, temperature, shale volume, water resistivity, and mud resistivity available in the LAS files. These are preliminary interpretations that were not performed by any member of the TWDB or UT-Austin. They were originally received in the well logs' files.

We match the resistivity logs and the SP log assuming shallow invasion since there is no available medium resistivity log to validate the salt concentration distribution of the invaded region. We use the R_{mf} reported in the well header even though this measurement has inconsistencies within the header report. Figure 5-25 and Table 5-15 present the well logs simulation results.

The LAS interpretations of shale volume, porosity, NaCl salinity, and Rw are in tracks 2, 4, 7, and 8, respectively. Spontaneous potential log and resistivity logs, both LAS and simulated, are in tracks 3, 5 and 6. We match these logs using an *m*-exponent of 2 for a proper representation of the sandstone lithology of the Lower Cretaceous formation. We assume a clean matrix and use Archie's equation to solve for resistivities, despite the considerable shale volume available in the given petrophysical interpretation. We could not

confirm the origin of this interpretation and high shale concentrations are not consistent with the GR log response. The following equation presents an empirical correlation between R_w and TDS for Reeves-State #1.

$$TDS = 0.7461\left(\frac{10{,}000}{R_w\frac{T}{75}}\right) \quad \text{..... (15)}$$

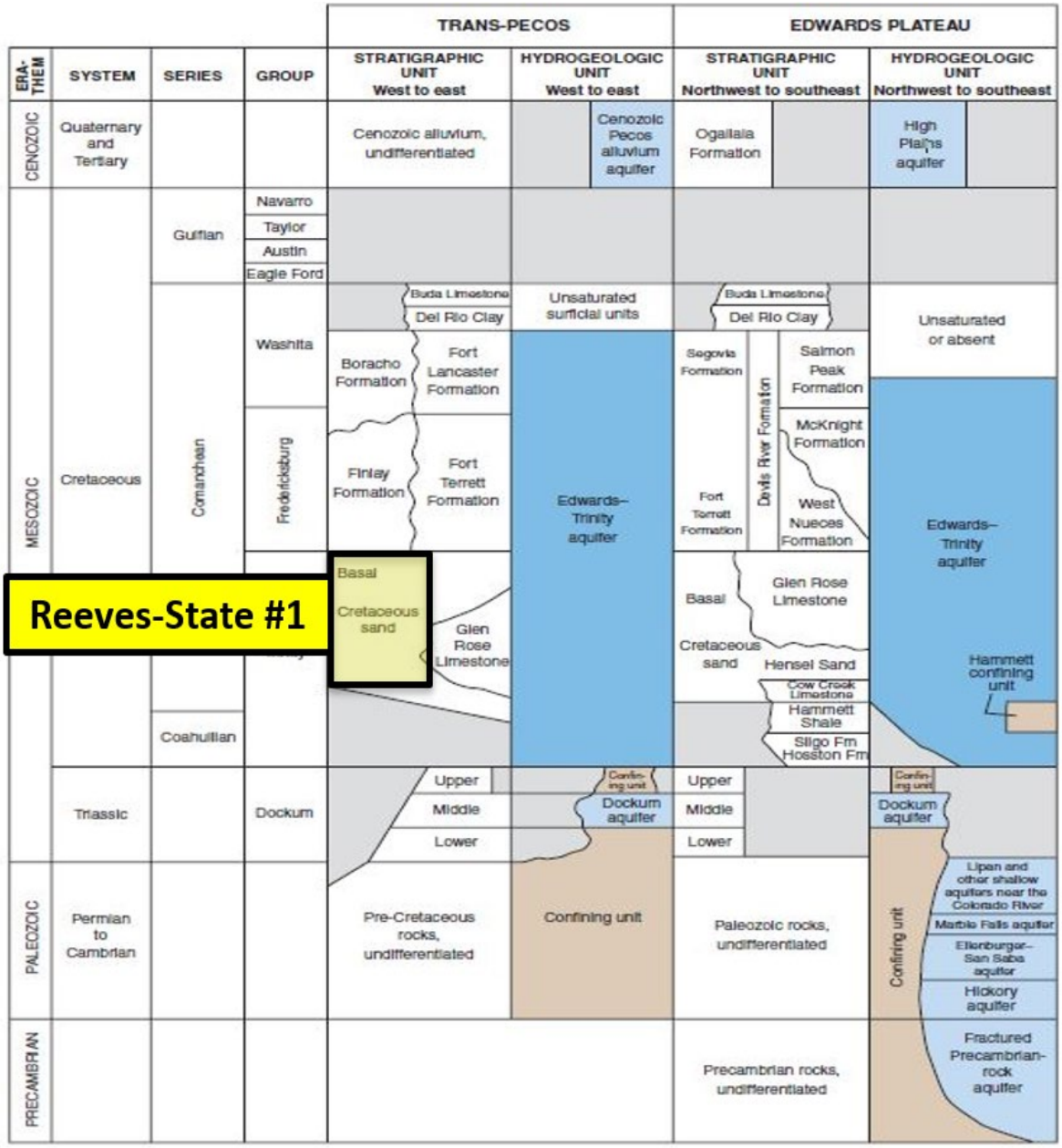

Figure 5-23. Reeves-State #1 stratigraphy. Edwards-Trinity Plateau stratigraphic and hydrogeologic units available in the Trans-Pecos and Edwards Plateau geographic subareas. Reeves-State #1 stratigraphy is highlighted in yellow.

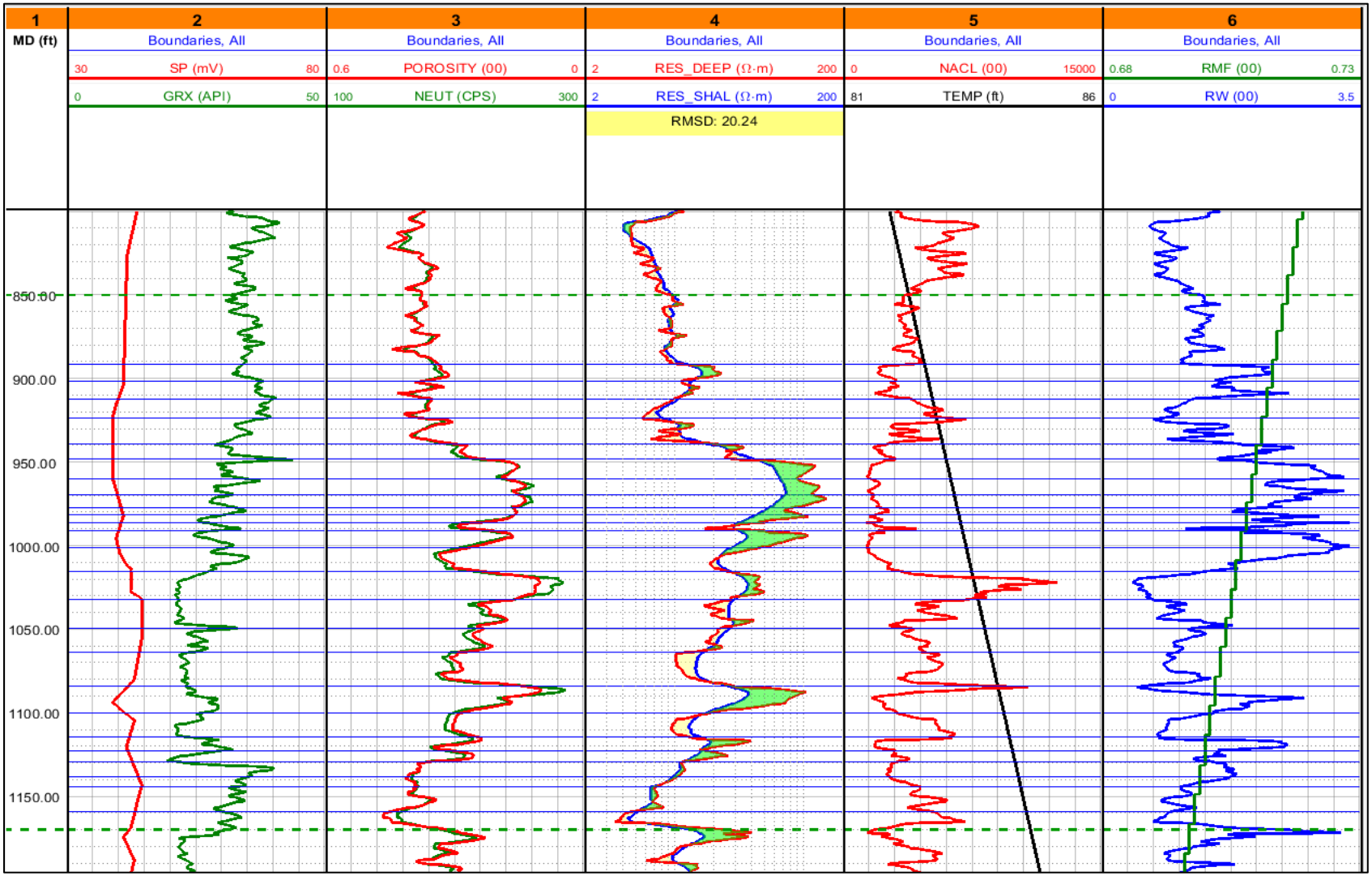

Figure 5-24. Reeves-State #1 well logs.

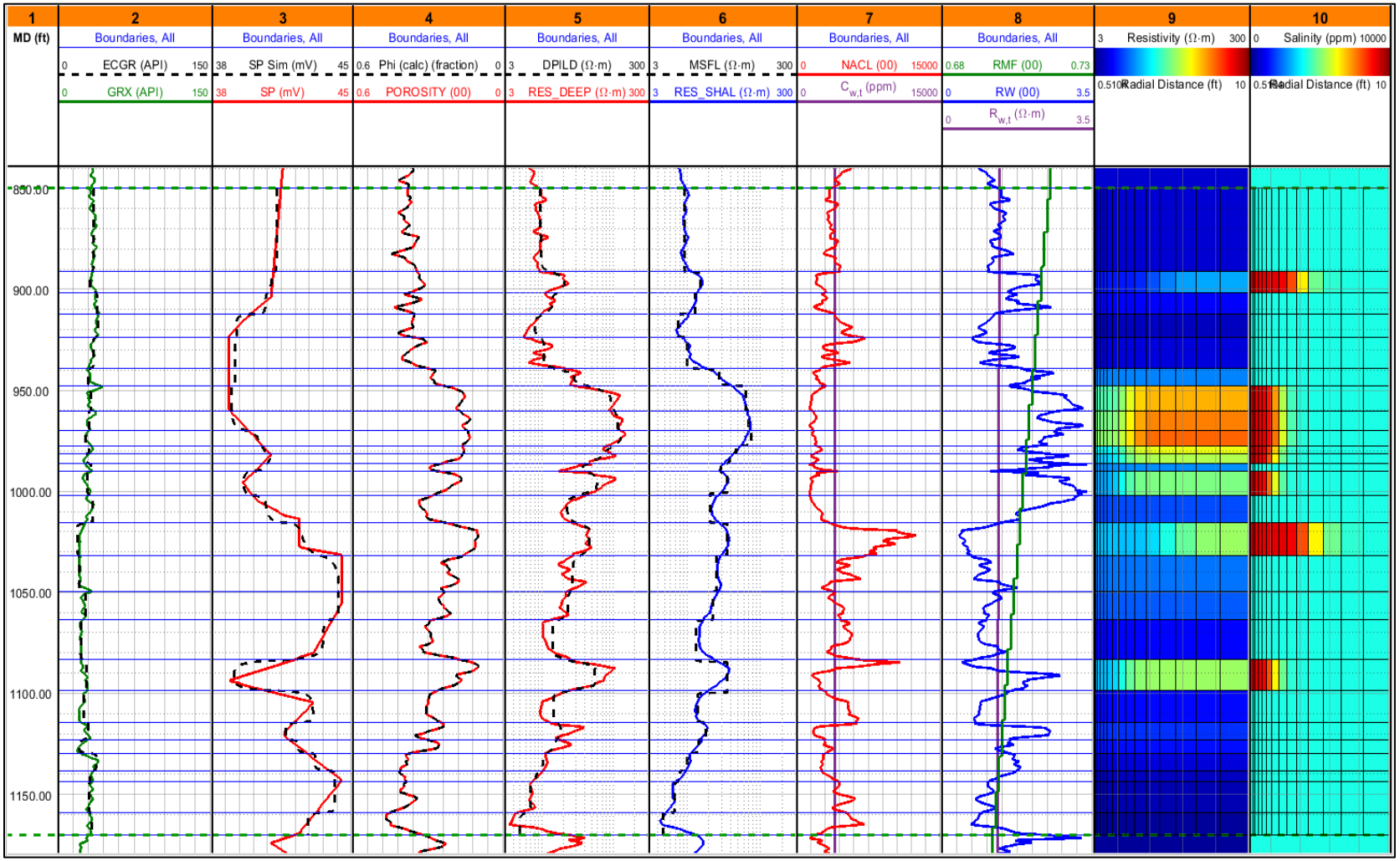

Figure 5-25. Numerical simulation results for the Reeves-State #1 well logs. Black dashed line in each track represents the numerical simulation of the respective log.

Table 5-15. Summary of water salinity estimation from the numerical simulation results for the Reeves State #1 well logs.

Depth (ft)	R_{mf} [a] (ohm.m)	R_w [b] (ohm.m)	C_{mf} [c] (ppm)	C_w [d] (ppm)[e]	TDS [f] (mg/L)	Method	Error (%)
970	0.618	1.3586	9,030	3,916	5,468	Simulation	2.0
		0.9647		5,626	7,701	Archie's Equation	38.0
		0.9566		5,677	7,766	Resistivity Ratio	39.2
		0.9190		5,924	8,084	Spontaneous Potential	44.9

Note: Error calculation assumes input formation water salinity as the true formation water salinity. We use the earth model computed values as inputs to calculate the simulation results using the Archie's equation method. The estimated temperature at the reported depth is 75.32 F. This temperature is used to compute salt concentration and electrical resistivity of mud-filtrate and formation water.
[a] R_{mf} = mud-filtrate resistivity.
[b] R_w = formation water resistivity.
[c] C_{mf} = mud-filtrate salinity.
[d] C_w = formation water salinity.
[e] ppm = parts per million.
[f] TDS = total dissolved solids.

In general, the error in the estimation of formation water salinity is high for all conventional methods. Even the simulation results present its higher error among all simulated wells with 2%. These high uncertainties rely on the quality of the shallow resistivity and the unreliability of the interpreted porosity and shale concentration. These issues with the GR log also escalate to the quantification of salt concentration using the SP method, which could be an interesting method to corroborate the results and assess the formation factor. However, the uncertainty in shale characterization limits the reliability of this method and the identification of an adequate shale baseline.

5.4.5 Earl Vest #1

Very close to Reeves-State #1, we have another well for simulation in Reeves County. The well logs dataset for Earl Vest #1 only includes SP log and laterolog resistivity logs (long normal and short normal). We correlate this well with Reeves-State #1, and its respective modeling intervals from 650 ft MD to 950 ft MD. Figure 5-26 displays this correlation using SP log and resistivity logs. As we observe, Earl Vest #1 shows higher shallow resistivity than deep resistivity, which implies a higher salt concentration in formation water than in mud-filtrate. This pose a different scenario than well Reeves-State #1 where formation water salinity was lower than mud-filtrate salinity. Since both wells are located in the same geographic area and show great geologic correlation of the aquifers, we would assume similar a salt concentration in the formation water. This suggests that the difference in the resistivity logs profile is due to the mud-filtrate salinity. However, Earl Vest #1 log header does not provide reliable measurements of T and R_{mf}. We communicate issue with the TWDB and we obtained an estimated R_{mf} of 0.52 at 75 F, estimated from correlations for other Reeves County wells. This mud-filtrate resistivity at this temperature conditions

results in a mud-filtrate salinity of 10,917 ppm NaCl, which is similar to the value computed for well Reeves-State #1. Nevertheless, this mud-filtrate salinity implies an even higher formation water salinity for Earl Vest #1 Lower Cretaceous sands. Indeed, if we perform a quick resistivity ratio calculation at 783 ft MD, we determine a salt concentration of 16,715 ppm NaCl. This value is extremely high compared with the expected salinity for these sandstones in Reeves County, and with the results reported on Table 5-15 for neighbor well Reeves-State #1. Consequently, we develop a synthetic case to understand the observations extracted from the available well logs acquired in these two wells located in Reeves County, and evaluate the effect of induction and laterolog electrical resistivity measurements in the preliminary results of these wells.

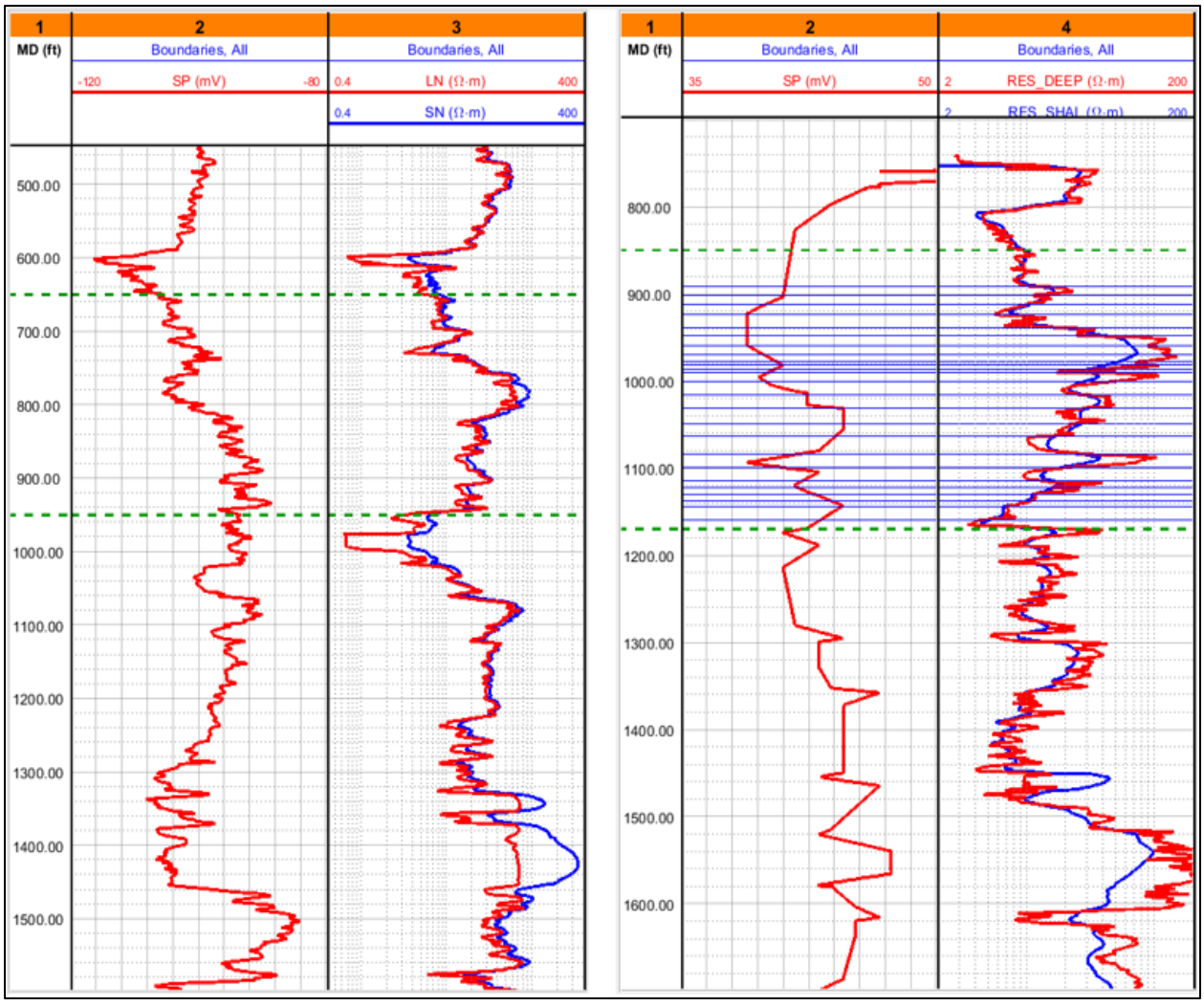

Figure 5-26. **Earl Vest #1 and Reeves-State #1 well logs correlation. Earl Vest #1 well logs are on the left image from tracks 1 to 3, presenting measured depth, SP log, and laterolog resistivities, respectively. Reeves-State #1 well logs are on the image to the right, including measured depth in track 1, SP log in track 2, and induction resistivity logs in track 3.**

Resistivity tools responses

Figure 5-27 and Table 5-16 include the simulation results for three different cases for wells Reeves-State #1, Earl Vest #1, and a purely synthetic model. These modeling renders 9 scenarios shown in layers 1 to 9. Each case is explained as follows:

- Resistivity Ratio: Uses the well logs resistivities and the estimated mud-filtrate resistivity to adjust the formation factor. We assume a clean sandstone with m = 2, and we estimate the total porosity by matching the earth model resistivities using Archie's equation. In this scenario, water salinity is estimated from the resistivity ratio method. This scenario is displayed in layers 1, 4, and 7.
- Shaly Sandstones: We have an uncertainty in shale concentration due to the uncertainties in Reeves-State #1 petrophysical interpretation and the lack of GR log in the Earl Vest #1 well logs. Therefore, we reproduce a case with shale concentration = 0.3. We change the saturation model to the one proposed by Juhasz (1979) using a = 1 and m = 2. We estimate the total porosity by matching the shallow resistivity log. Subsequently, we assume this estimated porosity as the true porosity, and we adjust the formation water salinity in the earth model to match the deep resistivity log. In this scenario, the water salinity is estimated from the simulations output. This scenario is shown in layers 2, 5, and 8.
- Match: This scenario includes the same assumptions as the Resistivity Ratio scenario. In addition, we adjust the formation water salinity in the earth model to match the deep resistivity log. In this scenario, the water salinity is estimated from the numerical simulation results. This scenario is available in layers 3, 6, and 9.

We perform these scenarios for both Reeves County wells, and we label them in track 2 as EV #1 for Earl Vest #1 (layers 1 to 3 highlighted in light blue), and RS #1 for Reeves-State #1 (layers 7 to 9 highlighted in light green). Between these wells, we develop an ideal case varying the formation water salinity at a constant mud-filtrate salinity (highlighted in yellow). On layer 4, we have a case where formation water salinity is higher than filtrate salinity ($R_w < R_{mf}$); on layer 5, we have equal salinities; and on layer 6 we have lower formation water salinity than mud-filtrate salinity ($R_w > R_{mf}$).

From these synthetic cases, we corroborate our observation regarding high variations in salinity from the two wells located in Reeves County. Differences between laterolog and induction resistivity logs, and presence of shale do not explain the salinity variations for this particular case. In fact, both scenarios would increase the salinity difference as shown in the higher salt concentrations computed for layers 2 and 3 with respect to layer 1, and layers 8 and 9 with respect to layer 7. This reinforces the hypothesis of severe issues in the information related to electrical measurements of the mud-filtrate salinity of Earl-Vest #1. Likewise, laterolog performance and uncertainty in freshwater aquifers pose problems for computing formation water salinity and modeling this well. Therefore, Earl-Vest #1 is removed from the simulations and is not considered for the results of this report. Nevertheless, we use this well to validate the observations and simulation outcomes of well Reeves-State #1.

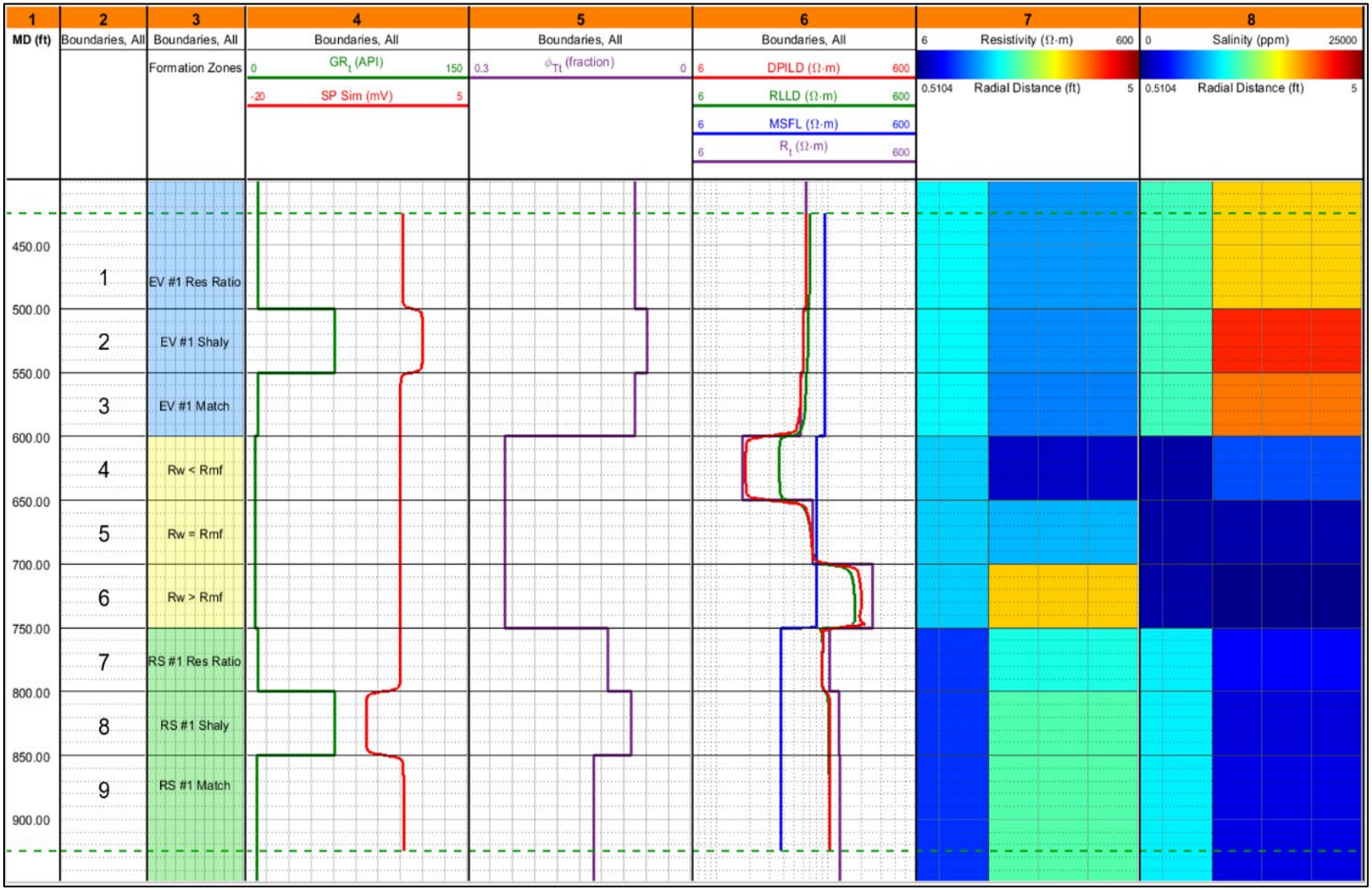

Figure 5-27. Synthetic case comparing induction resistivity and laterolog tools.

Table 5-16. Input parameters for the Reeves County synthetic models.

Layer	Scenario	Depth (ft)	C_{mf} [a] (ppm) [b]	C_w [c] (ppm) [b]	R_{mf} [d] (ohm.m)	R_w [e] (ohm.m)	$\emptyset$ [f]
1	Res. [g] Ratio	450	10,917	16,715	0.5349	0.3604	0.0750
2	Shaly SS [h]	500	10,917	21,000	0.5349	0.2923	0.0585
3	Match	550	10,917	19,000	0.5349	0.3203	0.0750
4	$R_w < R_{mf}$	600	1,000	5,000	4.9896	1.0825	0.2500
5	$R_w = R_{mf}$	650	1,000	1,100	4.9896	4.5566	0.2500
6	$R_w > R_{mf}$	700	1,000	300	4.9896	15.7283	0.2500
7	Res. [g] Ratio	750	9,030	3,915	0.4707	1.2883	0.1110
8	Shaly SS [h]	800	9,030	2,300	0.4707	1.7127	0.0795
9	Match	850	9,030	2,475	0.4707	2.1675	0.1300

Note: All depths are top-layer's depth. Water resistivities and salt concentrations are computed at their respective temperatures according to the geothermal gradient of Reeves-State #1 well, which is the only available and reliable information for formation temperature. Earl Vest #1 cases are available from layers 1 to 3. Ideal model cases are available from layers 4 to 6. Reeves-State #1 cases are available from layers 7 to 9.

[a] C_{mf} = mud-filtrate salinity.

[b] ppm = parts per million.

[c] C_w = formation water salinity.

[d] R_{mf} = mud-filtrate resistivity.

[e] R_w = formation water resistivity.

[f] $\emptyset$ = total porosity.

[g] Res. = resistivity.

[h] SS = sandstone.

Reeves-State #1 validation using Earl Vest #1 model

We use Earl Vest #1 for validating the results of Reeves-State #1. Basically, we assume the same rock classes and petrophysical trends correlate between the wells. We estimate the formation factor and mud-filtrate resistivity from the SP log, and we utilize this input as the initial guess for water resistivity and total porosity. We adjust and update these parameters by matching the electrical resistivity logs and the SP log along with the invasion simulations. The lower part of the SP log is not possible to match at the same time with the upper section, which is probably due to an increase in shale concentration. Unfortunately, we do not have a GR log available to confirm this response or to properly assess shale concentration. Figure 5-28 shows the simulated match of the available well logs and the invasion front. Table 5-17 compares the calculations for water salinity in ppm NaCl and TDS using different methods. We compute TDS from water resistivity using equation 15.

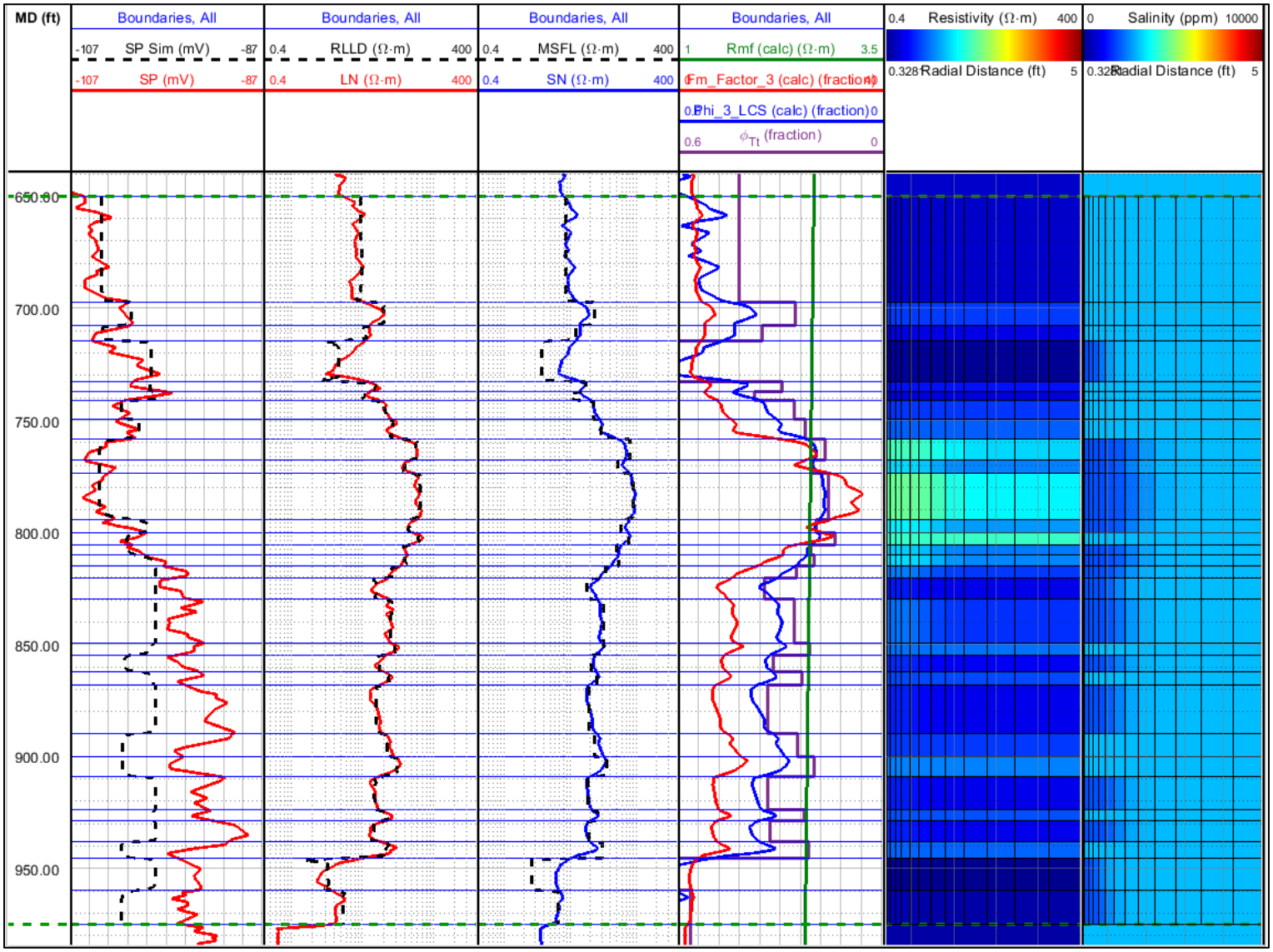

Figure 5-28. Numerical simulation results for the Earl Vest #1 well logs. Black dashed line in each track represents the numerical simulation of the respective log.

Table 5-17. Summary of water salinity estimations from the numerical simulation results for the Earl Vest #1 well logs.

Depth (ft)	R_{mf} [a] (ohm.m)	R_w [b] (ohm.m)	C_{mf} [c] (ppm)	C_w [d] (ppm)[e]	TDS [f] (mg/L)	Method	Error (%)
783	2.623	1.4622	2,025	3,749	5,263	Simulation	0.0
		1.5821		3,449	4,864	Archie's Equation	7.6
		1.7509		3,099	4,395	Resistivity Ratio	16.5
		1.5522		3,402	4,957	Spontaneous Potential	5.8

Note: Error calculation assumes input formation water salinity as the true formation water salinity. We use the earth model computed values as inputs to calculate the simulation results using the Archie's equation method. The estimated temperature at the reported depth is 72.72 F. This temperature is used to compute salt concentration and electrical resistivity of mud-filtrate and formation water.
[a] R_{mf} = mud-filtrate resistivity.
[b] R_w = formation water resistivity.
[c] C_{mf} = mud-filtrate salinity.
[d] C_w = formation water salinity.
[e] ppm = parts per million.
[f] TDS = total dissolved solids.

5.4.6 Mendel Estate #1

Mendel Estate #1 is also located to the northwest of the study area in the Trans-Pecos region. This Pecos County well exhibits an inverted electrical resistivity profile when passing from the Fort Terrett formation at the bottom of Edwards unit to the Lower Cretaceous sands at the top of the Trinity hydrogeologic unit. At the Edwards unit, the deep sensing resistivity response is larger than the shallow sensing resistivity, indicating higher salt concentration in the mud-filtrate than in the formation water. Conversely, the deep sensing resistivity response is lower than the shallow sensing resistivity in the Trinity unit, indicating lower salt concentration in the mud-filtrate than in the formation water. Since both sections were drilled with the same mud properties, Edwards contains a lower salinity water than Trinity. This resistivity signature allows to identify the limit between these two formations and hydrogeologic units. Figure 5-29 shows the available well logs, where we identify the shale located from 380 ft MD to 405 ft MD as the boundary between both hydrogeologic units.

In addition, the information received for Mendel Estate #1 contains a preliminary petrophysical interpretation available in the LAS file. This interpretation includes estimated curves for total porosity, water resistivity, formation temperature, water salinity in NaCl ppm, and shale concentration. Since this well does not have enough well logs to perform a reliable numerical model, we focus on constructing our earth model to match the available interpretation with our simulations. From the well log header mud-filtrate resistivity and the interpreted R_{mf}, we estimate a filtrate salinity of 998 ppm NaCl.

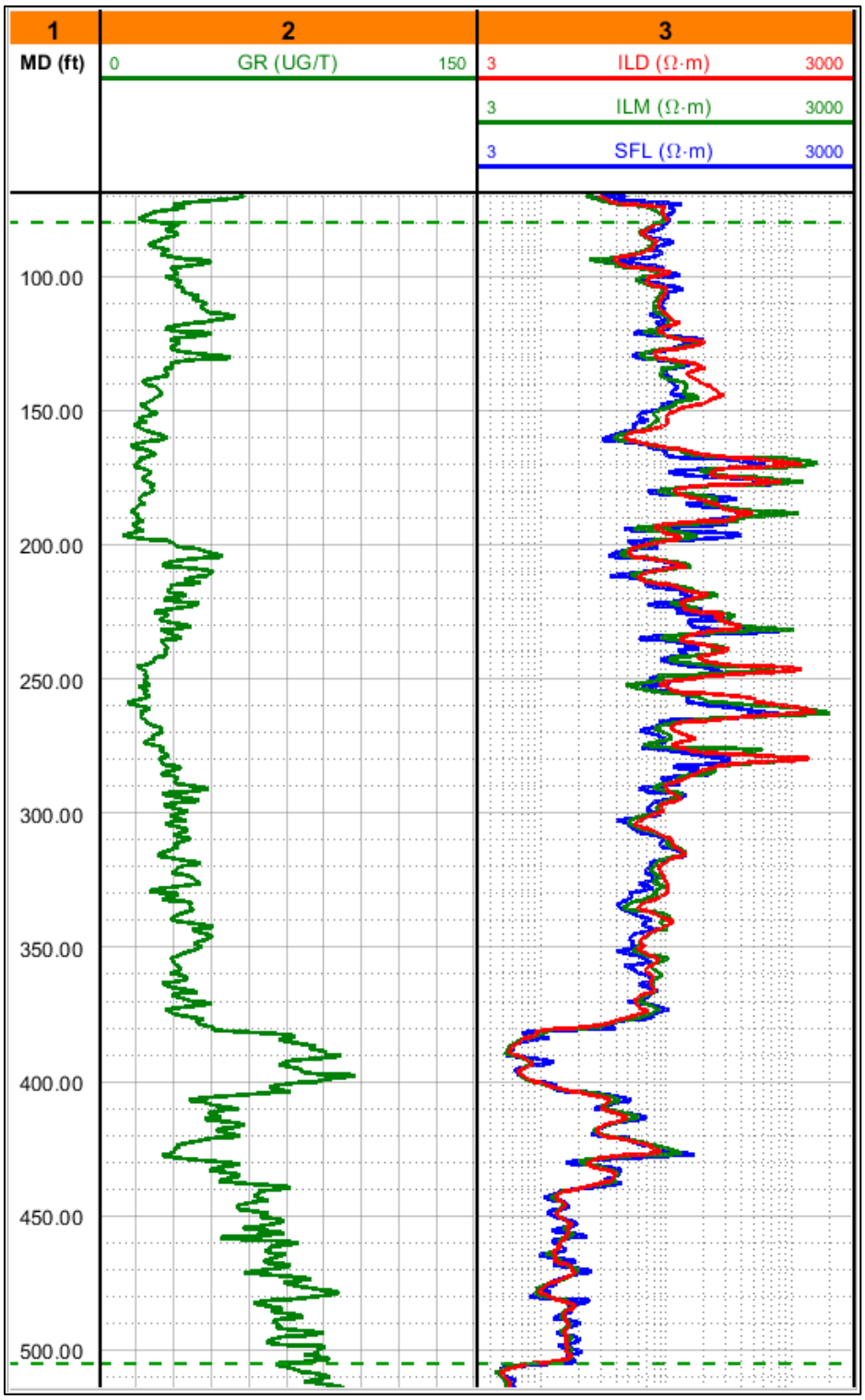

Figure 5-29. Available well logs in Mendel Estate #1. Track 1 presents the measured depth in ft,

track 2 presents the gamma ray log, and track 3 presents the electrical resistivity logs.

Figure 5-30 displays the simulations results. The average formation water salinity is 840 ppm NaCl for the Edwards hydrogeologic unit, and 1094 ppm NaCl for the Lower Cretaceous Sands of the Trinity hydrogeologic unit. However, these average values consider the full simulated sections, where shale concentration is considerable according to the available interpretation. Consequently, we chose a clean layer to perform the resistivity-based methods to compute formation water salinity using the well logs and the simulations results. These results and methods are compared in Table 5-18 and Table 5-19 for Edwards and Trinity, respectively. We employ equations 14 and 15 as empirical correlations to convert from water resistivity to total dissolved solids in the Fort Terrett carbonates and the Lower Cretaceous sandstones, respectively.

We can evaluate several factors from these results and perform interesting comparisons with the synthetic cases developed to understand the simulations outcomes. For the carbonates section in Edwards Unit, we observe a shallow invasion profile and a salinity contrast of three times higher mud-filtrate salinity than formation water salinity. This scenario yields an error of 34.3% for the resistivity ratio method with dual induction logs, which is consistent with the error of 37% encountered for the shallow invaded synthetic case and the performance of induction resistivity logs. However, the Archie's equation method computes a highly uncertain salt concentration in the formation water resulting in an extremely large error. Uncertainties in total porosity estimations extracted from the petrophysical interpretation could be the cause of the large errors. We match the well section around 170 ft MD assuming dolomite as the main rock composition. Porosity interpretation could have been developed assuming a different rock matrix rendering the remarked uncertainties.

On the other hand, we encounter low salinity contrast between filtrate and in-situ water for the Lower cretaceous sands, with respective salt concentrations of 998 ppm NaCl and 1333 ppm NaCl. In addition, the average formation water salinity for these sandstones is 1094 ppm NaCl, which is even more similar to the mud-filtrate salinity. Therefore, we detect a scenario of low invasion radius and low salinity contrast at slightly higher salt concentration in the formation water of Trinity sands. The resistivity ratio method yields an error of 4.9%, which is consistent with the error of 7.7% found in the synthetic case for shallow invasion with negligible salinity contrast using induction resistivity logs. For Trinity sands, the computed error in the assessment of salt concentration using Archie's equation is not as high as the error computed for the Edwards hydrogeological unit. Archie's equation method shows an error of 14.2%, which is not distant from the expected synthetic error of approximately 6%. Again, the uncertainty in the rock matrix during the porosity estimation is key to understand the error in the Archie's method.

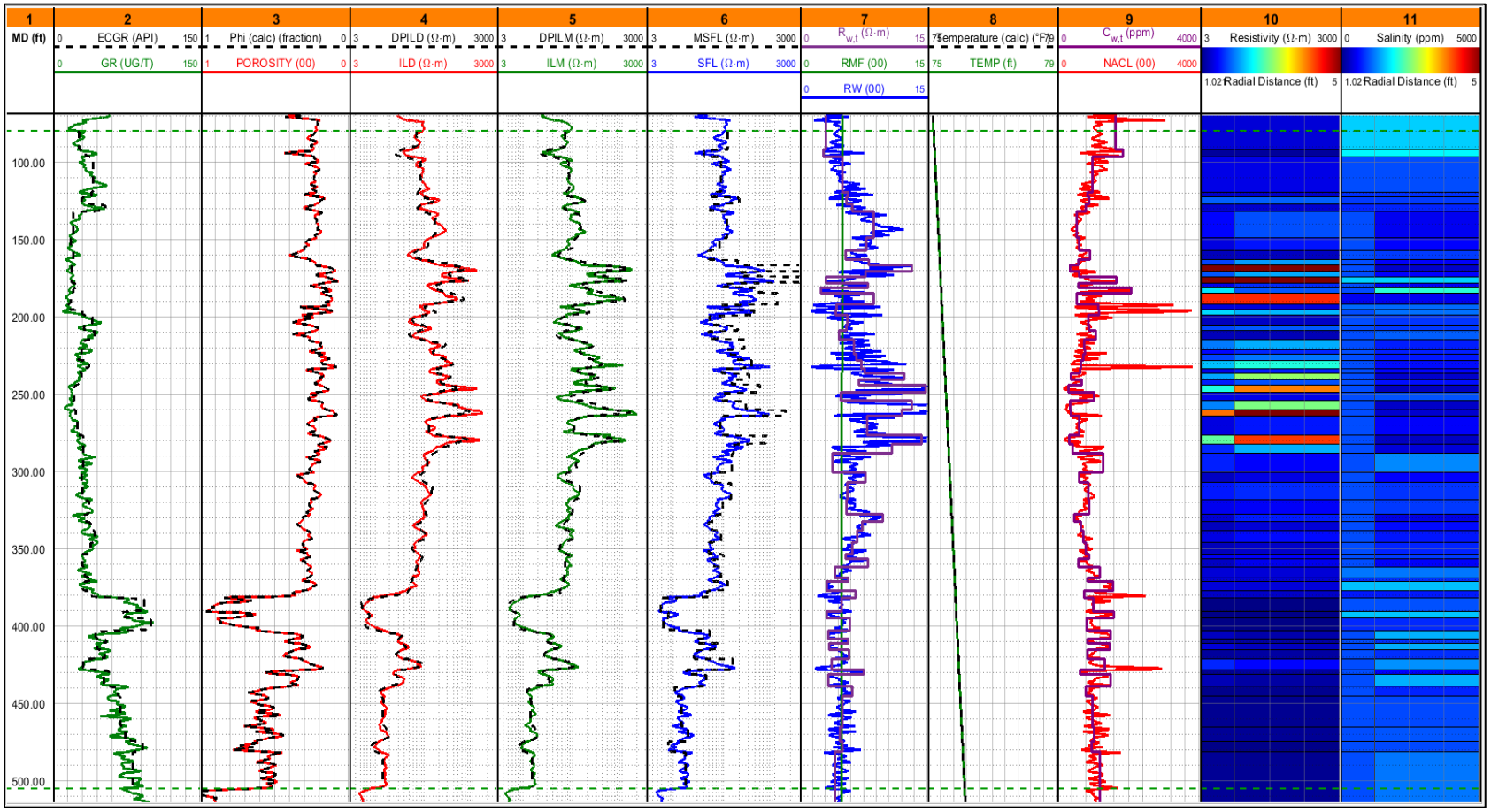

Figure 5-30. Numerical simulation results for the Mendel Estate #1 well logs. Black dashed line in each track represents the numerical simulation of the respective log.

Table 5-18. Summary of water salinity estimations from the numerical simulation results for the Mendel Estate #1 well logs in the upper section of the Fort Terrett formation in the Edwards hydrogeologic unit.

Depth (ft)	R_{mf} [a] (ohm.m)	R_w [b] (ohm.m)	C_{mf} [c] (ppm)	C_w [d] (ppm)[e]	TDS [f] (mg/L)	Method	Error (%)
		13.1928		358	555	Simulation	0.2
170	4.976	2.8120	998	1,818	2,393	Archie's Equation	330.2
		9.5357		504	747	Resistivity Ratio	34.3

Note: Error calculation assumes input formation water salinity as the true formation water salinity. We use the earth model computed values as inputs to calculate the simulation results using the Archie's equation method.
[a] R_{mf} = mud-filtrate resistivity.
[b] R_w = formation water resistivity.
[c] C_{mf} = mud-filtrate salinity.
[d] C_w = formation water salinity.
[e] ppm = parts per million.
[f] TDS = total dissolved solids.

Table 5-19. Summary of water salinity estimations from the numerical simulation results for the Mendel Estate #1 well logs in the upper section of the Lower Cretaceous sands in the Trinity hydrogeologic unit.

Depth (ft)	R_{mf} [a] (ohm.m)	R_w [b] (ohm.m)	C_{mf} [c] (ppm)	C_w [d] (ppm)[e]	TDS [f] (mg/L)	Method	Error (%)
		3.7596		1,330	1,959	Simulation	0.2
425	4.942	3.2851	998	1,532	2,242	Archie's Equation	14.2
		3.9449		1,264	1,867	Resistivity Ratio	4.9

Note: Error calculation assumes input formation water salinity as the true formation water salinity. We use the earth model computed values as inputs to calculate the simulation results using the Archie's equation method.
[a] R_{mf} = mud-filtrate resistivity.
[b] R_w = formation water resistivity.
[c] C_{mf} = mud-filtrate salinity.
[d] C_w = formation water salinity.
[e] ppm = parts per million.
[f] TDS = total dissolved solids.

6 Conclusions

Ultimately, we conducted laboratory measurements on 24 core samples which were obtained from 4 rock classes of the Trinity formation and one representative rock class of the Edwards formation. We faced some challenges in the core preparation process for rock class 1, because the core samples imbibed the water injected into the core samples or that used for core cutting, then got swelled and were cracked and broken. Our hypothesis is that the presence of preexisting micro-fractures in the samples as well as swelling clay minerals could be the reason behind this observation. Furthermore, during experimental procedures such as permeability measurements, these core samples tend to damage when they get exposed to heat and/or pressure.

NMR T_2 measurements show a bi-modal behavior in all Trinity rock classes except rock class 1. The bi-modal behavior is an indication of bi-modal pore-size distribution. Initial permeability measurements showed that rock classes 2 and 4 are very tight. Therefore, we used the pulse-decay permeameter technique for permeability measurements in these rock types since the conventional techniques including brine core-flood and gas permeameter failed to reliably estimate their permeability. These two rock classes showed permeability values ranging from 0.08 mD to 0.0004 mD. On other hand, rock class 3 has a wide range of permeability ranging from 7 mD to 1,378 mD which can indicate the presence of microfractures in some core samples. In the case of porosity quantification, rock class 2 had low porosity values of 2% to 6%, while other classes had porosity values ranging from 6% to 20%. In general, Trinity rock classes are very tight except class 3. Therefore, careful core samples preparation should take place to ensure full saturation of samples while performing experimental measurements. Moreover, the limitation of the laboratory equipment should be considered when dealing with such tight core samples to ensure that the results fall within the reliability margin of the equipment.

In addition, numerical simulations of well logs accurately estimate rock and fluid properties, including formation water salinity. Our simulations demonstrate the effect of mud-filtrate invasion on electrical resistivity logs response and the estimation of formation water salinity using conventional methods. For induction resistivity tools, the errors in the resistivity ratio and the Archie's equation methods increase with increasing salinity contrast between the formation water and the mud-filtrate salt concentrations. At low formation water salinities, below 2,100 ppm NaCL, the errors might achieve values as high as 50% for shallow invasions and 80% for deeply invaded formations. Whereas the errors at high salt concentrations, above 4,250 ppm NaCl, stay below 10%. However, under deeper invasions, the errors in the estimation of salt concentration for high formation water salinity aquifers might increase up to 30%. On the other hand, the errors for the resistivity ratio and Archie's equation methods might increase up to three times when laterolog tools are used instead of induction resistivity logs. In addition, the SP method shows an error varying between 20% and 30% for high water salinities and low water salinities, respectively, when the salinity contrast between formation water and mud-filtrate is high.

Moreover, the SP method requires certain conditions that are normally absent in West

Texas shallow aquifers, such as the presence of shale seals between permeable beds and a sufficient mud column in the wellbore. For all methods, the error in the calculation of formation water salinity decreases when the formation water and mud-filtrate salinity contrast decreases, and both salinities have similar values. Picket plot is a reliable and useful graphical method, but requires a considerable amount of data and sufficient porosity variation, which is not easily to find in practical applications of formation evaluation. According to these observations, the numerical simulations of well-logs provide an alternative and reliable solution for assessing formation water salinity in geohydrology under the presence of mud-filtrate invasion

7 References

Anaya, R., and Jones, I.C., 2009, Groundwater availability model for the Edwards-Trinity (Plateau) and Pecos Valley aquifers of Texas: Texas Water Development Board Report 373, 103 p.

Archie, G.E., 1942, The electrical resistivity logs as an aid in determining some reservoir characteristics: Trans. AIME 146, 54–67 p. doi: https://doi.org/10.2118/942054-G

Blanchard, K.S., 1970, Geothermal gradient in the Delaware-Val Verde Basin of West Texas and Southeast New Mexico: Paper presented at the Drilling and Production Practice, Washington, D.C., January 1970.

Crary, S., Jacobsen, S., Rasmus, J.C. et al, 2001, Effect of resistive invasion on resistivity logs. Presented at the SPE Annual Technical Conference and Exhibition, New Orleans, Louisiana, 30 September-3 October. SPE-71708-MS. doi: http://dx.doi.org/10.2118/71708-MS

Griffiths, R., Barber, T., and Faivre, O., 2000, Optimal evaluation of formation resistivities using array induction and array laterolog tools. Paper BBB presented at the 2000 SPWLA Annual Logging Symposium, Dallas, 4–7 June.

Juhasz, I., 1979, The central role of Qv and formation-water salinity in the evaluation of shaly formations: The Log Analyst 20 (04), p.

Kuniansky, Eve L., and Ardis, Ann F., 2004, Hydrogeology and ground-water flow in the Edwards-Trinity aquifer system, west-central Texas: Regional aquifer-system analysis—Edwards-Trinity: U.S. Geological Survey Professional Paper 1421-C, p.

Pickett, G.R., 1966, A review of current techniques for determination of water saturation from log: Journal of Petroleum Technology 18, 1425–1433 p. doi: https://doi.org/10.2118/1446-PA

Schlumberger, 1972, Log interpretation: Vol. 1. New York: Schlumberger Limited.

Semmelbeck, M. E., and Holditch, S.A., 1988, The effects of mud-filtrate invasion on the interpretation of induction logs: SPE Formation Evaluation 3, 386–392 p. doi: https://doi.org/10.2118/14491-PA

Voss, B., Torres-Verdín, C., Gandhi, A., Alabi, G., and Malek, L., 2009, Common stratigraphic framework to simulate well logs and to cross-validate static and dynamic petrophysical interpretations: Paper presented at the SPWLA 50th Annual Logging Symposium, The Woodlands, Texas, June 2009.